State University of Londrina
Center of Technology and Urbanization
Department of Electrical Engineering
Electrical Engineering Master Program

Gabriel Avanzi Ubiali

Antenna Selection Schemes for Energy Efficiency Increasing of XL-MIMO Systems Under Non-Stationary Channels

Londrina,
June 21, 2021

Gabriel Avanzi Ubiali

Antenna Selection Schemes for Energy Efficiency Increasing of XL-MIMO Systems Under Non-Stationary Channels

A Dissertation submitted to the Electrical Engineering Graduate Program at the State University of Londrina in fulfillment of the requirements for the degree of Master in Electrical Engineering.

Area: Telecommunications Systems

Supervisor: Taufik Abrão

Londrina,
June 21, 2021

Ubiali, Gabriel Avanzi

Antenna Selection Schemes for Energy Efficiency Increasing of XL-MIMO Systems Under Non-Stationary Channels. Londrina, 2021. 128 p.

Supervisor: Taufik Abrão

Dissertation (Master) – Department of Electrical Engineering – State University of Londrina

1. Massive MIMO, 2. Extra-Large MIMO, 3. Spatially Non-Stationary Channels, 4. Spectral Efficiency, 5. Energy Efficiency, 6. Telecommunications Systems

Gabriel Avanzi Ubiali

Antenna Selection Schemes for Energy Efficiency Increasing of XL-MIMO Systems Under Non-Stationary Channels

A Dissertation submitted to the Electrical Engineering Graduate Program at the State University of Londrina in fulfillment of the requirements for the degree of Master in Electrical Engineering.

Area: Telecommunications Systems

Examination Board

Dr. Taufik Abrão
Department of Electrical Engineering
State University of Londrina
Supervisor

Dr. José Carlos Marinello Filho
Department of Electrical Engineering
Federal Technological University of Paraná - Cornélio Procópio Campus
Member

Dr. Marcello Gonçalves Costa
Department of Electrical Engineering
State University of Londrina
Member

Londrina,
June 21, 2021

Acknowledgements

First of all, I thank God, from whom all life and grace comes.

I am very grateful to my supervisor, Prof. Taufik Abrão, for his invaluable advice and support during my M.Sc. study.

To my parents for all their support, understanding, and prayers during these years.

To all my friends (from school times, university, prayer groups and swim workouts) and relatives, for the moments of fun, and especially to friends and colleagues in the laboratory, with whom I lived very friendly day after day during this period.

To the State University of Londrina for the support for the development of the work.

This study was financed in part by the Coordenação de Aperfeiçoamento de Pessoal de Nível Superior - Brasil (CAPES) - Finance Code 001.

Abstract

Increasing the number of antennas at the base station (BS) of a massive MIMO network is useful to improve the throughput and the energy efficiency. However, when employing hundreds or thousands of antennas, the weight of the antenna array may become a challenge, as well as holding the antenna separation to at least half wavelength, which is opportune to make real advantage from an array composed by thousands of antenna elements. Consequently, the array length increases a lot. The main consequence is that the majority of the energy sent by a given user achieves only a small portion of the antenna array, which is called spatial non-stationarity. Thus, selecting the antennas that will participate in the receive combining of the signal sent by each user, instead of using all the available antennas, may be a very useful strategy to reduce considerably the power consumption without degrading the throughput. In this context, there are two possible situations: the subset of the antennas selected for a given user may be any combination of the available antennas, or the array is previously divided into multiple subarrays, corresponding to separate hardware entities, and one or more subarrays are assigned to each user. This work proposes three antenna selection (AS) and two subarray selection (SS) schemes. Numerical results proved that the selection schemes are capable of reducing the number of active antennas in low user-density non-stationary scenario, reducing the power consumption considerably. When assigning a small number of BS antennas per user to perform receive combining for each user, the processing complexity and analog RF front-end power consumption are also reduced. The proposed algorithms select properly the subset of antennas that are designated to each user, preferring the ones whose channel between them and the user are stronger and also considering the potential interference from the other users. Therefore, the throughput reduces only slightly, although zero-forcing (ZF) combiner is more efficient in mitigating the interference when many antennas are used. As the power consumption decays much more than the throughput, the energy-efficiency (EE) is dramatically improved. One of the proposed algorithms, namely fair-AS, arbitrarily maintain a limited number of antennas active. It was more efficient than the other algorithms at maximizing the EE, as it can provide a greater reduction in the power consumption than the other schemes, while the resulting throughput is not severely compromised. Fair-AS can provide big improvements in the system EE even under moderate user density scenarios.

Keywords: Massive MIMO, Extremely-Large MIMO, Antenna Selection, Energy Efficiency, Non-Stationarities, Near-Field Propagation

Resumo

Aumentar o número de antenas na estação rádio base de um sistema MIMO Massivo garante uma melhoria nas taxas de dados e na eficiência energética. Entretanto, ao empregar centenas ou milhares de antenas, o peso do *array* de antenas pode se tornar uma dificuldade, bem como manter a separação entre antenas em no mínimo meio comprimento de onda, o que é oportuno para aproveitar inteiramente a disponibilidade de um grande número de antenas. Consequentemente, o *array* de antenas torna-se muito mais comprido. A principal consequência disto é que a maior parte da energia contida no sinal enviado por um determinado usuário atinge apenas uma pequena porção do *array*, o que é conhecido como não-estacionariedade espacial. Portanto, selecionar as antenas que irão atuar na detecção do sinal transmitido por cada usuário, ao invés de usar todas as antenas, é uma ótima estratégia tendo em vista reduzir a complexidade computacional e o consumo de potência, sem comprometer a taxa de dados. Nesse contexto, existem duas possíveis situações: o subconjunto de antenas selecionadas para cada usuário pode ser qualquer combinação entre as antenas disponíveis no *array*, ou então o *array* é previamente dividido em múltiplos *subarrays*, que seriam entidades de *hardware* independentes, e um ou mais subarrays são atribuídos a cada usuário. Este trabalho propõe três esquemas de seleção de antenas (AS) e de dois esquemas de seleção de subarrays (SS). Os resultados numéricos demonstraram que os esquemas de seleção foram capazes de reduzir o número de antenas ativas em um cenário de baixa ou média densidade de usuários, e consequentemente reduzir consideravelmente o consumo de potência. Ao definir uma pequena quantidade de antenas para realizar o *receive combining* para cada usuário, a complexidade também é reduzida nesse cenário. Os algoritmos propostos selecionam os subconjuntos de antenas criteriosamente, dando preferência àqueles(as) cujo canal até o usuário está mais forte, também considerando a interferência potencial devido aos demais usuários. Portanto, a taxa de dados apresenta apenas uma pequena redução, mesmo que o combinador zero-forcing (ZF) seja mais eficiente em combater a interferência quando o número de antenas é alto. Enfim, como o consumo de potência diminui muito mais que a taxa de dados, a eficiência energética (EE) melhora colossalmente. Um dos algoritmos propostos, chamado *fair-AS*, mantém o número de antenas ativas limitado arbitrariamente. Este algoritmo mostrou-se mais eficiente que os demais em maximizar a eficiência energética, por garantir maior redução de potência que os demais, sem no entanto comprometer consideravelmente a taxa de dados do sistema. O esquema *fair-AS* mostrou-se capaz de aumentar consideravelmente a EE, mesmo em cenários de moderada densidade de usuários.

Palavras-chave: MIMO Massivo, Seleção de Antenas, Eficiência Energética, Não estacionariedades

List of abbreviations and acronyms

5G	5th Telecommunication Generation
AS	Antenna Selection
BS	Base Station
CPU	Central Processing Unit
CSI	Channel state information
DL	Downlink
EE	Energy Efficiency
FDD	Frequency-division duplex
GA	Genetic algorithm
HUD	High user-density
LoS	Line-of-sight
LS	Least-Squares
LUD	Low user-density
MCS	Monte-Carlo simulations
MIMO	Multiple-Input Multiple-Output
M-MIMO	Massive MIMO
MMSE	Minimum Mean-Square Error
NLoS	non-LoS
no-S	non-Antenna Selection
PSO	Particle swarm optimization
SE	Spectral Efficiency
SINR	Signal-to-interference-plus-noise ratio
SS	Subarray Selection
TDD	Time-division duplex

UE	User Equipment
UL	Uplink
ULA	Uniform linear array
VR	Visibility Region
XL-MIMO	Extra-Large MIMO
ZF	Zero-Forcing

List of Notations

k , γ , M	scalars are denoted by italic characters
$\mathbf{a}$	vectors are denoted by lower case bold characters
$\mathbf{A}$	matrices are denoted by upper case bold characters
$\mathcal{A}$	sets are denoted by upper case calligraphic characters
$\|\mathbf{a}\|_2$	norm-2 of $\mathbf{a}$
$\mathbf{0}_N$	N-length zero vector
$\mathbf{I}_N$	$N \times N$ identity matrix
$\odot$	element-wise matrix product
$\mathbf{A}^*$	conjugate of matrix $\mathbf{A}$
$\mathbf{A}^{\mathrm{T}}$	transpose of matrix $\mathbf{A}$
$\mathbf{A}^{\mathrm{H}}$	conjugate transpose of matrix $\mathbf{A}$
$\mathbf{A}^{-1}$	inverse of matrix $\mathbf{A}$
a_{ij} , $[\mathbf{A}]_{ij}$	element present in the ith row and jth column of matrix $\mathbf{A}$
$\mathbf{a}_k$, $[\mathbf{A}]_k$, $\mathbf{A}_{(:,k)}$	k-th column of matrix $\mathbf{A}$
$\mathbf{A}_{(k,:)}$	k-th row of matrix $\mathbf{A}$
$\mathbf{A}_{(\mathcal{D},:)}$	submatrix of $\mathbf{A}$ containing only the rows whose indices are in the set $\mathcal{D}$
$\mathbf{A}_{(:,\mathcal{D})}$	submatrix of $\mathbf{A}$ containing only the columns whose indices are in the set $\mathcal{D}$
a_i , $[\mathbf{a}]_i$	i-th element of vector $\mathbf{a}$
$\mathcal{A}\backslash\{a\}$	set containing all the elements of the set $\mathcal{A}$, except a
$\mathcal{CN}(\mathbf{0}_M, \mathbf{I}_M)$	complex normal distribution with mean $\mathbf{0}_M$ and covariance $\mathbf{I}_M$
$\underset{a\in\mathcal{A}}{\operatorname{argmax}}\ [.]$	element of the set $\mathcal{A}$ that maximizes the argument
$\|a\|$	absolute value of the scalar a
$\|\mathcal{A}\|$	number of elements in the set $\mathcal{A}$
$\log_b a$	logarithm of a in base b
$\mathbb{E}\{.\}$	expectation operator

List of Symbols

K	number of users
S	number of scatterers
M	number of BS antennas
N	number of subarrays
k	user index: $1 \leq k \leq K$
s	scatterer index: $1 \leq s \leq S$
m	antenna index: $1 \leq m \leq M$
n	subarray index: $1 \leq n \leq N$
$\mathcal{M}$	set containing the indices of the M antennas: $\mathcal{M} = \{1, \ldots, M\}$
$\mathcal{N}$	set containing the indices of the N subarrays: $\mathcal{N} = \{1, \ldots, N\}$
M_k	number of antennas serving the k-th user
L	number of antennas serving each user (fixed-AS)
N_k	number of subarrays serving the k-th user (multiple-SS and single-SS)
$\mathcal{D}_k$	set containing the indices of the antennas (fixed-AS and variable-AS) or subarrays (multiple-SS and single-SS) selected for the k-th user
$\mathcal{D}$	set containing the indices of the active antennas
M_{act}	number of active antennas
M_{s}	number of selected antennas (fair-AS)
$M_{\text{s,A}}$	number of antennas selected in stage A of fair-AS algorithm
$M_{\text{s,B}}$	number of antennas selected in stage B of fair-AS algorithm
N_{act}	number of active subarrays (multiple-SS and single-SS)
K_n	number of users served by the n-th subarray (multiple-SS and single-SS)
$\mathcal{F}_n$	number of users served by the n-th subarray (multiple-SS and single-SS)
B	bandwidth
B_{C}	coherence bandwidth
T_{C}	coherence time
τ_{c}	number of symbols that fit in each coherence block
τ_{u}	number of symbols dedicated to the UL data transmission

τ_{p} length of the pilot sequences, which is also the number of symbols in the coherence block that are dedicated to the UL pilot transmission

$\boldsymbol{\psi}_k$ pilot sequence assigned to the k-th user

$\boldsymbol{\Psi}$ set containing the K pilot sequences

d antenna separation

λ wavelength

(x, y) position of a user, scatterer or antenna, considering an xy coordinate system, with the constraints $\mathrm{x}_{\min} \leq x \leq \mathrm{x}_{\max}$ and $\mathrm{y}_{\min} \leq y \leq \mathrm{y}_{\max}$

$\mathrm{x}_{\min}$, $\mathrm{x}_{\max}$ limits of the cell regarding the coordinates in the x-axis

$\mathrm{y}_{\min}$, $\mathrm{y}_{\max}$ limits of the cell regarding the coordinates in the y-axis

$(\bar{x}_s, \bar{y}_s)$ location of the center of the UE-VR associated to the s-th scatterer

$(x_s^{\mathrm{sc}}, y_s^{\mathrm{sc}})$ coordinates of the s-th scatterer

$(x_k^{\mathrm{UE}}, y_k^{\mathrm{UE}})$ coordinates of the k-th user

r_s radius of the s-th scatterer

$D_0(x, y)$ distance between the antenna array and the point (x, y)

$D_m(x, y)$ distance between the m-th antenna and the point (x, y)

D_{mk}^{UE} distance between the k-th user and the m-th antenna: $D_{mk}^{\mathrm{UE}} = D_m(x_k^{\mathrm{UE}}, y_k^{\mathrm{UE}})$

D_{ms}^{sc} distance between the s-th user and the m-th antenna: $D_{ms}^{\mathrm{sc}} = D_m(x_s^{\mathrm{sc}}, y_s^{\mathrm{sc}})$

D_{ks} distance between the k-th user and the s-th scatterer

d_{ks} distance between the k-th user and the center of the UE-VR associated to the s-th scatterer

$\mathbf{a}(x, y)$ array response vector

$\boldsymbol{\Xi}_k$ set containing the antennas that are seen by the k-th user through LoS propagation

$\boldsymbol{\Phi}_s$ set containing the indices of the antennas that see the s-th scatterer

α_{ks} indicates whether the k-th user is (1) or not (0) located inside the UE-VR associated to the s-th scatterer

$\mathbf{h}_k$ channel vector between the antenna array and the k-th user

$\mathbf{h}_k^{\mathrm{LoS}}$ LoS channel between the antenna array and the k-th user

$\mathbf{h}_{ks}^{\mathrm{NLoS}}$ NLoS channel between the antenna array and the k-th user

$\bar{\mathbf{h}}_{ks}$ small-scale fading between the k-th user and the s-th scatterer

$\mathbf{h}_{kn}$ channel vector between the k-th user and the antennas in the n-th subarray

$\widehat{\mathbf{h}}_k$ estimated channel vector between the antenna array and the k-th user

$\widehat{\mathbf{h}}_{kn}$ estimated channel vector between the k-th user and the antennas in the n-th subarray

$\mathbf{H}$ channel matrix

$\mathbf{H}_n$ channel matrix of the n-th subarray

$\widehat{\mathbf{H}}$ estimated channel matrix

$\widehat{\mathbf{H}}_n$ estimated channel matrix of the n-th subarray

$\mathbf{b}_k^{\mathrm{LoS}}$ vector containing the path loss coefficients from the k-th user to each of the M antennas, considering the LoS channel

$\mathbf{b}_{ks}^{\mathrm{NLoS}}$ vector containing the path loss coefficients from the k-th user to each of the M antennas, in the case of NLoS propagation, when the signal travels from the k-th user to the s-th scatterer and then from the scatterer to the BS

$\beta_{mk}^{\mathrm{LoS}}$ path loss coefficient between the k-th user and the m-th antenna, considering the LoS channel

$\beta_{mks}^{\mathrm{NLoS}}$ path loss coefficient between the k-th user and the s-th scatterer, and the s-th scatterer and the m-th antenna (NLoS channel)

β_0 median channel gain for the reference distance $d_0 = 1$ m

γ path-loss exponent

w probability of occurance of the LoS-BS-VRs

$\mathbf{s}_k$ signal transmitted by the k-th user during the UL pilot transmission

x_k signal transmitted by the k-th user during the UL data transmission

$\mathbf{Y}^{\mathrm{p}}$ signal received by the BS during the UL pilot transmission

$\mathbf{r}$ received signal at the BS during the UL data transmission

$\mathbf{r}_n$ signal received by the antennas in the n-th subarray during the UL data transmission

$\mathbf{N}^{\mathrm{p}}$ noise matrix at the receiver of the BS during the UL pilot transmission

$\mathbf{n}$ noise vector at the BS receiver during the UL data transmission

$\mathbf{n}_n$ noise vector at the receiver of the antennas in the n-th subarray

y_k detected signal for the k-th user

y_{kn} detected signal for the k-th user in the n-th subarray

p_{p} transmit power during the UL pilot transmission

p_k k-th user transmit power during the UL pilot transmission

σ_{n}^2 noise power

γ_k SINR of the k-th user

$\mathbf{v}_k$ combining vector of the k-th user

$\mathbf{v}_{kn}$ combining vector of the k-th user, considering only the antennas in the n-th subarray

$\mathbf{V}_n$ collection of the combining vectors used by the n-th subarray

$\boldsymbol{\theta}_k$ quantitative indicator of the quality of the channel between the k-th user and each of the M antennas

z_0 predefined fraction of the total cumulative channel power (variable-AS and multiple-SS)

Z_k total cumulative channel power of the k-th user

Z_{kn} cumulative channel power of the k-th user, considering the n-th subarray

δ_k factor used to normalized the receive signal power (multiple-SS)

C_{tot} total computational complexity

C_{CE} channel estimation complexity

$C_{\text{C-UL}}$ complexity of the computation of the ZF combining vectors

C_{SR} complexity of the UL signal reception

C_{sel} complexity of the antenna/subarray selection (fixed-AS, variable-AS, multiple-SS and single-SS)

C_{PD} complexity of the precision detection (multiple-SS)

P_{tot} total power consumption

$P_{\text{TX}}^{\text{UL}}$ total power consumed by the power amplifiers during the UL data transmission

$P_{\text{TX}}^{\text{tr}}$ total power consumed by the power amplifiers during the UL pilot transmission

P_{CP} circuit power consumption

P_{FIX} fixed power consumption

P_{TC} transceiver chains power consumption

$P_{\text{CE/SP}}$ channel estimation and signal processing power consumption

$P_{\text{C/D}}$ coding and decoding power consumption

P_{BH} load-dependent backhaul power consumption

P_{LO} power consumed by the local oscillator

P_{BS} power consumed by the circuit components of each BS antenna

P_{UE} power consumed by the circuit components of each single-antenna user

L_{BS} computational efficiency at the BS

$\mathcal{P}_{\mathrm{COD}}$	coding power density
$\mathcal{P}_{\mathrm{DEC}}$	decoding power density
$\mathcal{P}_{\mathrm{BT}}$	backhaul traffic power density
η^{UL}	efficiency of the power amplifiers of the BS antennas

List of Figures

List of Tables

Contents

1 Introduction

Massive MIMO (M-MIMO) is considered a crucial component for fulfilling the demands of the fifth generation (5G) wireless communication standard and beyond (Boccardi et al., 2014). Specifically, equipping the BS with thousands of antennas provides extreme spatial resolution that can be used to boost both capacity and energy efficiency (EE). However, practical challenges appear when the array dimension is increased to the order of thousands or more, such as the size and weight of the array (Wang et al., 2020), as current cellular networks deploy compact and colocated antenna array, with antenna separation in the order of the wavelength. In order to make real advantage from the deployment of such a large number of antenna elements, a proper antenna separation is important to achieve great spatial resolution (BJöRNSON et al., 2017). These difficulties advocate for distributing the antennas over a substantially large area.

One potential approach is to divide the antenna array into disjoint subsets of antennas and distributing them over a large area, coordinated by a central processing unit (CPU), which is known as distributed M-MIMO (Wang et al., 2020). Another approach, called extra-large-scale MIMO (XL-MIMO), is the integration of the antenna array into large structures, such as the facades of buildings, shopping malls or stadiums (Carvalho et al., 2020).

When a moderate number of antennas is compactly deployed in the BS, the wavefront from a far user can be reasonably approximated as planar wavefront, while the channel is spatially stationary, which means that the entire array receives approximately the same amount of energy from each user (Han et al., 2020). On the other hand, an antenna array with extreme dimensions yields different channel conditions. As the availability of sufficiently accurate propagation channel models is of critical importance to the design and evaluation of new wireless systems (Flordelis et al., 2020), one must take such conditions into account in order to define a consistent channel model.

First, due to the use of large aperture arrays and the close distance between the array and the users' antenna, the BS antenna array will experience spherical wavefronts instead of planar wavefronts (Yin et al., 2017), which is called *near-field propagation*. Second, in large aperture arrays, different parts of the array might observe the same propagation paths with varying power or distinct propagation paths (Carvalho et al., 2020). Consequently, the majority of energy received from a specific user concentrates on small portions of the antenna array (Ali et al., 2019; Amiri et al., 2018), according to recent channel measurements (Hou et al., 2020; Li et al., 2018; Chen et al., 2017). It is called spatial *non-stationarity*, and such channel property can be introduced in the M-MIMO and XL-MIMO channel modelling by defining the concept of *visibility region* (VR). Section 2.1 contains a discussion on these two additional aspects on the propagation pattern and

the concept of VR, where the traditional M-MIMO channel model is modified in order to aggregate the spherical wavefront and the spatial non-stationarity assumptions.

When employing extremely large arrays, say thousands of antenna-elements, the computational complexity for signal processing becomes a bottleneck if a centralized processing architecture is implemented, specially in crowded scenarios, due to the excessively large amounts of data being transferred between the array and the processing unit (Wang et al., 2020). A promising solution is to divide the antenna array into subarrays, which are disjoint units with individual processing units that accesses only its locally received signals to estimate them (Wang et al., 2020), consequently reducing the complexity. The number and size of subarrays may be fixed, when they correspond to separate hardware entities, or adjustable, when they correspond to software-defined logical interconnections between different antenna elements (Wang et al., 2020).

Numerous benefits arise from the subarray-based processing architecture, including: **a**) *Simplification of the channel acquisition:* as the channel of each subarray individually can be approximated as stationary, one can simply apply MMSE channel estimation, which is known to provide very good channel estimation quality in stationary channels. Furthermore, as the channel matrix is divided into multiple submatrices and each one can be estimated individually, the associated computational complexity is reduced. **b**) *Computational complexity reduction:* due to the spatial non-stationarities along the array, the energy received from each user is mostly concentrated in small portions of the array. Thus, the majority of the energy coming from that user can be received by using only a few antennas, instead of the whole antenna array. Hence, the complexity associated to computing the combining and precoding matrices, as well as the complexity associated to the UL reception and DL transmission, decreases. **c**) *Energy saving:* the channel estimation and signal processing power consumption decreases, due to the reduction in the computational complexity associated to tasks such as signal processing and channel estimation; the power consumption due to the antennas activation also reduces considerably.

By appropriately selecting a subset of BS antennas to communicate to each user, the BS may receive almost all the energy that would be received if all the antennas were used, while reducing the interference coming from the other users if maximum-ratio (MR) combiner is used. If zero-forcing (ZF) combiner is employed, the interference power after the combiner increases when less antennas are utilized. However, if the antennas are properly selected, this increase may be attenuated.. Consequently, although less antennas participate in the signal detection, the spectral efficiency (SE) is not significantly compromised, while the power consumption considerably decreases. As a result, such configuration attains higher EE. Finally, one can summarise the aforementioned benefits from the subarray-based architecture and a judicious antenna selection as:

1. simplification of the channel acquisition;

2. computational complexity reduction;
3. energy saving;
4. increased SE;
5. increased EE.

This work deals with XL-MIMO systems with subarray-based processing architecture, which itself is promising for providing very high spectral and energy efficiencies. Furthermore, this work contains five novel algorithms to judiciously select the BS antennas that communicate with each user in order to reduce the overall computational complexity and the power consumption, consequently ensuring a considerable EE improvement, when compared to using the whole antenna array to communicate to every user.

Aside the necessity of improving the SE, minimizing the power consumption is a growing concern in the XL-MIMO implementation systems, including green communication technologies issues (HUANG et al., 2018). The EE is a performance metric that can manage both objectives. For this reason, the numerical results in Chapter 4 discuss both SE and EE.

1.1 Literature Review

1.1.1 Near-field propagation when employing large antenna arrays

In (Jeng-Shiann Jiang; Ingram, 2005), spherical wave model is empirically shown to be more accurate than plane wave model in short-range MIMO with a line-of-sight (LoS) component, for example, in indoor wireless local area network applications. In (Bohagen et al., 2009), authors provide a tool that can be employed to determine the distances for which the spherical wave model should be applied instead of the plane wave model, in pure LoS conditions and using uniform linear MIMO arrays. In (Zhou et al., 2015), authors propose an analytical spherical-wave channel model for large linear arrays, and investigate how users can be spatially separated in simple LoS scenarios. The results show that spherical wavefront models help decorrelate the channels more effectively than planar wavefront models.

Considering a large-scale antenna array scenario, (Chen et al., 2016) proposes a spherical wavefront signal model and an algorithm to localize the first- and last-hop scatterers along the propagation paths between the user and the BS antennas. Particularly, the algorithm estimates the distance between the last-hop scatterer to a reference antenna element, as well as the angle-of-arrival (AoA) and the angle-of-departure (AoD). Simulations and outdoor measurements with a 1600-element planar array are carried out to verify the

estimation performance of the algorithms. A significant extension of this estimation scheme is presented in (Yin et al., 2017), with a complete generic signal model being proposed.

1.1.2 Channel non-stationarities when employing large antenna arrays

A generic multipath model is proposed in (Wang et al., 2020), based on spherical wavefront, to characterize the propagation path. Some parameteres of the propagation path are used to localize the scatterers in the first and last hops.

The spatial non-stationarity impact on the signal-to-interference-plus-noise ratio (SINR) performance is analysed in (Ali et al., 2019). In (Carvalho et al., 2020), authors show that, when M-MIMO systems operate in extra-large scale regime, several important MIMO design aspects change, due to spatial non-stationarities. In (Amiri et al., 2018), three low-complexity data detection algorithms are proposed for uplink communication in XL-MIMO systems. Efficient detector for XL-MIMO systems based on the subarray processing architecture is proposed in (Wang et al., 2020), by extending the application of the expectation propagation principle to each subarray. A different approach to the antenna selection in XL-MIMO is proposed in (AMIRI et al., 2020), which is based on machine learning to select a small portion of the array that contains a considerable portion of beamforming energy, aiming at overcoming the prohibitive antenna activation consumption/complexity in conventional XL-MIMO systems.

1.2 Objectives

This Master Dissertation has the following objectives:

1. **General:** Systematic analysis of the deployment of antenna selection schemes in XL-MIMO systems.

2. **Specific:**

   a) Perform a systematic comparison between the traditional strategy of utilizing all the antennas of the BS to perform receive combining to detect the signal sent by each user, and the proposed strategy of selecting only a small number of antennas or subarrays to do this task. The strategies are compared regarding the EE, the throughput, the complexity and the power consumption resulting from each strategy.

   b) Make a systematic comparison among each of the five proposed selection schemes, in order to define which one achieves the best results regarding the five performance metrics above mentioned.

1.3 Contributions

The contributions of this work are threefold:

1. Five novel antenna selection procedures are proposed to improve the EE of XL-MIMO systems while reducing the computational complexity and the power consumption, utilizing a detailed circuit power consumption model.

2. A simplified XL-MIMO channel model that takes into account the spatial non-stationarity and the near-field propagation assumptions is developed.

3. A comprehensive analysis on how each proposed AS algorithm impacts on the system performance has been carried out, highlighting the benefits arising from the algorithms compared to the case of using the whole antenna array to communicate to every user.

1.4 Summary of generated articles

1. G.A. Ubiali, T. Abrão. **XL-MIMO energy-efficient antenna selection under non-stationary channels**. Full paper published in the journal *Physical Communication* (IF = 1.830, A3 - Eng. IV in QUALIS-CAPES), in August 2020. A copy of the article is in Appendix A.

2. G.A. Ubiali, J. C. Marinello F., T. Abrão. **Energy-Efficient Flexible and Fixed Antenna Selection Methods for XL-MIMO Systems**. Full paper published in the journal *International Journal of Electronics and Communications* (IF = 3.510, A2 - Eng. IV in QUALIS-CAPES), in December 2020. A copy of the article is in Appendix B.

1.5 Organization of the Text

The remainder of this Dissertation is organized as follows:

- Chapter 2 presents the system model and develops the adopted channel model, describing how the conventional Massive MIMO channel model was modified to include the non-stationarity and near-field propagation scenario.

- Chapter 3 describes the UL Pilot and UL Data Transmission phases and the five proposed strategies of antenna and subarray selection in XL-MIMO scenarios. The computational complexity related to each algorithm and the adopted power consumption model are also presented and comprehensively developed. Section 3.3 suggests a different philosophy in antenna selection for XL-MIMO systems: the number of active

antennas becomes an input parameter to be optimized in the AS algorithm, and all the active antennas collaborate in detecting the signal sent by all active users. The goal is to arbitrarily hold the number of active antennas low, even in medium system loading, so that the energy efficiency is improved over the non antenna selection approach.

- Chapter 4 contains extensive numerical results showing how the EE, the throughput, the complexity and the power consumption are affected depending on which antenna selection scheme is employed.

- Chapter 5 brings the conclusions, summarizes the main findings of this mastership's work and addresses some interesting future research directions in efficient antenna selection issues in XL-MIMO scenarios.

2 System Model

The system model adopted in this chapter involves the UL of a single-cell multiuser XL-MIMO system with an M-antenna BS and K single-antenna users, operating over a bandwidth of B Hz in the time-division duplex (TDD) operation mode. Due to channel reciprocity, TDD mode does not require CSI to be sent from the user equipments (UE) to the BS via feedback, avoiding excessive overhead (Flordelis et al., 2018; MARZETTA et al., 2016). Channel state information (CSI) is acquired via UL synchronous pilot transmission, and the pilot sequences are taken from the same pilot codebook. Their length is denoted by τ_{p} and they form an orthogonal set. Herein, it is assumed that each user uses a different pilot sequence. Then, the pilot sequences' set is $\boldsymbol{\Psi} = [\boldsymbol{\psi}_1 \dots \boldsymbol{\psi}_K] \in \mathbb{C}^{\tau_{\mathrm{p}} \times K}$ and the orthogonality condition states that $\boldsymbol{\Psi}^{\mathrm{H}}\boldsymbol{\Psi} = \tau_{\mathrm{p}}\mathbf{I}_{\tau_{\mathrm{p}}}$, *i.e.*:

$$\boldsymbol{\psi}_i^{\mathrm{H}}\boldsymbol{\psi}_k = \begin{cases} \tau_{\mathrm{p}} & i = k, \\ 0 & i \neq k. \end{cases} \tag{2.1}$$

The channel coherence block is divided into UL pilot and UL data transmission. Being B_{C} and T_{C} the coherence bandwidth and the coherence time, respectively, the number of symbols that fits in a channel coherence block is determined by $\tau_{\mathrm{c}} = T_{\mathrm{C}}B_{\mathrm{C}}$, in which τ_{p} symbols are dedicated to UL pilot transmission and $\tau_{\mathrm{u}} = \tau_{\mathrm{c}} - \tau_{\mathrm{p}}$ symbols are dedicated to UL data transmission (MARZETTA, 2010). During the UL pilot transmission, a different pilot sequence is assigned to each user. The number of available orthogonal pilot sequences is equal their length (τ_{p}). As we need K sequences, we can take $\tau_{\mathrm{p}} = K$, which means that the time required for pilots is proportional to K. Thus, the number of users that can be served is limited by the coherence time, which itself depends on the mobility of the users (MARZETTA, 2010).

We consider a BS equipped with an M-elements uniform linear array (ULA). The distance between two adjacent ULA elements is d. Figure 2.1 shows the ULA lying along the y-axis of an xy coordinate system and centered at its origin. Therefore, the m-th antenna is located at $\left[0,\ \left(m - \frac{M+1}{2}\right) d\right]$. Users are located in the positive x-axis region, inside the rectangular cell defined by $\mathrm{x}_{\min} \leq x \leq \mathrm{x}_{\max}$, $x > 0$, and $\mathrm{y}_{\min} \leq y \leq \mathrm{y}_{\max}$, being (x, y) the coordinates of the user. The distance between any point (x, y) and the antenna array is $D_0(x, y) = x$ and the distance to the m-th antenna is

$$D_m(x, y) = \sqrt{x^2 + \left(y - d\left(m - \frac{M+1}{2}\right)\right)^2} \tag{2.2}$$

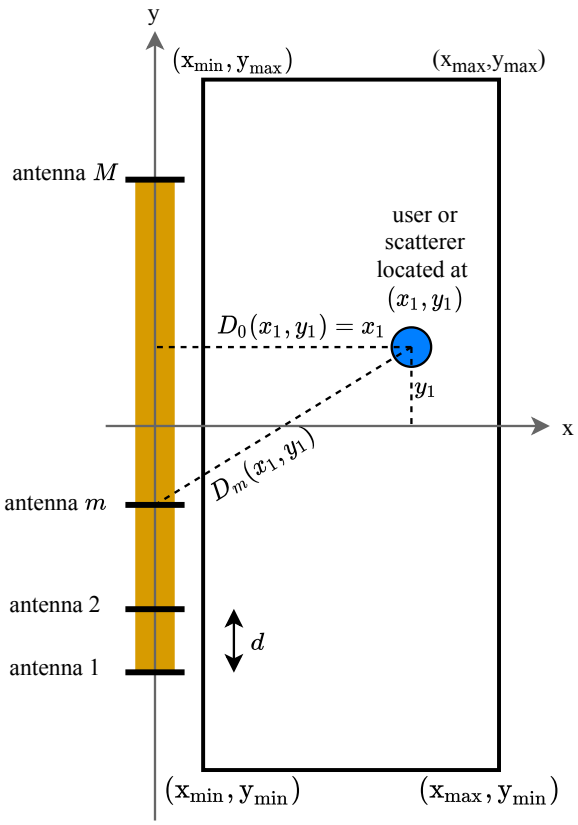

Figure 2.1 – XL-MIMO system represented with an xy coordinate system, with the ULA situated over the y-axis and the user located inside a rectangular cell positioned in (x_1, y_1). $D_0(x, y)$ is the distance between the user and the array; $D_m(x, y)$ is the distance between the user and the m-th antenna element, while d denotes the antenna separation.

2.1 XL-MIMO Channel

The XL-MIMO channel model adopted in this work takes into consideration the spherical wavefront assumption and the spatial non-stationarities.

2.1.1 Near-Field Propagation

The radiation field of antennas can be divided into the near-field region and the far-field region (KRAUS; MARHEFKA, 2002). The boundary between the two regions is approximately the Rayleigh distance (MOLISCH, 2012):

$$\text{Rayleigh distance} = \frac{2l^2}{\lambda} \tag{2.3}$$

where l is the length of the antenna array and λ is the wavelength. In the far-field region, the wavefront can be reasonably assumed as planar. Massive MIMO channel models are usually based on the planar wavefront assumption, as the objects are far beyond the Rayleigh distance (Zhou et al., 2015). However, in XL-MIMO systems, where the arrays

are physically large, this assumption does not hold, as the majority of users and scatterers are situated inside the near-field region. Therefore, the spherical wavefront assumption over large arrays must be taken into consideration when modeling XL-MIMO channels.

The spherical wavefront causes the signal to arrive with different inclination angles along the antenna array, and consequently with different intensities. Furthermore, the distance between a scatterer or user located at the point (x, y) and the antenna array varies significantly on the antenna index. Figure 2.2 illustrates this phenomenon. We can model these properties associated with spherical wavefront assumption deploying the *array response* vector $\mathbf{a}(x, y) \in \mathbb{C}^{M\times 1}$, which is excited by a user or scatterer located at (x, y), whose m-th entry can be expressed as (Han et al., 2020):

$$[\mathbf{a}(x, y)]_m = \frac{D_0(x, y)}{D_m(x, y)} e^{j2\pi D_m(x,y)/\lambda} \tag{2.4}$$

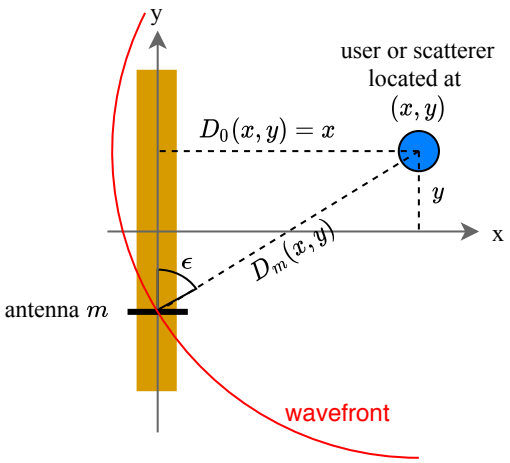

Figure 2.2 – The spherical wavefront causes the signal to arrive with different inclination angles along the antenna array, and consequently with different intensities.

2.1.2 Spatial Non-Stationarity

In (Flordelis et al., 2020), authors propose the notion of BS-side visibility region (BS-VR) and UE-side visibility region (UE-VR) to model spatial non-stationarities. Throughout this work, when the k-th user is said to "see" the m-th antenna, it means that the m-th antenna receives the signal transmitted by the k-th user with non-zero energy.

The transmitted signal interacts with the objects in the environment such as building facades, trees and street furniture, in outdoor environments, or inner walls, pillars and office equipment, in indoor settings. Interactions happen at so-called scattering points (Flordelis et al., 2020). The signal may travel from the user to the BS or from the BS to the user through LoS propagation or through the interactions with the scattering points, *i.e.*, non-LoS (NLoS) propagation configurations. If there is no obstacle in the straight line between the k-th user and the m-th antenna, then there is a LoS propagation and we say

that the m-th antenna is located in the k-th user's LoS-BS-VR. The set containing the antennas that are seen by the k-th user through LoS propagation is denoted by $\mathbf{\Xi}_k$.

Each scatterer has an associated UE-VR and an associate BS-VR. The UE-VR of the s-th scatterer is a circle centered in $(\bar{x}_s, \bar{y}_s)$, whose radius is denoted by r_s. The scatterers and the associated UE-VR centers are uniformly distributed over the cell area. The set containing the antennas that are in the BS-VR of the s-th scatterer is denoted by $\mathbf{\Phi}_s$. If the k-th user is located inside the UE-VR of the s-th scatterer, it will see the antennas that are inside the BS-VR of the s-th scatterer.

Figure 2.3 illustrates a scenario with one user (UE1) and two scattering points, denoted by sc1 and sc2. The UE1 sees a portion of the array through LoS propagation. We say that this portion of the array is inside the BS-VR associated to the line-of-sight of UE1, which is denoted by LoS-BS-VR1. However, UE1 may also see other portions of the array, through NLoS propagation. In the case represented by Figure 2.3, UE1 is inside the UE-VR of sc1, namely, UE-VR1, what means that it sees the portion of the array that is inside the BS-VR of sc1, namely, NLoS-BS-VR1. Then, the portion of the array seen by UE1 corresponds to the union of the regions LoS-BS-VR1 and NLoS-BS-VR1. The antennas that are not inside any of these two BS-VRs are assumed to receive zero energy from UE1, and the signal transmitted by these antennas will not achieve UE1 as well.

Figure 2.4 illustrates a simplificated example of a XL-MIMO system, with 2 users or scatterers and their BS-VRs. If the user or scatterer is located at (x, y), then its BS-VR is assumed to be centered in $(0, y)$ and to have length x, *i.e.*, it extends from $y - x/2$ to $y + x/2$. Thus, the farther a given user or scatterer is located relative to the array, the longer the associated BS-VR will be. This way of modeling the extension of the BS-VRs is proposed in this work as a simple manner of taking into consideration that there are obstacles in the propagation environment and they prevent the signal from arriving at many of the BS antennas, mainly the most distant ones.

The NLoS-BS-VR of the s-th scatterer has length x_s^{sc} and is centered in $(0, y_s^{\text{sc}})$, *i.e.*, it stands from the point $(0, y_s^{\text{sc}} - x_s^{\text{sc}}/2)$ to the point $(0, y_s^{\text{sc}} + x_s^{\text{sc}}/2)$. If the m-th antenna is in this interval, then $m \in \mathbf{\Phi}_s$. The LoS-BS-VR of the k-th user has length x_k^{UE} and is centered in $(0, y_k^{\text{UE}})$, *i.e.*, it stands from $(0, y_k^{\text{UE}} - x_k^{\text{UE}}/2)$ to $(0, y_k^{\text{UE}} + x_k^{\text{UE}}/2)$. Due to the obstacles in the propagation environment, even antennas that are close to a given user may sometimes not receive the signal sent by it. To make the modeling described in the last paragraph more realistic, we can consider that the LoS-BS-VRs occur with a probability of occurrence w, which means there is a probability $1 - w$ that there are obstacles blocking the signal that comes directly from the user (*i.e.*, via LoS propagation). In other words, w is the probability that the signal transmitted by the user will achieve at least one point in the y-axis. If the energy sent by a given user achieves an interval in the y-axis, and there is at least one antenna in this interval, then the LoS-BS-VR of the given user will contain a portion of the array, *i.e.*, this user will see a portion of the array

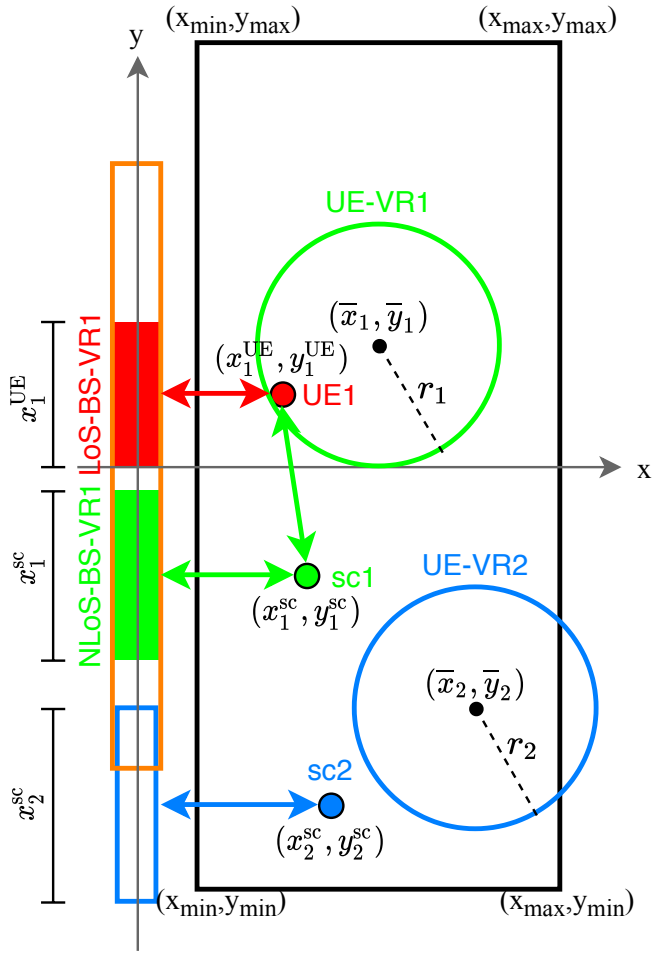

Figure 2.3 – Simplified example of a XL-MIMO system, with 1 user and two scatterers. The user sees a portion of the array through a LoS propagation and other portion of the linear array through a NLoS propagation via scatterer sc1.

through LoS propagation. Recall that (x_s^{sc}, y_s^{sc}) and (x_k^{UE}, y_k^{UE}) represent the points where the s-th scatterer and the k-th user are located, respectively.

2.2 Modeling the XL-MIMO Channel

The channel vector between the BS and the k-th user is defined by both LoS and NLoS terms:

$$\mathbf{h}_k = \mathbf{h}_k^{\text{LoS}} + \sum_{s=1}^{S} \mathbf{h}_{ks}^{\text{NLoS}} \alpha_{ks} \tag{2.5}$$

with the LoS component defined as:

$$\mathbf{h}_k^{\text{LoS}} = \sqrt{\mathbf{b}_k^{\text{LoS}}} \odot \mathbf{a}(x_k^{UE}, y_k^{UE}) \odot \mathbf{q}(\boldsymbol{\Xi}_k) \tag{2.6}$$

and the NLoS components associated to S scatterers:

$$\mathbf{h}_{ks}^{\text{NLoS}} = \sqrt{\mathbf{b}_{ks}^{\text{NLoS}}} \odot \bar{\mathbf{h}}_{ks} \odot \mathbf{a}(x_s^{sc}, y_s^{sc}) \odot \mathbf{q}(\boldsymbol{\Phi}_s) \tag{2.7}$$

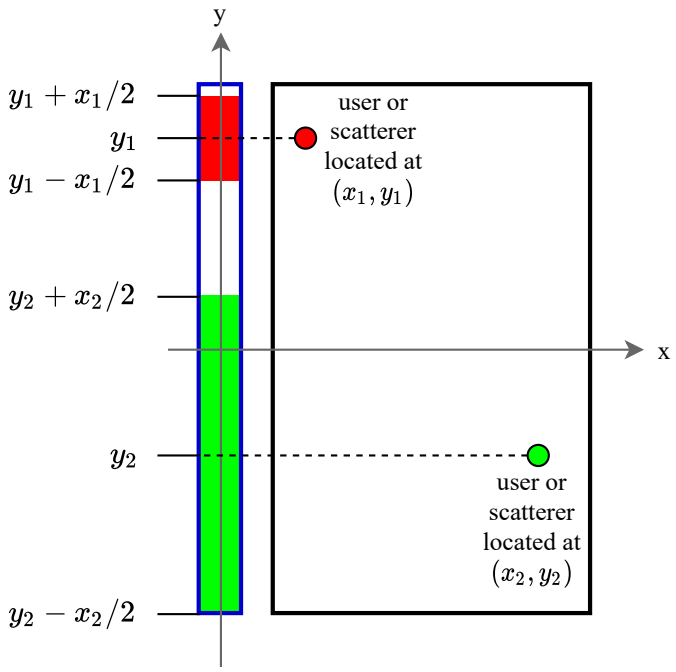

Figure 2.4 – Simplified example of a XL-MIMO system, with 2 users or scatterers and their BS-VRs. The BS-VRs are assumed to be centered in y-axis coordinate of the user or scatterer, and to have length equal to its x-axis coordinate.

where $(x_k^{\mathrm{UE}}, y_k^{\mathrm{UE}})$ and $(x_s^{\mathrm{sc}}, y_s^{\mathrm{sc}})$ are the position of the k-th user and the s-th scatterer, respectively; $\mathbf{\Phi}_s$ is the set containing the indices of the antennas that see the s-th scatterer, while

$$[\mathbf{q}(\mathbf{\Phi})]_m = \begin{cases} 1 & \text{if } m \in \mathbf{\Phi}, \\ 0 & \text{otherwise.} \end{cases} \tag{2.8}$$

indicates whether the m-th antenna is in the BS-VR associated to the set $\mathbf{\Phi}$ or not, and α_{ks} indicates if the k-th user is located inside the UE-VR associated to the s-th scatterer. Then,

$$\alpha_{ks} = \begin{cases} 1 & \text{if } d_{ks} \leq r_s, \\ 0 & \text{otherwise.} \end{cases} \tag{2.9}$$

where $d_{ks} = \sqrt{(x_k^{\mathrm{UE}} - \bar{x}_s)^2 + (y_k^{\mathrm{UE}} - \bar{y}_s)^2}$ is the distance between the k-th user and the center of the UE-VR associated to the s-th scatterer.

The vector $\mathbf{b}_k^{\mathrm{LoS}} = [\beta_{1k}^{\mathrm{LoS}}, \ldots, \beta_{Mk}^{\mathrm{LoS}}]^{\mathrm{T}}$ groups the path loss coefficients from the k-th user to each of the M antennas, in the case of the LoS channel. Considering that $D_{mk}^{\mathrm{UE}} = D_m(x_k^{\mathrm{UE}}, y_k^{\mathrm{UE}})$ is the distance between the k-th user and the m-th antenna, according to Eq. (2.2), the LoS propagation has a path loss determined by:

$$\beta_{mk}^{\mathrm{LoS}} = \beta_0 \left(\frac{D_{mk}^{\mathrm{UE}}}{1 \text{ m}} \right)^{-\gamma} \tag{2.10}$$

where β_0 defines the *median channel gain* for the *reference distance* $d_0 = 1$ m and $\gamma \geq 2$ is the path-loss exponent. The parameters β_0 and γ are functions of the carrier frequency,

antenna gains, and vertical heights of the antennas, which are derived from fitting (2.10) and (2.11) to measurements (BJöRNSON et al., 2017).

On the other side, the vector $\mathbf{b}_{ks}^{\text{NLoS}} = [\beta_{1ks}^{\text{NLoS}}, \ldots, \beta_{Mks}^{\text{NLoS}}]^{\text{T}}$ groups the path loss coefficients in the case of NLoS propagation, when the signal travels from the user to the scatterer and then from the scatterer to the BS. Being $D_{ks} = \sqrt{(x_k^{\text{UE}} - x_s^{\text{sc}})^2 + (y_k^{\text{UE}} - y_s^{\text{sc}})^2}$ the distance between the k-th user and the s-th scatterer, and $D_{ms}^{\text{sc}} = D_m(x_s^{\text{sc}}, y_s^{\text{sc}})$ the distance between the s-th scatterer and the m-th antenna, the NLoS path loss is determined as:

$$\beta_{mks}^{\text{NLoS}} = \beta_0 \left(\frac{D_{ms}^{\text{sc}} + D_{ks}}{1 \text{ m}} \right)^{-\gamma} \tag{2.11}$$

In the NLoS propagation scenarios, the transmitted signal interacts with the objects in the environment, what changes its module and phase. This is the small-scale fading, which can be modeled as an independent Rayleigh fading; hence, in (2.7), the vector $\bar{\mathbf{h}}_{ks}$ can be modeled as complex Gaussian distribution with zero mean and unity variance, $\bar{\mathbf{h}}_{ks} \sim \mathcal{CN}(\mathbf{0}, \mathbf{I}_M)$.

2.3 UL Pilot Transmission and Channel Estimation

During the UL pilot transmission, the k-th user transmits the pilot sequence $\boldsymbol{\psi}_k \in \mathbb{C}^{\tau_{\text{p}}}$, with transmit power p_{p}. The elements of $\boldsymbol{\psi}_k$ are scaled by $\sqrt{p_{\text{p}}}$, forming the signal $\mathbf{s}_k = \sqrt{p_{\text{p}}}\boldsymbol{\psi}_k^{\text{H}}$, to be transmitted over τ_{p} UL symbols. As a result, the BS receives the signal $\mathbf{Y}^{\text{p}} \in \mathbb{C}^{M \times \tau_{\text{p}}}$:

$$\mathbf{Y}^{\text{p}} = \sum_{i=1}^{K} \sqrt{p_{\text{p}}} \mathbf{h}_i \boldsymbol{\psi}_i^{\text{H}} + \mathbf{N}^{\text{p}} \tag{2.12}$$

where $\mathbf{N}^{\text{p}} \in \mathbb{C}^{M \times \tau_{\text{p}}}$ is the noise matrix at the receiver of the BS with i.i.d. elements following a complex normal distribution with zero mean and variance σ_{n}^2.

As the information about which antennas are visible for each user is unknown, it might be necessary to consider obtaining the channel estimates by using estimators that require no prior statistical information, such as the *Least-Squares* (LS). The LS estimate of $\mathbf{h}_k$ is attained by (BJöRNSON et al., 2017):

$$\widehat{\mathbf{h}}_k = \frac{1}{\tau_{\text{p}}\sqrt{p_{\text{p}}}} \mathbf{Y}^{\text{p}} \boldsymbol{\psi}_k \tag{2.13a}$$

$$= \mathbf{h}_k + \frac{1}{\tau_{\text{p}}\sqrt{p_{\text{p}}}} \mathbf{N}^{\text{p}} \boldsymbol{\psi}_k \tag{2.13b}$$

The last term in (2.13b) is the equivalent noise vector, which adds imperfections to the channel estimates and follows a complex normal distribution: $\mathbf{N}^{\text{p}}\boldsymbol{\psi}_k \sim \mathcal{CN}(\mathbf{0}_M, \tau_{\text{p}}\sigma_{\text{n}}^2\mathbf{I}_M)$. Finally, the estimated channel matrix is $\widehat{\mathbf{H}} = [\widehat{\mathbf{h}}_1 \ \ldots \ \widehat{\mathbf{h}}_K]$, while $\mathbf{H} = [\mathbf{h}_1 \ \cdots \ \mathbf{h}_K] \in \mathbb{C}^{M \times K}$ is the true channel matrix.

3 Energy Efficiency in XL-MIMO Systems

This chapter presents the five proposed antennas and subarrays selection schemes, as well as the computational complexity resulting from each algorithm.

The *antenna selection* (AS) algorithms assign the BS subset of antennas to perform receive combining to each user. Section 3.1 presents two AS schemes, namely fixed-AS and variable-AS. Both select the best antennas to communicate to each user, so that not every selected antenna is used to communicate to all the users. By allowing the users to be served by different antenna elements, this approach is particularly adequate to reduce the interference power after the combiner when employing maximum-ratio (MR) combiner. However, as ZF combiner usually provides much greater SE and EE than MR, all the signal models described in this chapter attain to ZF processing only.

Section 3.2 presents two *subarray selection* (SS) algorithms, namely multiple-SS and single-SS. In this approach, the antenna array is divided into a number of fixed-size subarrays, which can be implemented in a distributed way, as separate hardware entities, while selecting one or more subarrays to communicate with each user. It is an advantage over the AS approach, as the implementation complexity is reduced. Thus, it is important to test, via numerical results, for example, if this implementation complexity reduction is sufficient to consider the SS schemes more promising than the AS schemes, or if the resulting SE and EE are worse, as the SS schemes have less flexibity on choosing the best antenna elements for each user because the antenna arrays was previously divided into subarrays. Chapter 4 presents the results concerning these comparisons.

In this work, all the users are assigned different orthogonal pilot sequence, such that there is no pilot contamination and the channel estimation is corrupted only by the noise received in the BS antennas during the UL pilot transmission. In this scenario, the CSI is almost perfect and the ZF is efficient at mitigating interference. Therefore, when detecting the signal sent from the k-th user, even if the antenna m, contained in the set $\mathcal{D}$, receives much energy from other users, it is convenient to utilize this antenna to perform the receive combining operation for the k-th user.

Considering these facts, Section 3.3 presents a AS approach different from the AS schemes depicted in Section 3.1. In this scheme, namely fair-AS, all the selected antennas communicate to every user. Thus, the fair-AS scheme was particularly designed for ZF receive combining, where the more antennas are used, the more the interference is mitigated. Employing the fair-AS scheme, it is easier to prevent the whole antenna array from being active, saving power and increasing the overall system EE, when compared to the other strategies. It has been demonstrated by the numerical results in Chapter 4.

3.1 Antenna Selection (AS)

Here, two different algorithms, fixed-AS and variable-AS, are proposed for selecting the antenna elements in the XL-MIMO system that will be used to detect the signal sent by each of the K users during the UL data transmission. The set $\mathcal{D}_k$ contains the indices of the $M_k = |\mathcal{D}_k|$ antennas selected for the k-th user.

One advantage of using $M_k \leq M$ antennas instead of all the M available antennas is the reduction of the computational complexity, as the combining vector for a given user will be based only on the rows of the estimated channel matrix corresponding to the antennas that the algorithm designated to be active for that user, instead of the full estimated channel matrix. As a consequence, when the number of users is not elevated, it is possible to maintain a portion of the array inactivated, and the complexity is reduced, resulting in a considerable reduction in the power consumption. Besides, even ZF combiner being more efficient at mitigating interference when more antennas are utilized, the throughput will not be severely compromised, because the antennas are properly selected. Consequently, the EE certainly increases.

The ZF combining vector $\mathbf{v}_k$ is M-length, but only the elements corresponding to the indices of the antennas selected for that user are non-zero. Thus, the m-th entry of the combining vectors is given by:

$$[\mathbf{v}_k]_m = \begin{cases} \widehat{\mathbf{H}}_{(m,:)} \left(\left[\widehat{\mathbf{H}}^{\mathrm{H}}_{(\mathcal{D}_k,:)} \widehat{\mathbf{H}}_{(\mathcal{D}_k,:)} \right]^{-1} \right)_{(:,k)} & \text{if } m \in \mathcal{D}_k, \\ 0 & \text{otherwise,} \end{cases} \tag{3.1}$$

Notice that the rows of the combining matrix corresponding to the antennas whose indices are not in the set $\mathcal{D}_k$ are set equal zero.

The vector $\boldsymbol{\theta}_k = [\theta_{1k}, \theta_{2k}, \ldots, \theta_{Mk}] \in \mathbb{C}^M$ is a quantitative indicator of the quality of the channel between the k-th user and each of the M antennas, being defined by:

$$\theta_{mk} = \frac{|\widehat{h}_{mk}|^2}{\sum\limits_{\substack{i=1 \\ i \neq k}}^{K} |\widehat{h}_{mi}|^2} \tag{3.2}$$

where $\widehat{h}_{mk} = [\widehat{\mathbf{h}}_k]_m$. A high signal intensity may be obtained when $|\widehat{h}_{mk}|^2$ is strong. On the other hand, the terms $|\widehat{h}_{mi}|^2$, $i \neq k$, are related to the interference intensity. Higher θ_{mk} values are therefore associated to higher SINRs on the signal detection, as defined by (3.6), and consequently higher spectral and energy efficiencies.

Both algorithms select the M_k antennas associated to the M_k highest elements of the vector $\boldsymbol{\theta}_k$ to detect the signal of the k-th user. In other words, being $\theta_{m_{ik}k}$ the i-th highest element of the vector $\boldsymbol{\theta}_k$, they define:

$$\mathcal{D}_k = \{m_{1k}, \ldots, m_{M_k k}\} \tag{3.3}$$

The condition $M_k > K$ is necessary to guarantee that the matrix to be inverted in (3.1) is not singular. Being $\mathcal{D} = \mathcal{D}_1 \cup \ldots \cup \mathcal{D}_K$ the set containing the indices of the antennas that are active for some user, $M_{\text{act}} = |\mathcal{D}|$ denotes the number of active antennas.

The received signal $\mathbf{r} \in \mathbb{C}^M$ at the BS during the UL data transmission is:

$$\mathbf{r} = \sum_{k=1}^{K} \mathbf{h}_k x_k + \mathbf{n} \tag{3.4}$$

where x_k is the signal sent by the k-th user and $\mathbf{n} \sim \mathcal{CN}(\mathbf{0}_M, \sigma_{\text{n}}^2 \mathbf{I}_M)$ contains the noise received at the BS antennas. The detected signal for the k-th user after the combiner is given by:

$$y_k = \mathbf{v}_k^{\text{H}} \mathbf{r} \tag{3.5}$$

where $\mathbf{v}_k \in \mathbb{C}^M$ is the k-th user receive combining vector. The SINR of the k-th user during the UL data transmission can be defined as

$$\gamma_k = \frac{p_k |\mathbf{v}_k^{\text{H}} \mathbf{h}_k|^2}{\sum\limits_{\substack{i=1 \\ i \neq k}}^{K} p_i |\mathbf{v}_k^{\text{H}} \mathbf{h}_i|^2 + \sigma_{\text{n}}^2 ||\mathbf{v}_k||^2} \tag{3.6}$$

where $p_k = \mathbb{E}\{|x_k|^2\}$ is the k-th user UL transmit power.

3.1.1 No selection (no-S)

The no-S is the traditional processing scheme: the whole antenna array (all the M antennas), is utilized to detect the signal sent by each user in the BS receiver through a linear combining technique, *i.e.*, $M_k = M$ and $\mathcal{D}_k = \{1, \ldots, M\}$. It means that none of the M elements of the combining vectors of the K users are intentionally set to zero. Consequently, the k-th user ZF receive combining vector in (3.1) can be rewritten as:

$$\mathbf{v}_k = [\widehat{\mathbf{H}} (\widehat{\mathbf{H}}^{\text{H}} \widehat{\mathbf{H}})^{-1}]_{(:,k)} \tag{3.7}$$

3.1.2 Fixed number of antennas per user (fixed-AS)

In the fixed-AS scheme, described by Algorithm 3.1, the number of antennas to be selected for each user is fixed, *i.e.*, it is an input parameter of the algorithm, and is the same for all users, denoted by L, so that $M_k = L$, $k \in \{1, \ldots, K\}$. Therefore, $\mathcal{D}_k = \{m_{1k}, \ldots, m_{Lk}\}$. Lines 1-3 attend the condition $M_k \geq K$.

Figure 3.1 shows an example of the XL-MIMO system user spatial distribution, where the number of users and BS antennas are low, for simplicity: $K = 4$ and $M = 16$. Each triangle represents one of the 16 BS antennas, while the colored circles represents the mobile users, which are randomly distributed over a rectangular cell. Taking a random channel realization, the portion of the array that each user sees is indicated by the

Algorithm 3.1 Fixed-AS for receive combining in XL-MIMO systems

Input: M, L, K, $\hat{\mathbf{H}}$
if $L \leq K$ **then**
  $L = K$
end if
for $k = 1$ to K **do**
  Reinitialize the set containing the indices of the M antennas: $\mathcal{M} = \{1, \ldots, M\}$
  Initialize the set containing the indices of the antennas that will communicate with the user k: $\mathcal{D}_k = \emptyset$
  Compute $\boldsymbol{\theta}_k$, according to (3.2)
  for $l = 1$ to L **do**
    find $m^* = \underset{m \in \mathcal{M}}{\operatorname{argmax}}\ \theta_{mk}$
    $\mathcal{M} = \mathcal{M} \backslash \{m^*\}$
    $\mathcal{D}_k = \mathcal{D}_k \cup \{m^*\}$
  end for
end for
Output: $\mathcal{D}_k$, $k = 1, \ldots, K$

horizontal line with its correspondent color. User 1, for example, sees the antennas 1 to 10, while user 2 sees the antennas 9 to 15, excepting the antenna 13. This fragmentation of the VR into two parts may occur if any object is blocking the signal in that region.

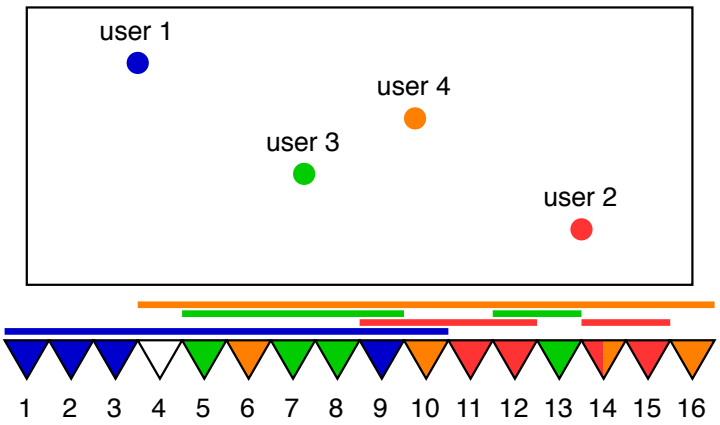

Figure 3.1 – Example of a XL-MIMO system, with 4 users being served by a BS equipped with a 16-antenna linear antenna array. The figure illustrates each user's VR and the antennas that the proposed algorithm designates to communicate with each user.

In this example, the fixed-AS algorithm was set up to define $L = 4$ antennas to communicate with each user. In the figure, the triangle that represents a given antenna m is painted with the color of the k-th user if the k-th user is being served by the m-th antenna. For example, antennas 1, 2, 3 and 9, which are in blue, were designated by to communicate with user 1. Notice that all these 4 antennas are part of the VR of user 1. Although the signal from user 1 probably achieves the antennas 4 to 8 with higher intensity than antenna 9, choosing one of these antennas would increase the received interference

power, mainly due to user 3. Observe that antenna 4 is not active, while antenna 14 serves users 2 and 4, simultaneously. Therefore, considering that only one antenna was designated to communicate with 2 users at the same time, we can say that , if MR combining is employed, the algorithm will be successful in avoiding the interference from other users to affect the SINR, while simultaneously reducing the computational complexity.

However, the fair-AS scheme would be much more promising when employing ZF combining, specially when there is not pilot contamination, as all the selected antennas would be used to estimate the signal sent by all the users. Furthermore, we could maintain more antennas inactive, achieving higher energy efficiency.

3.1.3 Variable number of antennas per user (variable-AS)

In the variable-AS scheme, described by Algorithm 3.2, the number of antennas to be selected for each user is not fixed and is not the same for all users. Therefore, variable-AS scheme may select only a few antennas if the energy coming from an individual user signal is concentrated over a small portion of the array, for example. On the other hand, it may select more antennas if the energy is more uniformly distributed over the array. Thus, the objective is to verify via numerical results if the flexibilizing the number of selected antennas per user is advantageous or not for improving the EE over the fixed-AS scheme. In this approach, M_k is the minimum number of antennas that satisfies

$$\sum_{i=1}^{M_k} |\widehat{h}_{m_{ik}k}|^2 \geq z_0 Z_k \tag{3.8}$$

where $0 \leq z_0 \leq 1$, and Z_k is the total cumulative power associated to the k-th user, defined as:

$$Z_k = \sum_{m=1}^{M} |\widehat{h}_{mk}|^2 \tag{3.9}$$

Indeed, $z_0 Z_k$ represents a fraction of the total cumulative power for the kth user. For instance, setting $z_0 = 0.9$ represents 90% of the total cumulative power. Hence, setting $z_0 = 1$ corresponds to using all the M antennas to process the signal of the k-th user. In practice, it is the same as not applying antenna selection procedure for that user. On the other hand, setting $z_0 = 0$ will simply force the BS to ignore that user. Finally, setting z_0 as low values implies that the main concern is reduce the power consumption.

Line 13 of Algorithm 3.2 attends the condition $M_k \geq K$.

In the example given in Figure 3.1, the variable-AS scheme would probably select a different number of antennas for each user, depending on the amount of antennas that are necessary to receive a fraction z_0 of the total energy coming from each user.

Algorithm 3.2 Variable-AS for receive combining in XL-MIMO systems

Input: M, K, $\widehat{\mathbf{H}}$, z_0

1: **for** $k = 1$ to K **do**
2: Reinitialize the set containing the indices of the M antennas: $\mathcal{M} = \{1, \ldots, M\}$
3: Initialize the set containing the indices of the antennas that will communicate with the user k: $\mathcal{D}_k = \emptyset$
4: Compute $\boldsymbol{\theta}_k$, according to (3.2)
5: Compute Z_k, according to (3.9)
6: Initialize $z_k = 0$
7: **while** $z_k < z_0 Z_k$ **do**
8: $m^* = \underset{m \in \mathcal{M}}{\arg\max}\ \theta_{mk}$
9: $z_k = z_k + |\widehat{h}_{m^*k}|^2$
10: $\mathcal{D}_k = \mathcal{D}_k \cup \{m^*\}$
11: $\mathcal{M} = \mathcal{M} \backslash \{m^*\}$
12: **end while**
13: Repeat lines 8–11 until $|\mathcal{D}_k| \geq K$.
14: **end for**

Output: $\mathcal{D}_k$, $k = 1, \ldots, K$

3.2 Subarray Selection (SS)

In the subarray selection (SS) approach, the antenna array is divided into subarrays, which can be implemented as separate hardware entities. It is an advantage over the AS approach, as the implementation complexity is reduced. The number of subarrays (N) is fixed, as well as their size. We consider the specific case where all subarrays have the same length, *i.e.*, M/N, antennas. Then, the antennas in the n-th subarray form the set $\mathcal{M}_n = \{\frac{M}{N}(n-1)+1\ ,\ \ldots\ ,\ \frac{M}{N}n\}$. For instance, considering a ULA with $M = 100$ antennas, if we want to divide it into $N = 10$ subarrays of the same size, then each one will have 10 antennas, and subarray 1 will correspond to the antennas 1 to 10.

In this section, two SS schemes are proposed, namely multiple-SS and single-SS, which defines the sets $\mathcal{F}_1, \ldots, \mathcal{F}_N$ containing the indices of the users that will be served by each of the N subarrays. The set $\mathcal{D}_k$ contains the indices of the subarrays designated to perform receive combining for the k-th user. The number of users served by the n-th subarray is $K_n = |\mathcal{F}_n|$, and the number of subarrays serving the k-th user is $N_k = |\mathcal{D}_k|$. If $k \in \mathcal{F}_n$, then $n \in \mathcal{D}_k$, and vice-versa.

If N_{act} denotes the number of non-empty $\mathcal{F}_n$ sets, and consequently the number of subarrays that serve at least one user, then $M_{\text{act}} = M \cdot N_{\text{act}}/N$ is the number of active antennas.

During the UL, the received signal $\mathbf{r}_n \in \mathbb{C}^{M/N}$ at the n-th subarray is:

$$\mathbf{r}_n = \sum_{k=1}^{K} \mathbf{h}_{kn} x_k + \mathbf{n}_n \tag{3.10}$$

where $\mathbf{h}_{kn} = \mathbf{H}_{(\mathcal{M}_n,k)}$ and $\widehat{\mathbf{h}}_{kn} = \widehat{\mathbf{H}}_{(\mathcal{M}_n,k)}$ are respectively the channel vector and the estimated channel vector between the n-th subarray and the k-th user and $\mathbf{n}_n \sim \mathcal{CN}(\mathbf{0}_{M/N}, \sigma_{\mathrm{n}}^2 \mathbf{I}_{M/N})$. The estimated channel matrix of the n-th subarray is $\widehat{\mathbf{H}}_n = \widehat{\mathbf{H}}_{(\mathcal{M}_n,:)} = [\widehat{\mathbf{h}}_{1n}, \ldots, \widehat{\mathbf{h}}_{Kn}] \in \mathbb{C}^{M/N \times K}$, which contains only the rows corresponding to its antennas. If $k \in \mathcal{F}_n$, the n-th subarray will detect the signal transmitted by the k-th user:

$$y_{kn} = \mathbf{v}_{kn}^{\mathrm{H}} \mathbf{r}_n \tag{3.11}$$

where the ZF combining vector $\mathbf{v}_{kn} \in \mathbb{C}^{M/N}$ is given by:

$$\mathbf{v}_{kn} = \begin{cases} [\widehat{\mathbf{H}}_n (\widehat{\mathbf{H}}_n^{\mathrm{H}} \widehat{\mathbf{H}}_n)^{-1}]_{(:,k)} & \text{if } k \in \mathcal{F}_n, \\ \mathbf{0}_{M/N} & \text{otherwise.} \end{cases} \tag{3.12}$$

The matrix $\mathbf{V}_n = [\mathbf{v}_{1n} \ldots \mathbf{v}_{Kn}]$ is the collection of the combining vectors used by the n-th subarray. As defined in (3.12), if $k \notin \mathcal{F}_n$, then $\mathbf{v}_{kn}$ is an all-zero vector. Thus, there is a complexity reduction, as only $\sum_{n=1}^{N} K_n$ vectors will be computed, instead of NK if there was no subarray selection. Notice that each subarray computes its receive combining matrix independently, based on the matrix $\widehat{\mathbf{H}}_n$, which contains only the rows of the matrix $\widehat{\mathbf{H}}$ that corresponds to the antennas that are part of the n-th subarray.

Both multiple-SS and single-SS assign the N_k subarrays associated to the highest θ_{nk} values to communicate with the k-th user. In other words, they define the set $\mathcal{D}_k$ as:

$$\mathcal{D}_k = \{n_{1k}, \ldots, n_{N_k k}\} \tag{3.13}$$

being $\theta_{n_{ik}k}$ the i-th highest element of the vector $\boldsymbol{\theta}_k$. The condition $M/N > K$ is necessary to guarantee that the matrix to be inverted in (3.12) is not singular. The n-th entry of the vector $\boldsymbol{\theta}_k \in \mathbb{C}^N$ is defined as

$$\theta_{nk} = \frac{Z_{kn}}{\sum\limits_{\substack{i=1 \\ i \neq k}}^{K} Z_{in}} \tag{3.14}$$

where Z_{kn} is the cumulative power associated to the k-th user in the n-th subarray, given by:

$$Z_{kn} = \sum_{m \in \mathcal{M}_n} |\widehat{h}_{mk}|^2 \tag{3.15}$$

Notice that θ_{nk} in (3.14) is a metric that indicates the quality of the channel between the k-th user and the n-th subarray, while in (3.2) it indicates the quality of the channel between the user and each antenna individually.

The CPU will then combine the detected signals y_{kn}, $n \in \mathcal{D}_k$, in each of the N_k subarrays, featuring a precision detector:

$$y_k = \frac{1}{\delta_k} \sum_{n \in \mathcal{D}_k} \theta_{nk} y_{kn} \tag{3.16}$$

Thus, after the receive combining at the BS, during the UL data transmission, the average desired signal power and the average interference power for the k-th user are given by

$$\mathcal{S}_k = p_k \frac{t_{kk}}{\delta_k^2} \tag{3.17}$$

and

$$\mathcal{I}_k = \sum_{\substack{k'=1 \\ k' \neq k}}^{K} p_{k'} \frac{t_{kk'}}{\delta_k^2} \tag{3.18}$$

respectively, where

$$t_{kk'} = \left| \sum_{n=1}^{N} \theta_{nk} \mathbf{v}_{kn}^{\mathrm{H}} \mathbf{h}_{k'n} \right|^2 \tag{3.19}$$

In order to normalize the received signal power in (3.17), so that $\mathcal{S}_k = p_k$, δ_k is defined as:

$$\delta_k = \sum_{n \in \mathcal{D}_k} \theta_{nk} \tag{3.20}$$

The average noise power for the k-th user after the combining is:

$$\mathcal{N}_k = \sigma_{\mathrm{n}}^2 \sum_{n=1}^{N} \frac{\theta_{nk}^2}{\delta_k^2} ||\mathbf{v}_{kn}||^2 \tag{3.21}$$

Thus, analogously to (3.6), the resulting SINR is given by:

$$\gamma_k = \frac{p_k t_{kk}}{\sum\limits_{\substack{k'=1 \\ k' \neq k}}^{K} p_{k'} t_{kk'} + \sigma_{\mathrm{n}}^2 \sum\limits_{n=1}^{N} \theta_{nk}^2 ||\mathbf{v}_{kn}||^2} \tag{3.22}$$

3.2.1 Multiple number of subarrays per user (multiple-SS)

In the multiple-SS scheme, described by Algorithm 3.3, the number of subarrays to be selected for each user is not fixed and is not the same for all users. N_k is the minimum number of subarrays that satisfies

$$\sum_{i=1}^{N_k} Z_{kn_{ik}} \geq z_0 Z_k \tag{3.23}$$

where Z_k is the cumulative power associated to the k-th user, given by:

$$Z_k = \sum_{n=1}^{N} Z_{kn} \tag{3.24}$$

The condition $M/N > K$ is attended in lines 1-3 of Algorithm 3.3.

Algorithm 3.3 Multiple-SS for receive combining in XL-MIMO systems

Input: M, N, K, $\widehat{\mathbf{H}}$, z_0
1: **if** $M/N \leq K$ **then**
2: $N = M/(K+1)$
3: **end if**
4: Initialize the set of the users that will be served by each subarray: $\mathcal{F}_n = \emptyset$, for $n = 1, \ldots, N$.
5: Initialize the sets $\mathcal{M}_n = \{\frac{M}{N}(n-1)+1\ ,\ \ldots\ ,\ \frac{M}{N}n\}$, which will be used to compute Z_{kn} in line 9.
6: **for** $k = 1$ to K **do**
7: Reinitialize the set containing the indices of the N subarrays: $\mathcal{N} = \{1, \ldots, N\}$.
8: Initialize the set containing the indices of the subarrays that will communicate with the k-th user: $\mathcal{D}_k = \emptyset$.
9: Compute Z_{kn}, $n = 1, \ldots, N$, according to (3.15).
10: Compute Z_k, according to (3.24).
11: Compute $\boldsymbol{\theta}_k$, according to (3.14).
12: Initialize $z_k = 0$.
13: **while** $z_k < z_0 Z_k$ **do**
14: $n^* = \underset{n \in \mathcal{N}}{\operatorname{argmax}}\ \theta_{nk}$
15: $z_k = z_k + Z_{kn^*}$
16: $\mathcal{D}_k = \mathcal{D}_k \cup \{n^*\}$
17: $\mathcal{F}_{n^*} = \mathcal{F}_{n^*} \cup \{k\}$
18: $\mathcal{N} = \mathcal{N} \backslash \{n^*\}$
19: **end while**
20: **end for**
Output: $\mathcal{F}_n$, $n = 1, \ldots, N$, and $\mathcal{D}_k$, $k = 1, \ldots, K$

3.2.2 Only one subarray per user (single-SS)

Multiple-SS may select multiple subarrays to detect the signal sent by each user during the UL data transmission, which means that $1 \leq N_k \leq N$. Single-SS, described by Algorithm 3.4, is a variant of multiple-SS where only one subarray is selected per user, *i.e.*, $N_k = 1$. Thus, $\mathcal{D}_k = \{n_{1k}\}$, which means that the selected subarray is the one associated with the highest element of the vector $\boldsymbol{\theta}_k$, and y_k is simply the detected symbol in the n_{1k}-th subarray. The objective of single-SS is to obtain a larger complexity reduction than with the former methods (fixed-AS, variable-AS and multiple-SS), as less antennas are likely to be active, while not deteriorating considerably the SE. By replacing $\mathcal{D}_k$ with $\{n_{1k}\}$ in (3.16) and (3.20), (3.16) can be rewritten as:

$$y_k = y_{kn_{1k}} \tag{3.25}$$

The SINR in (3.22) can be rewritten as:

$$\gamma_k = \frac{p_k \left| \mathbf{v}_{kn_{1k}}^{\mathrm{H}} \mathbf{h}_{kn_{1k}} \right|^2}{\sum\limits_{\substack{k'=1 \\ k' \neq k}}^{K} p_{k'} \left| \mathbf{v}_{kn_{1k}}^{\mathrm{H}} \mathbf{h}_{k'n_{1k}} \right|^2 + \sigma_{\mathrm{n}}^2 ||\mathbf{v}_{kn_{1k}}||^2} \tag{3.26}$$

The condition $M/N > K$ is attended in lines 1-3 of Algorithm 3.4.

Algorithm 3.4 Single-SS for receive combining in XL-MIMO systems

Input: M, N, K, $\widehat{\mathbf{H}}$
1: **if** $M/N \leq K$ **then**
2: $N = M/(K+1)$
3: **end if**
4: Initialize the set containing the indices of the N subarrays: $\mathcal{N} = \{1, \ldots, N\}$.
5: Initialize the set of the users that will be served by each subarray: $\mathcal{F}_n = \emptyset$, for $n = 1, \ldots, N$.
6: Compute Z_{kn}, $n = 1, \ldots, N$, $k = 1, \ldots, K$, according to (3.15).
7: Compute $\boldsymbol{\theta}_k$, $k = 1, \ldots, K$, according to (3.14).
8: **for** $k = 1$ to K **do**
9: $n^* = \underset{n \in \mathcal{N}}{\operatorname{argmax}}\ \theta_{nk}$
10: $\mathcal{D}_k = \{n^*\}$
11: $\mathcal{F}_{n^*} = \mathcal{F}_{n^*} \cup \{k\}$
12: **end for**
Output: $\mathcal{F}_n$, $n = 1, \ldots, N$, and $\mathcal{D}_k$, $k = 1, \ldots, K$

3.3 Arbitrary Low Number of Antennas Selection – Fair-AS Scheme

The schemes proposed in Section 3.1 select the best antennas for each user, so that when the number of users is relatively large, the number of active antennas is almost the total number of available antennas. This section defines another selection scheme, based on (Marinello et al., 2020), with a different philosophy: the number of active antennas is an input of the algorithm and all the active antennas collaborate on detecting the signal sent from all the K users. The objective is to arbitrarily maintain the number of active antennas low, even when $K = 100$, for instance, so that the energy efficiency is improved over the no-S approach even in the HUD scenario.

The ZF combining vector $\mathbf{v}_k$ is M-length, but only the elements corresponding to the indices of the M_s selected antennas are non-zero. Thus, the m-th entry of the combining vectors is given by:

$$[\mathbf{v}_k]_m = \begin{cases} \widehat{\mathbf{H}}_{(m,:)} \left(\left[\widehat{\mathbf{H}}^{\mathrm{H}}_{(\mathcal{D},:)} \widehat{\mathbf{H}}_{(\mathcal{D},:)} \right]^{-1} \right)_{(:,k)} & \text{if } m \in \mathcal{D}, \\ 0 & \text{otherwise.} \end{cases} \tag{3.27}$$

where the set $\mathcal{D}$ contains the indices of the antennas that the algorithm designates to be active. Notice that this strategy requires just one matrix inversion to obtain the ZF combining matrix, unlike fixed-AS and variable-AS, which requires K matrix inversions, one for each of the K users.

3.3.1 Fairness criterion antenna selection (fair-AS)

The fair-AS scheme gives attention to the strength of the channel of all the K users when selecting the active antennas, in order to try to provide good rates for all the users while simultaneously improving the EE.

The vector $\boldsymbol{\theta}_k = [\theta_{1k}, \theta_{2k}, \ldots, \theta_{Mk}] \in \mathbb{C}^M$ indicates the strength of the channel between the k-th user and each of the M antennas, being defined by:

$$\theta_{mk} = |\widehat{h}_{mk}|^2 \tag{3.28}$$

Similarly to the schemes described in Chapter 3, this selection scheme chooses the $M_k = \lfloor M_\mathrm{s}/K \rfloor$ antennas associated to the M_k highest elements of the vector $\boldsymbol{\theta}_k$. In other words, being $\theta_{m_{ik}k}$ the i-th highest element of the vector $\boldsymbol{\theta}_k$:

$$\mathcal{D}_k = \{m_{1k}, \ldots, m_{M_k k}\} \tag{3.29}$$

This process is done for the K users, so that $\sum_{k=1} M_k$ antennas are chosen. This is the stage A of the algorithm, when $M_{\mathrm{s,A}} = |\mathcal{D}_\mathrm{A}|$ antennas are selected, being $\mathcal{D}_\mathrm{A} = \mathcal{D}_1 \cup \ldots \cup \mathcal{D}_K$. If $M_{\mathrm{s,A}} \neq M_\mathrm{s}$, the algorithm will select other $M_{\mathrm{s,B}} = M_\mathrm{s} - M_{\mathrm{s,A}}$ antennas, in the stage B of the algorithm. If $M_{\mathrm{s,A}} = M_\mathrm{s}$, the stage B will not be executed and, consequently, $M_{\mathrm{s,B}} = 0$.

During the stage B, the fair-AS algorithm obtains the set $\mathcal{D}_\mathrm{B}$, which defines other $M_{\mathrm{s,B}} = |\mathcal{D}_\mathrm{B}|$ antennas to be activated. The selected antennas during stage B are the ones associated to the $M_{\mathrm{s,B}}$ highest elements of the vector $\boldsymbol{\rho}$, whose m-th entry is defined as:

$$\rho_m = \sum_{k=1}^{K} |\widehat{h}_{mk}|^2 \tag{3.30}$$

Notice that all the M_s selected antennas will be used to perform the receive combining for the k-th user, although only M_k antennas had been chosen considering the strength of the channel of this user. The selection procedure is depicted in Algorithm 3.5. Lines 5-14 and lines 15-28 correspond to the stages A and B, respectively. The condition $M_\mathrm{s} > K$ is necessary to guarantee that the matrix to be inverted in (3.27) is not singular.

3.4 Computational Complexity

This section develops the computational complexity resulting from employing each of the antenna/subarray selection strategies. The complexity may be discriminated in five parts: channel estimation, computation of the ZF combining vectors, signal reception at the BS during the UL data transmission, antenna or subarray selection (only on fixed-AS, variable-AS, multiple-SS, single-SS and fair-AS strategies) and precision detection (only on multiple-SS strategy). Table 3.1 gathers all these complexities, while Table 3.2 contains the total complexity associated to each selection scheme.

Algorithm 3.5 Fair-AS for receive combining in XL-MIMO systems

Input: M, M_{s}, K, $\hat{\mathbf{H}}$
if $M_{\mathrm{s}} \leq K$ **then**
  $M_{\mathrm{s}} = K + 1$
end if
Initialize $M_{\mathrm{user}} = \lfloor M_{\mathrm{s}}/K \rfloor$.
Initialize $\mathcal{D}_{\mathrm{A}} = \emptyset$.
for $k = 1$ to K **do**
  Reinitialize the set containing the indices of the M antennas: $\mathcal{M} = \{1, \ldots, M\}$.
  Compute $\boldsymbol{\theta}_k$, according to (3.28)
  for $l = 1$ to M_{user} **do**
    Find $m^* = \underset{m \in \mathcal{M}}{\operatorname{argmax}}\ \theta_{mk}$
    $\mathcal{M} = \mathcal{M} \backslash \{m^*\}$
    $\mathcal{D}_{\mathrm{A}} = \mathcal{D}_{\mathrm{A}} \cup \{m^*\}$
  end for
end for
if $|\mathcal{D}_{\mathrm{A}}| \neq M_{\mathrm{s}}$ **then**
  Reinitialize $\mathcal{M} = \{1, \ldots, M\}$.
  Initialize the set containing the indices of the antennas that have not been selected already: $\mathcal{N} = \mathcal{M} \backslash \mathcal{D}_{\mathrm{A}}$.
  Initialize $\mathcal{D}_{\mathrm{B}} = \emptyset$.
  Compute $\boldsymbol{\rho}$, as in (3.30).
  for $l = 1$ to $M_{\mathrm{s}} - |\mathcal{D}_{\mathrm{A}}|$ **do**
    Find $m^* = \underset{m \in \mathcal{N}}{\operatorname{argmax}}\ \rho_m$
    $\mathcal{N} = \mathcal{N} \backslash \{m^*\}$
    $\mathcal{D}_{\mathrm{B}} = \mathcal{D}_{\mathrm{B}} \cup \{m^*\}$
  end for
  $\mathcal{D} = \mathcal{D}_{\mathrm{A}} \cup \mathcal{D}_{\mathrm{B}}$
else
  $\mathcal{D} = \mathcal{D}_{\mathrm{A}}$
end if
Output: $\mathcal{D}$

Notice that the complexity reduction provided by the selection schemes over the no-selection strategy comes from utilizing fewer antennas to perform receive combining for each user, which considerably reduces the number of complex multiplications when applying the ZF combiner over the received signal, as well as the size of the channel matrix to be inverted in order to compute the ZF vectors. However, the AS schemes performs one matrix inversion for each of the K users, which will possibly make the complexity scale when K is high. Numerical results addressing complexity comparisons among the proposed schemes are presented in Chapter 4.

3.4.1 Channel estimation

According to (2.13a), the channel estimation process corresponds to the inner product of M complex vectors of length τ_{p}, requiring $M\tau_{\mathrm{p}}$ multiplications between complex numbers (or $3M\tau_{\mathrm{p}}$ multiplications between real numbers[1]) to estimate the channel vector of each of the K UEs. Herein, both multiplication and division between real numbers correspond to 1 floating-point operation (flop). As the channel estimation (CE) process is performed once per coherence block, its computational complexity, defined in number of flops per coherence block [fpcb], is:

$$C_{\mathrm{CE}} = 3\tau_{\mathrm{p}}MK \text{ [fpcb]} \tag{3.31}$$

3.4.2 Computation of the ZF combining vectors

- **no-S:** Multiplying $\widehat{\mathbf{H}}^{\mathrm{H}}$ by $\widehat{\mathbf{H}}$, following (3.7), requires $\frac{K^2+K}{2}M$ complex multiplications[2], using the Hermitian symmetry. According to (BJöRNSON et al., 2017), when the inverse of a matrix is multiplied by another matrix, the $\mathbf{LDL}^{\mathrm{H}}$ decomposition can be used to achieve an efficient hardware implementation. The decomposition of $\widehat{\mathbf{H}}^{\mathrm{H}}\widehat{\mathbf{H}}$ requires $\frac{K^3-K}{3}$ complex multiplications (BJöRNSON et al., 2017). Finally, we need to multiply $\widehat{\mathbf{H}}$ by the matrix $(\widehat{\mathbf{H}}^{\mathrm{H}}\widehat{\mathbf{H}})^{-1}$, which requires K^2M complex multiplications plus K complex divisions to compute $\mathbf{D}^{-1}$ (BJöRNSON et al., 2017; BOYD; VANDENBERGHE, 2004). Considering complex multiplications and complex divisions to correspond to 3 and 7 flops[3], respectively, the computation of the combining matrix $\mathbf{V}$ has a complexity of $3\left(\frac{K^2+K}{2}M + \frac{K^3-K}{3} + K^2M\right) + 7K$ flops per coherence block, which is the same as:

$$C_{\text{C-UL}}^{\text{no-S}} = K^3 + \frac{9}{2}MK^2 + \frac{3}{2}(M+4)K \text{ [fpcb]} \tag{3.32}$$

- **variable-AS:** Multiplying $\widehat{\mathbf{H}}_{(\mathcal{D}_k,:)}^{\mathrm{H}}$ by $\widehat{\mathbf{H}}_{(\mathcal{D}_k,:)}$, according to (3.1), requires $\frac{K^2+K}{2}M_k$ complex multiplications. The decomposition of $\widehat{\mathbf{H}}_{(\mathcal{D}_k,:)}^{\mathrm{H}}\widehat{\mathbf{H}}_{(\mathcal{D}_k,:)}$ requires $\frac{K^3-K}{3}$ complex multiplications. Finally, we need to multiply the matrix $\widehat{\mathbf{H}}_{(\mathcal{D}_k,:)}$ by the k-th column of the matrix $\left[\widehat{\mathbf{H}}_{(\mathcal{D}_k,:)}^{\mathrm{H}}\widehat{\mathbf{H}}_{(\mathcal{D}_k,:)}\right]^{-1}$, which requires KM_k complex multiplications plus K complex divisions to compute $\mathbf{D}^{-1}$. Then, the computation of the combining vector

[1] Consider $x = a + jb$ and $y = c + jd$. The hardware implementation of the complex multiplication $xy = ac - bd + j[(a+b)(c+d) - ac - bd]$ involves 3 real multiplications and 5 real sums. Only those will be considered, due to their very greater hardware complexity compared to the real sum operation.

[2] Being $\mathbf{A} \in \mathbb{C}^{a\times b}$ and $\mathbf{B} \in \mathbb{C}^{b\times c}$, the multiplication $\mathbf{A}\cdot\mathbf{B}$ requires ac inner products between b-length vector, what corresponds to abc complex multiplications. However, if $\mathbf{B} = \mathbf{A}^{\mathrm{H}}$, the Hermitian symmetry is utilized. Thus, only the a diagonal elements of $\mathbf{A}\cdot\mathbf{B}$ and half of the $a^2 - a$ off-diagonal elements need to be computed, resulting in $\frac{a^2+a}{2}b$ complex multiplications(BJöRNSON et al., 2017).

[3] Considering $x = a + jb$ and $y = c + jd$, then $\frac{x}{y} = \frac{xy^*}{yy^*} = \frac{xy^*}{|y|^2}$. The computation of xy^* requires 3 real multiplications. The computation of $|y|^2 = c^2 + d^2$ requires 2 real multiplications. Finally, the complex division $\frac{xy^*}{|y|^2}$ corresponds to 2 real divisions, making a total of 7 real operations.

$\mathbf{v}_k$ has a complexity of $3\left(\frac{K^2+K}{2}M_k + \frac{K^3-K}{3} + KM_k\right) + 7K$ flops per coherence block, and the computational complexity to obtain the whole combining matrix $\mathbf{V}$ is given by:

$$C_{\text{C-UL}}^{\text{variable-AS}} = K^4 + 6K^2 + \frac{3}{2}(K+3)K\sum_{k=1}^{K} M_k \text{ [fpcb]} \tag{3.33}$$

- **fixed-AS:** The complexity of computing the ZF combining vectors, when employing the fixed-AS scheme, can be obtained from (3.33) by replacing M_k with L:

$$C_{\text{C-UL}}^{\text{fixed-AS}} = K^4 + \frac{3}{2}LK^3 + \frac{3}{2}\left(3L+4\right)K^2 \text{ [fpcb]} \tag{3.34}$$

- **multiple-SS:** The multiplication of $\widehat{\mathbf{H}}_n^{\text{H}}$ by $\widehat{\mathbf{H}}_n$, according to (3.12), has a complexity of $\frac{K^2+K}{2}\frac{M}{N}$ flops per coherence block, using the Hermitian symmetry. The $\mathbf{LDL}^{\text{H}}$ decomposition of the matrix $\widehat{\mathbf{H}}_n^{\text{H}}\widehat{\mathbf{H}}_n$ requires $\frac{K^3-K}{3}$ complex multiplications. Multiplying $\widehat{\mathbf{H}}_n$ by the k-th column of $(\widehat{\mathbf{H}}_n^{\text{H}}\widehat{\mathbf{H}}_n)^{-1}$, in order to obtain $\mathbf{v}_{kn}$, $k \in \mathcal{F}_n$, requires $K\frac{M}{N}$ complex multiplications plus K complex divisions to compute $\mathbf{D}^{-1}$. Recalling that $|\mathcal{F}_n| = K_n$, the n-th subarray needs to compute the combining vectors of K_n users, and the complexity of obtaining the matrix $\mathbf{V}_n$ is $3\left(\frac{K^2+K}{2}\frac{M}{N} + \frac{K^3-K}{3} + K_nK\frac{M}{N}\right)+7K$ flops per coherence block. Finally, the complexity to compute the combining matrix of the N subarrays, when employing ZF combining, is given by:

$$C_{\text{C-UL}}^{\text{multiple-SS}} = NK^3 + \frac{3}{2}MK^2 + \frac{3}{2}(M+4N)K + MK\sum_{n=1}^{N} K_n \text{ [fpcb]} \tag{3.35}$$

- **single-SS:** In this case, each user is served by only one subarray. Thus, $\sum_{n=1}^{N} K_n = K$. As a consequence, (3.35) can be rewritten as:

$$C_{\text{C-UL}}^{\text{single-SS}} = NK^3 + \frac{5}{2}MK^2 + \frac{3}{2}(M+4N)K \text{ [fpcb]} \tag{3.36}$$

  and there is a complexity reduction over the multiple-SS strategy.

- **fair-AS:** Multiplying $\widehat{\mathbf{H}}_{(\mathcal{D},:)}^{\text{H}}$ by $\widehat{\mathbf{H}}_{(\mathcal{D},:)}$, following (3.27), requires $\frac{K^2+K}{2}M_{\text{s}}$ complex multiplications, using the Hermitian symmetry. The $\mathbf{LDL}^{\text{H}}$ decomposition of $\widehat{\mathbf{H}}_{(\mathcal{D},:)}^{\text{H}}\widehat{\mathbf{H}}_{(\mathcal{D},:)}$ requires $\frac{K^3-K}{3}$ complex multiplications. Finally, we need to multiply $\widehat{\mathbf{H}}_{(\mathcal{D},:)}$ by $\left[\widehat{\mathbf{H}}_{(\mathcal{D},:)}^{\text{H}}\widehat{\mathbf{H}}_{(\mathcal{D},:)}\right]^{-1}$, which requires K^2M_{s} complex multiplications plus K complex divisions. Finally, the computation of the combining matrix $\mathbf{V}$ has a complexity of $3\left(\frac{K^2+K}{2}M_{\text{s}} + \frac{K^3-K}{3} + K^2M_{\text{s}}\right) + 7K$ flops per coherence block, which is the same as:

$$C_{\text{C-UL}}^{\text{fair-AS}} = K^3 + \frac{9}{2}M_{\text{s}}K^2 + \frac{3}{2}(M_{\text{s}}+4)K \text{ [fpcb]} \tag{3.37}$$

When the number of users is small, M_k may be considerably smaller than M, as ZF combiner may be efficient at mitigating interference with less antennas in this scenario. When there are more users, on the other hand, the selection schemes complexity at computing the ZF combining vector increases, because M_k and the term K^4 both increase.

3.4.3 Signal reception

- **variable-AS:** Notice that the rows of the k-th user combining vector that correspond to the antennas whose indices are not in the set $\mathcal{D}_k$ are set equal zero. It reduces the complexity to obtain y_k, as described in (3.5), because the BS will use M_k elements of the vectors $\mathbf{v}_k$ and $\mathbf{r}$, instead of M elements, resulting in $3M_k$ flops. As this process is done τ_u times per coherence block, the computational complexity associated to the reception of the information is:

$$C_{\mathrm{SR}}^{\text{variable-AS}} = 3\tau_\mathrm{u} \sum_{k=1}^{K} M_k \text{ [fpcb]} \tag{3.38}$$

- **fixed-AS:** The complexity associated with the signal reception, when employing the fixed-AS scheme, can be obtained from (3.38) by simply replacing M_k with L:

$$C_{\mathrm{SR}}^{\text{fixed-AS}} = 3\tau_\mathrm{u} LK \text{ [fpcb]} \tag{3.39}$$

- **no-S:** The complexity associated with the signal reception, when employing the no-S scheme, can be obtained from (3.38) by simply replacing M_k with M:

$$C_{\mathrm{SR}}^{\text{no-S}} = 3\tau_\mathrm{u} MK \text{ [fpcb]} \tag{3.40}$$

- **multiple-SS:** As $\mathbf{v}_{kn}$ and $\mathbf{r}_n$ are (M/N)-length vectors, obtaining y_{kn}, as described in (3.11), requires M/N complex multiplications. This process is done τ_u times per coherence block. As the n-th subarray serves K_n users, the resulting complexity is $3\tau_\mathrm{u} MK_n/N$ [fpcb]. Recalling that there are N subarrays, the total computational complexity is:

$$C_{\mathrm{SR}}^{\text{multiple-SS}} = 3\tau_\mathrm{u} \frac{M}{N} \sum_{n=1}^{N} K_n \text{ [fpcb]} \tag{3.41}$$

  Notice that $\sum_{n=1}^{N} K_n \geq K$.

- **single-SS:** In the single-SS scheme, each user is attended by only one subarray. Then, $\sum_{n=1}^{N} K_n = K$, and (3.41) can be rewritten as:

$$C_{\mathrm{SR}}^{\text{single-SS}} = 3\tau_\mathrm{u} \frac{M}{N} K \text{ [fpcb]} \tag{3.42}$$

  Notice that there is a further complexity reduction when compared to the multiple-SS scheme.

- **fair-AS:** Notice that the rows of the combining matrix that correspond to the inactive antennas are set equal zero. It reduces the complexity to obtain y_k, because the BS will use M_s elements of the vectors $\mathbf{v}_k$ and $\mathbf{r}$, instead of M elements, resulting in $3M_\mathrm{s}$ flops. As this process is done τ_u times per coherence block, the computational complexity associated to the reception of the information is:

$$C_{\mathrm{SR}}^{\text{fair-AS}} = 3\tau_\mathrm{u} M_\mathrm{s} K \text{ [fpcb]} \tag{3.43}$$

3.4.4 Antenna/subarray selection

- **fixed-AS:** Obtaining θ_{mk} in (3.2) requires MK complex multiplications, to compute all the terms $|\widehat{h}_{mk}|^2$, $m = 1, \ldots, M$, $k = 1, \ldots, K$, plus MK real divisions, summing $4MK$ [fpcb]. The vector $\boldsymbol{\theta}_k$ must then be sorted, so that the antennas corresponding to the first L antennas of the sorted vector are selected for each user. As $\boldsymbol{\theta}_k$ has length M and there are K users, the associated complexity is $MK\log(M)$ [fpcb]. Thus, the complexity associated to the antenna selection itself is:

$$C_{\mathrm{sel}}^{\text{fixed-AS}} = MK(\log(M) + 4) \text{ [fpcb]} \tag{3.44}$$

- **variable-AS:** Obtaining Z_k, given by (3.9), requires M complex multiplications to obtain $\{|\widehat{h}_{1k}|^2, \ldots, |\widehat{h}_{Mk}|^2\}$. Considering that there are K users, the total complexity is $3MK$ [fpcb]. Then, obtaining $\{\boldsymbol{\theta}_1, \ldots, \boldsymbol{\theta}_K\}$ requires only MK real divisions, as all the modulus have already been computed. Sorting the vector $\boldsymbol{\theta}_k$ has a complexity of $MK\log(M)$ [fpcb]. Finally,

$$C_{\mathrm{sel}}^{\text{variable-AS}} = MK(\log(M) + 4) \text{ [fpcb]} \tag{3.45}$$

- **multiple-SS:** To obtain Z_{kn}, given by (3.15), the BS does M/N complex multiplications to obtain $|\widehat{h}_{mk}|^2$, $m \in \mathcal{M}_n$. As there are N subarrays and K users, it results in a complexity of $3MK$ [fpcb]. Given the values of Z_{kn}, obtaining Z_k (when employing multiple-SS scheme) according to (3.24) does not involve any further multiplication or division. Finally, obtaining $\boldsymbol{\theta}_k$, $k \in \{1, \ldots, K\}$, according to (3.14), requires only NK real divisions, while sorting this vector requires $\frac{M}{N}K\log(\frac{M}{N})$ [fpcb]. Thus,

$$C_{\mathrm{sel}}^{\text{multiple-SS}} = \left(\frac{M}{N}\log\left(\frac{M}{N}\right) + 3M + N\right) K \text{ [fpcb]} \tag{3.46}$$

- **single-SS:** The difference from the selection complexity of multiple-SS is that just the first iteration of the sorting algorithm must be executed. Thus, sorting the vectors $\boldsymbol{\theta}_k$, $k \in \{1, \ldots, K\}$ requires $\frac{M}{N}K$ [fpcb], so that,

$$C_{\mathrm{sel}}^{\text{single-SS}} = \left(\frac{M}{N} + 3M + N\right) K \text{ [fpcb]} \tag{3.47}$$

- **fair-AS:** Obtaining θ_{mk} in (3.28) requires MK complex multiplications, to compute all the terms $|\widehat{h}_{mk}|^2$, $m = 1, \ldots, M$, $k = 1, \ldots, K$, corresponding to $3MK$ [fpcb]. In the stage A of the algorithm, the vector $\boldsymbol{\theta}_k$ must then be sorted, so that the antennas corresponding to the first $\lfloor M_\mathrm{s}/K \rfloor$ antennas of the sorted vector are selected for each user. As $\boldsymbol{\theta}_k$ has length M and there are K users, the associated complexity is $MK\log(M)$ [fpcb]. During the stage B, in order to sort the vector $\boldsymbol{\rho}$, $M\log(M)$ [fpcb] will be required, in the worst case. Thus, the complexity associated to the antenna selection itself is:

$$C_{\mathrm{sel}}^{\text{fair-AS}} = M(K+1)\log(M) + 3MK \text{ [fpcb]} \tag{3.48}$$

3.4.5 Precision detection

- **multiple-SS:** To obtain δ_k, as in (3.20), N_k real multiplications are required. As there are K users, the resulting complexity, in [fpcb], is $\sum_{k=1}^{K} N_k$, which is equal to $\sum_{n=1}^{N} K_n$. Multiplying θ_{nk} by y_{kn}, as in (3.16), costs 1 complex multiplication. It is done for the N_k subarrays that serve k-th user. Then, the sum obtained in (3.16) is divided by δ_k, which costs 1 complex division. It is done for the K users, τ_u times per coherence block, resulting in $\tau_\mathrm{u} \sum_{k=1}^{K} (3N_k + 7) = 7\tau_\mathrm{u}K + 3\tau_\mathrm{u} \sum_{k=1}^{K} N_k$ [fpcb]. Thus, the total precision detector additional complexity is:

$$C_{\mathrm{PD}}^{\text{multiple-SS}} = 7\tau_\mathrm{u}K + (1 + 3\tau_\mathrm{u}) \sum_{n=1}^{N} K_n \text{ [fpcb]} \tag{3.49}$$

3.5 SE and EE Definitions and Power Consumption Model

The ergodic spectral efficiency is defined by (BJöRNSON et al., 2017):

$$\mathrm{SE} = \frac{\tau_\mathrm{u}}{\tau_\mathrm{c}} \sum_{k=1}^{K} \mathbb{E}\{\log_2(1 + \gamma_k)\} \tag{3.50}$$

where γ_k is the SINR of the k-th user, given by (3.6), when employing no-S, fixed-AS or variable-AS strategies, or given by (3.22) or (3.26) when employing multiple-SS or single-SS, respectively.

The energy efficiency of a cellular network is defined in (BJöRNSON et al., 2017) as the number of bits that can be reliably transmitted per unit of energy. Thus, its unit is $\left[\frac{\text{bit}}{\text{J}}\right]$, which is the same as the throughput per unit of power $\left[\frac{\text{bit/s}}{\text{W}}\right]$:

$$\mathrm{EE} = \frac{B \cdot \mathrm{SE}}{P_{\mathrm{tot}}} = \frac{B \cdot \mathrm{SE}}{P_{\mathrm{TX}}^{\mathrm{UL}} + P_{\mathrm{TX}}^{\mathrm{tr}} + P_{\mathrm{CP}}} \tag{3.51}$$

Table 3.1 – Complexity of the proposed selection schemes

Channel estimation [fpcb]:	
C_{CE}	$3\tau_{\text{p}}MK$
Computation of the ZF combining vectors [fpcb]:	
$C_{\text{C-UL}}^{\text{no-S}}$	$K^3 + \frac{9}{2}MK^2 + \frac{3}{2}(M+4)K$
$C_{\text{C-UL}}^{\text{fixed-AS}}$	$K^4 + \frac{3}{2}LK^3 + \frac{3}{2}(3L+4)K^2$
$C_{\text{C-UL}}^{\text{variable-AS}}$	$K^4 + 6K^2 + \frac{3}{2}(K+3)K\sum_{k=1}^{K} M_k$
$C_{\text{C-UL}}^{\text{multiple-SS}}$	$NK^3 + \frac{3}{2}MK^2 + \frac{3}{2}(M+4N)K + MK\sum_{n=1}^{N} K_n$
$C_{\text{C-UL}}^{\text{single-SS}}$	$NK^3 + \frac{5}{2}MK^2 + \frac{3}{2}(M+4N)K$
$C_{\text{C-UL}}^{\text{fair-AS}}$	$K^3 + \frac{9}{2}M_{\text{s}}K^2 + \frac{3}{2}(M_{\text{s}}+4)K$
Signal reception [fpcb]:	
$C_{\text{SR}}^{\text{no-S}}$	$3\tau_{\text{u}}MK$
$C_{\text{SR}}^{\text{fixed-AS}}$	$3\tau_{\text{u}}LK$
$C_{\text{SR}}^{\text{variable-AS}}$	$3\tau_{\text{u}}\sum_{k=1}^{K} M_k$
$C_{\text{SR}}^{\text{multiple-SS}}$	$3\tau_{\text{u}}\frac{M}{N}\sum_{n=1}^{N} K_n$
$C_{\text{SR}}^{\text{single-SS}}$	$3\tau_{\text{u}}\frac{M}{N}K$
$C_{\text{SR}}^{\text{fair-AS}}$	$3\tau_{\text{u}}M_{\text{s}}K$
Antenna or subarray selection [fpcb]:	
$C_{\text{sel}}^{\text{fixed-AS}}$	$MK(\log(M)+4)$
$C_{\text{sel}}^{\text{variable-AS}}$	$MK(\log(M)+4)$
$C_{\text{sel}}^{\text{multiple-SS}}$	$\left(\frac{M}{N}\log\left(\frac{M}{N}\right)+3M+N\right)K$
$C_{\text{sel}}^{\text{single-SS}}$	$\left(\frac{M}{N}\log\left(\frac{M}{N}\right)+3M+N\right)K$
$C_{\text{sel}}^{\text{fair-AS}}$	$M(K+1)\log(M)+3MK$
Precision detector [fpcb]:	
$C_{\text{PD}}^{\text{multiple-SS}}$	$7\tau_{\text{u}}K + (1+3\tau_{\text{u}})\sum\limits_{n=1}^{N} K_n$

Table 3.2 – Total complexity associated to each of the proposed selection schemes

Total complexity [fps]:	
$C_{\text{tot}}^{\text{no-S}}$	$\frac{B}{\tau_c}(C_{\text{CE}} + C_{\text{C-UL}}^{\text{no-S}} + C_{\text{SR}}^{\text{no-S}})$
$C_{\text{tot}}^{\text{fixed-AS}}$	$\frac{B}{\tau_c}(C_{\text{CE}} + C_{\text{C-UL}}^{\text{fixed-AS}} + C_{\text{SR}}^{\text{fixed-AS}} + C_{\text{sel}}^{\text{fixed-AS}})$
$C_{\text{tot}}^{\text{variable-AS}}$	$\frac{B}{\tau_c}(C_{\text{CE}} + C_{\text{C-UL}}^{\text{variable-AS}} + C_{\text{SR}}^{\text{variable-AS}} + C_{\text{sel}}^{\text{variable-AS}})$
$C_{\text{tot}}^{\text{multiple-SS}}$	$\frac{B}{\tau_c}(C_{\text{CE}} + C_{\text{C-UL}}^{\text{multiple-SS}} + C_{\text{SR}}^{\text{multiple-SS}} + C_{\text{sel}}^{\text{multiple-SS}} + C_{\text{PD}}^{\text{multiple-SS}})$
$C_{\text{tot}}^{\text{single-SS}}$	$\frac{B}{\tau_c}(C_{\text{CE}} + C_{\text{C-UL}}^{\text{single-SS}} + C_{\text{SR}}^{\text{single-SS}} + C_{\text{sel}}^{\text{single-SS}})$
$C_{\text{tot}}^{\text{fair-AS}}$	$\frac{B}{\tau_c}(C_{\text{CE}} + C_{\text{C-UL}}^{\text{fair-AS}} + C_{\text{SR}}^{\text{fair-AS}} + C_{\text{sel}}^{\text{fair-AS}})$

where the denominator contains the total power consumption (P_{tot}), including all power consumption terms required to make the wireless communication system operational. Being η^{UL} the power amplifier efficiency at the BS, the term

$$P_{\text{TX}}^{\text{UL}} = \frac{\tau_u}{\tau_c}\frac{1}{\eta^{\text{UL}}}\sum_{k=1}^{K} p_k \tag{3.52}$$

refers to the UL power consumed for data transmission, while

$$P_{\text{TX}}^{\text{tr}} = \frac{\tau_p}{\tau_c}\frac{1}{\eta^{\text{UL}}} K p_p \tag{3.53}$$

accounts for the total power consumed by the power amplifiers during the UL pilot transmission. Based on (UBIALI; ABRÃO, 2020; BJöRNSON et al., 2017), a detailed model for the circuit power consumption is:

$$P_{\text{CP}} = P_{\text{FIX}} + P_{\text{TC}} + P_{\text{CE/SP}} + P_{\text{C/D}} + P_{\text{BH}} \tag{3.54}$$

The fixed power consumption (P_{FIX}) is a constant quantity that accounts for the power consumption required for site-cooling, control signaling and load-independent power of backhaul infrastructure and baseband processors (BJöRNSON et al., 2017; Marinello et al., 2019). The transceiver chains power consumption (P_{TC}) involves the power consumed by the BS local oscillator (P_{LO}), the circuit components (converters, mixers and filters) of each BS antenna (P_{BS}) and the the circuit components (mixers, filters, amplifiers and oscillator) of each single-antenna user (P_{UE}), as described by:

$$P_{\text{TC}} = P_{\text{LO}} + M_{\text{act}} P_{\text{BS}} + K P_{\text{UE}} \tag{3.55}$$

The channel estimation and signal processing power consumption ($P_{\text{CE/SP}}$) can be obtained by simply dividing the total complexity in flops per second [fps] by the

computational efficiency at the BS (L_{BS}), which represents the number of flops per Joule of energy[4].

Finally, being $\mathcal{P}_{\mathrm{COD}}$, $\mathcal{P}_{\mathrm{DEC}}$ and $\mathcal{P}_{\mathrm{BT}}$ the coding, decoding and backhaul traffic power densities, respectively, given in $\left[\frac{\mathrm{watt}}{\mathrm{bit/s}}\right]$, the channel coding and decoding power consumption can be expressed as:

$$P_{\mathrm{C/D}} = B \cdot \mathrm{SE} \cdot (\mathcal{P}_{\mathrm{COD}} + \mathcal{P}_{\mathrm{DEC}}) \tag{3.56}$$

The load-dependent backhaul power consumption, necessary for the data transmission between the BS and the core network, is modeled as

$$P_{\mathrm{BH}} = B \cdot \mathrm{SE} \cdot \mathcal{P}_{\mathrm{BT}} \tag{3.57}$$

[4]A complexity of C flops per coherence block results in a power consumption of $\frac{BC}{\tau_{\mathrm{c}} L_{\mathrm{BS}}}$, where L_{BS} is the computational efficiency, representing the number of flops per Joule of energy, and consequently $\frac{C}{L_{\mathrm{BS}}}$ represents the energy consumption per coherence block.

4 Energy Efficiency in XL-MIMO Systems: Numerical Results

This chapter presents numerical results based on Monte-Carlo simulations (MCS) in order to demonstrate that the antenna and subarray selection algorithms proposed in Chapter 3 provide an EE increase while reducing considerably the computational complexity and the power consumption in XL-MIMO systems. From these results, we can see the advantages of appropriately selecting the antennas subset (fixed-AS, variable-AS, multiple-SS and single-SS schemes) against utilizing the whole antenna array to serve all users at the same time (no-S scheme). All UEs utilize the same transmit power, *i.e.*, $p_1, \ldots, p_K = p_{\text{UL}}$. Table 4.1 contains a list of the main deployed parameter values, similar to those adopted in (BJöRNSON et al., 2017; UBIALI; ABRÃO, 2020; Marinello et al., 2019) and (Björnson et al., 2015).

In the MCS, the antenna array contains $M = 1000$ antenna elements and the distance between the antennas is $d = \lambda/2$, where λ is the wavelength. The borders of the cell are defined by $\text{x}_{\text{min}} = 20\lambda$, $\text{x}_{\text{max}} = 200\lambda$, $\text{y}_{\text{min}} = -600\lambda$ and $\text{y}_{\text{max}} = 600\lambda$. Although the position of the users (and consequently the pathloss), the short-scale fading and the VRs are random variables, the numerical results represent an average over 1000 independent realizations, therefore they are statistically relevant.

In all simulations, $S = 50$ scatterers and $r_s = 5$ m (radium for all scatterers) have been adopted. Under these conditions, one can obtain information about the length of the visibility regions associated to the users and the scatterers, via numerical simulation. For example, the BS-VR of a scatterer contains, on average, 259.9 antennas; each antenna is inside the BS-VR of 12.9 scatterers, on average; and each user is inside the UE-VR of 2.0 scatterers, on average. Further information is presented in Table 4.2.

4.1 Influence of the algorithm parameters on the energy efficiency

In this section, numerical results are presented to show how the parameters L, z_0 and N influence the number of active antennas, the power consumption, the complexity, the throughput and the energy efficiency. All results refer to an example scenario of $K = 32$ users. Subsection 4.1.1 compares the performance of fixed-AS and the no-S strategies, as a function of the number of antennas selected per user L, which is the parameter of Algorithm 3.1. Subsection 4.1.2 compares the performance of variable-AS and multiple-SS to the performance of no-S, and the effect of the z_0 choices, which are parameters of the

Table 4.1 – System and Channel Parameter Values

Parameter	**Value**
Pathloss attenuation exponent: γ	2.5
Median channel gain at a distance of 1 m: β_0	$2.95 \cdot 10^{-4}$
$[x_{min}, x_{max}]$	$[20\lambda, 200\lambda]$
$[y_{min}, y_{max}]$	$[-600\lambda, 600\lambda]$
Wavelength: λ	5 cm
Antenna separation: d	$\lambda/2$
Number of BS antennas (ULA): M	1000
Number of scatterers: S	50
Radium of the UE-VRs: r_s	5 m
Probability of occurance of the LoS-BS-VRs: w	0.75
Number of mobile users: K	$\{4; 8; 16; 32; 64; 100\}$
Transmission bandwidth: B	20 MHz
Channel coherence bandwidth: B_C	100 kHz
Channel coherence time: T_C	2 ms
Total UL noise power: σ_n^2	$-$ 100 dBm
UL pilot transmit power per user (EPA): p_p	0.1 W
UL data transmit power per user (EPA): p_{UL}	0.1 W
Power amplifier efficiency at the BSs: η^{UL}	0.5
Computational efficiency at the BS: L_{BS}	75 $\left[\frac{\text{Gflop/s}}{\text{W}}\right]$
Fixed power consumption: P_{FIX}	10 W
Power consumed by local oscillators at BS: P_{LO}	1.0 W
Power consumed by circuit components at BS: P_{BS}	0.5 W
Power consumed by circuit components at UE: P_{UE}	0.2 W
Power density for coding of data signals: $\mathcal{P}_{COD}$	0.1 $\left[\frac{\text{W}}{\text{Gbit/s}}\right]$
Power density for decoding of data signals: $\mathcal{P}_{DEC}$	0.8 $\left[\frac{\text{W}}{\text{Gbit/s}}\right]$
Power density for backhaul traffic: $\mathcal{P}_{BT}$	0.25 $\left[\frac{\text{W}}{\text{Gbit/s}}\right]$
Number of Monte-Carlo realizations: $\mathcal{T}$	1000

algorithms 3.2 and 3.3, on the performance metrics. Finally, subsection 4.1.3 compares no-S, multiple-SS and single-SS, and the effect of the N choices, while subsection 4.1.4 shows the performance of the fair-AS scheme as a function on the number of active antennas, which is an entry of Algorithm 3.5.

4.1.1 no-S x fixed-AS

Figure 4.1 compares the no-S and fixed-AS strategies in terms of the average number of selected antennas per user ($\mathbb{E}\{M_k\} = M_k = L$) and the average number of active antennas ($\mathbb{E}\{M_{act}\}$), as a function of the value adopted for the parameter L of Algorithm 3.1. To avoid problems with the matrix inversion when obtaining the ZF combining vectors, L must be at least 32 antennas. When fixed-AS is set to select

Table 4.2 – Average VR size conditions resulting from the adopted XL-MIMO channel parameters

# antennas inside the BS-VR of a scatterer:	259.9
# antennas seen by each user via LoS propagation:	193.9
# antennas seen by each user via NLoS propagation:	406.2
# antennas seen by each user via LoS or NLoS propagation:	520.1
% users that don't see any antenna via LoS propagation:	49.5%
% users that don't see any antenna via NLoS propagation:	25.9%
% users don't see any antenna via neither LoS nor NLoS:	13.6%

less than one hundred antennas to detect the signal sent by each user through receive combining, the number of active antennas can be considerably reduced. As a consequence, the computational complexity and the total power consumption decrease, as Figures 4.4 and 4.5 show.

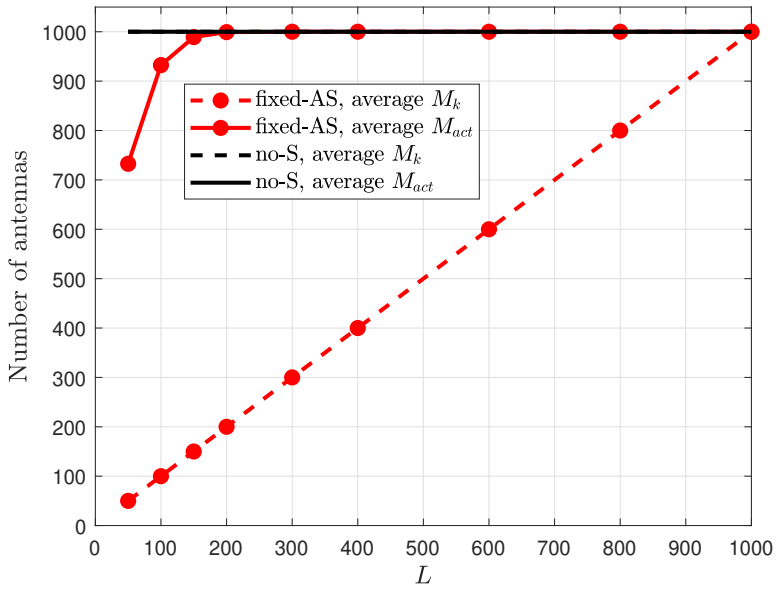

Figure 4.1 – Comparison between no-S and fixed-AS, regarding the average number of selected antennas per user and the average number of active antennas, as a function of the parameter L of Algorithm 3.1; $K = 32$; ZF combiner

Figure 4.2 shows the behavior of the average signal, interference and noise power after the combiner, according to the value of L. The average desired signal power (after the combiner) is close to 20 dBm, which is the UL transmit power of each user (0.1 W). The little difference is due to the channel estimation error. Conservating the signal power is a feature of the ZF combiner. The ZF combiner is more effective at mitigating the

interference and noise power when the number of antennas is high. Thus, when selecting less than 300 antennas for each user ($L < 300$), the interference and noise powers considerably increase. However, as long as the antennas are selected properly, the throughput does not deteriorate at all, as Figure 4.3 shows.

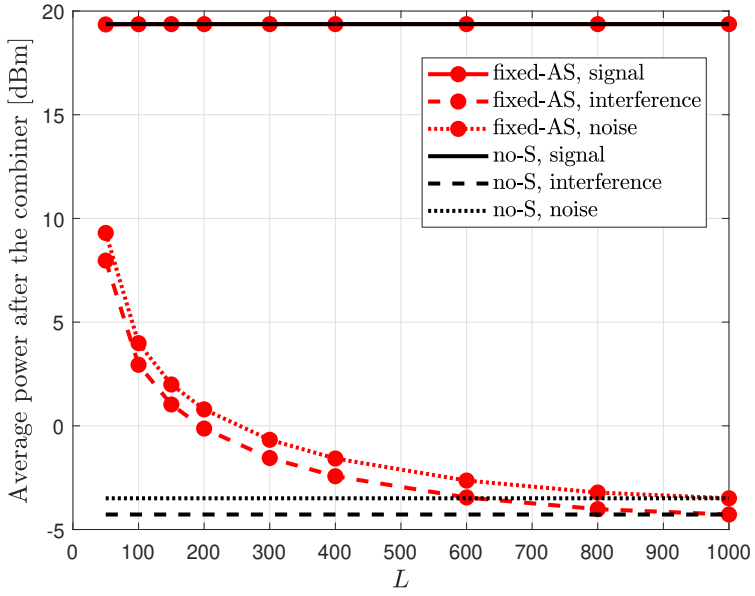

Figure 4.2 – Comparison between no-S and fixed-AS, regarding the average signal, interference and noise power, after the combiner, as a function of parameter L of Algorithm 3.1; $K = 32$; ZF combiner

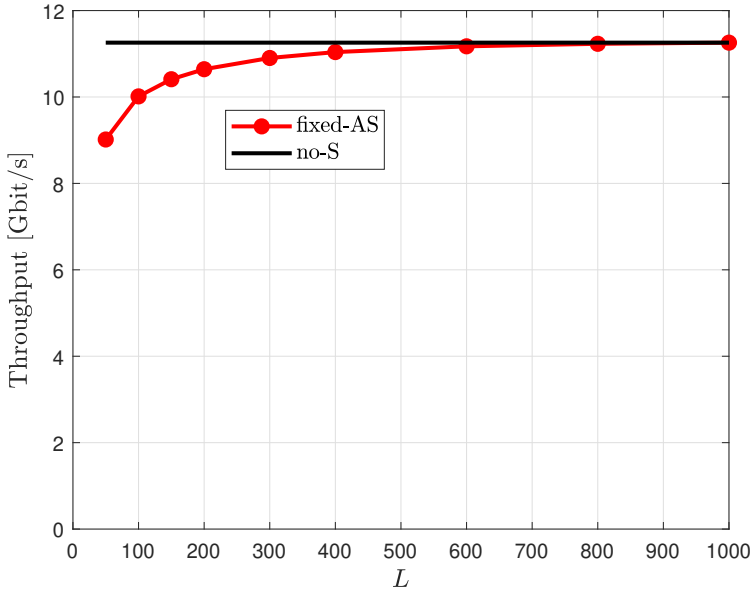

Figure 4.3 – Comparison between no-S and fixed-AS, regarding the throughput, as a function of the parameter L of Algorithm 3.1; $K = 32$; ZF combiner.

The most significant term in the total complexity is $C_{\text{C-UL}}$, which designates the

complexity of computing the ZF combining vectors. When employing fixed-AS or variable-AS, the matrix to be inverted is smaller than when employing no-S ($M_k \times K$ instead of $M \times K$). However, K different matrices need to be inverted to compute the combining vector of the K users. As a consequence, the total complexity behaves as shown in Figure 4.4: depending on the number of antennas that will be selected (L), the resulting complexity may be lower or higher than when not employing any selection scheme (no-S strategy). The complexity increase is the reason why the power consumption may also increase depending on the value of L (Figure 4.5).

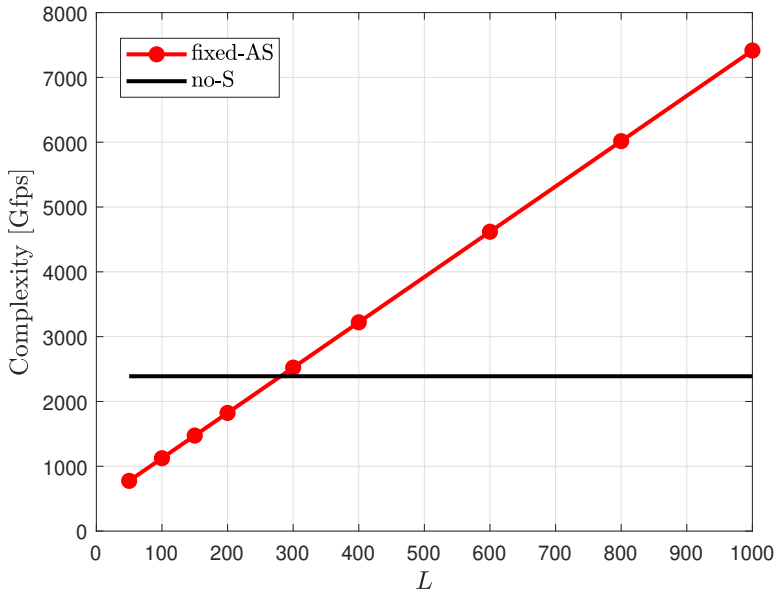

Figure 4.4 – Comparison between no-S and fixed-AS, regarding the complexity, as a function of the parameter L of Algorithm 3.1; $K = 32$; ZF combiner.

Finally, Figure 4.6 shows the dependency of the EE on L. Notice that, for $K = 32$ users, the EE can be improved by choosing an appropriate number of antennas to detect the signal sent by each user. From the left side graphic, among the different tested values of L, $L = 50$ is the best choice regarding the EE: when compared to the no-S strategy, the EE raises from 19.9 Mbit/J to 21.9 Mbit/J (an increase of 10.2%). On the other side, the throughput drops from 11.3 Gbit/s to 9.0 Gbit/s (a decrease of 20.4%). However, there is a huge complexity reduction of 67.6% (from 2389 Gfps to 775 Gfps), and the power consumption also decreases considerably: from 57.5 dBm to 56.1 dBm (27.6%). According to the right side graphic of Figure 4.6 we can see that the optimal value for L is not necessarily K. For $K = 32$, for example, the EE is maximized when $L = 38$.

4.1.2 no-S x variable-AS x multiple-SS

When employing the variable-AS or the multiple-SS schemes, the number of selected antennas is not the same for all the users, unlike the fixed-AS scheme. Thus, variable-AS

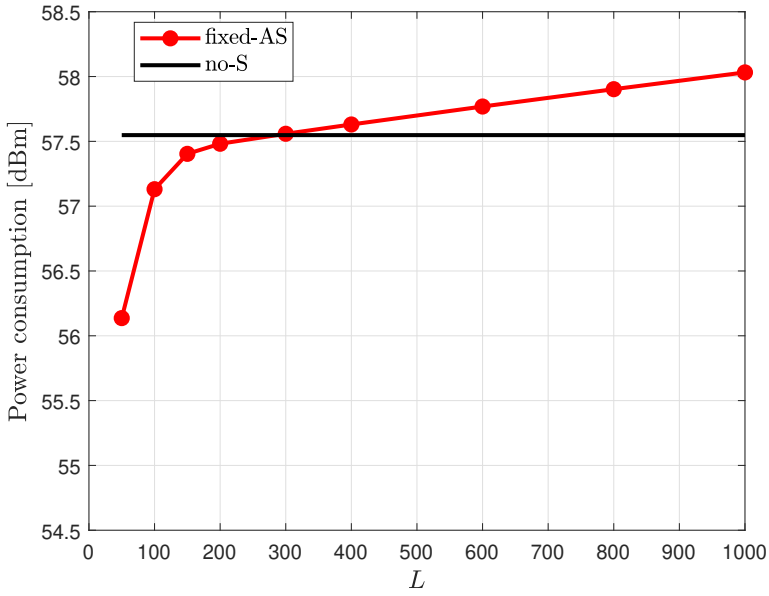

Figure 4.5 – Comparison between no-S and fixed-AS, regarding the power consumption, as a function of the parameter L of Algorithm 3.1; $K = 32$; ZF combiner.

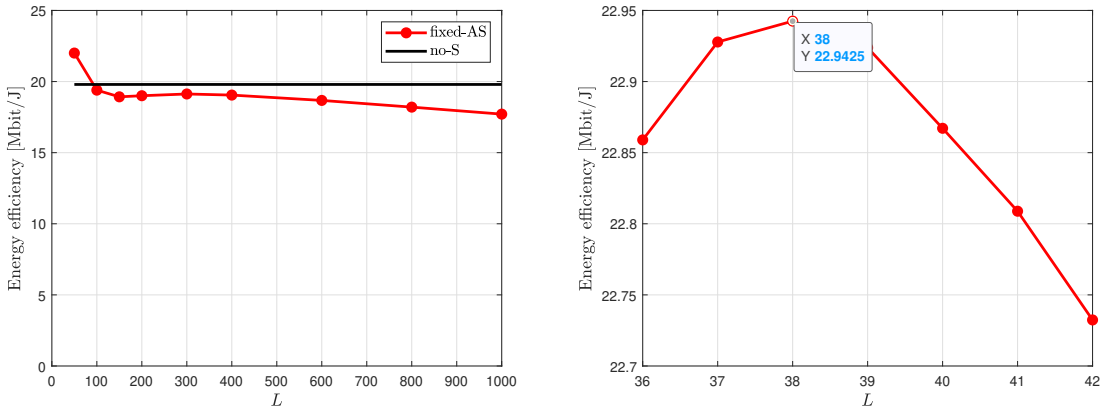

Figure 4.6 – Comparison between no-S and fixed-AS, regarding the energy efficiency, as a function of the parameter L of Algorithm 3.1; $K = 32$; ZF combiner.

and multiple-SS can personalize the number of selected antennas for a given user according to its channel profile. For example, if the energy coming from an individual user signal is concentrated over a small portion of the array, the schemes are capable of selecting only a few antennas, being more effective at reducing the number of active antennas while not considerably compromising the throughput. Consequently, they are expected to bring higher EE improvements than fixed-AS.

Figure 4.7 shows the relation between the parameter z_0 and $\mathbb{E}\{M_k\}$, as well as $\mathbb{E}\{M_{\text{act}}\}$, considering four different cases: no-S, variable-AS, multiple-SS with $N = 5$ subarrays and multiple-SS with $N = 25$ subarrays. The bigger the number of subarrays (N), the smaller the number of active antennas. The maximum possible number of subarrays is $N = M$, where the multiple-SS scheme converges to the variable-AS solution. On the

other side, dividing the antenna array into many subarrays (for example, $N = 25$) is more likely to deteriorate the throughput than if it was divided into only a few subarrays (for example, $N = 5$), as the lower number of antennas per subarray compromises the ZF signal detection as in (3.12) (see Figure 4.8).

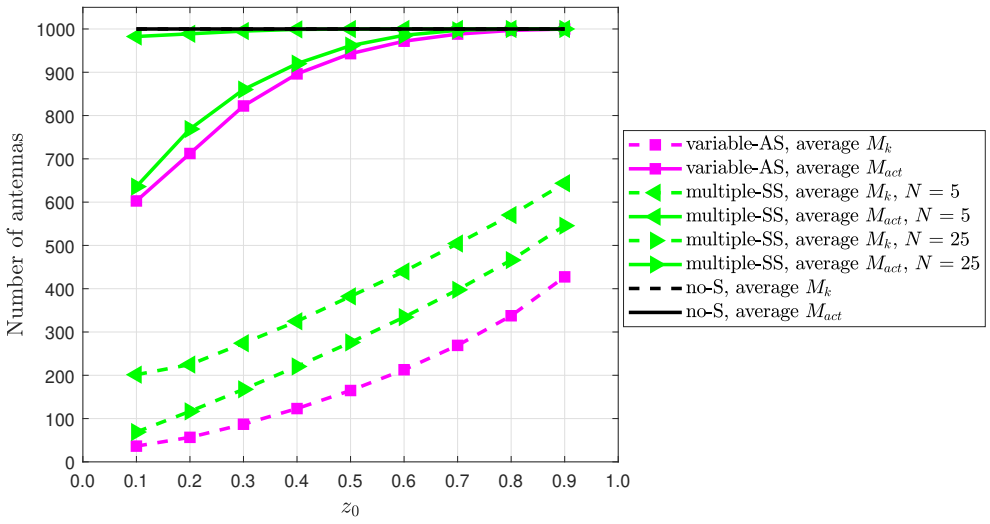

Figure 4.7 – Comparison among no-S, variable-AS and multiple-SS, regarding the average number of selected antennas per user and the average number of active antennas, as a function of the parameter z_0 of the algorithms 3.2 and 3.3; $K = 32$; ZF combiner.

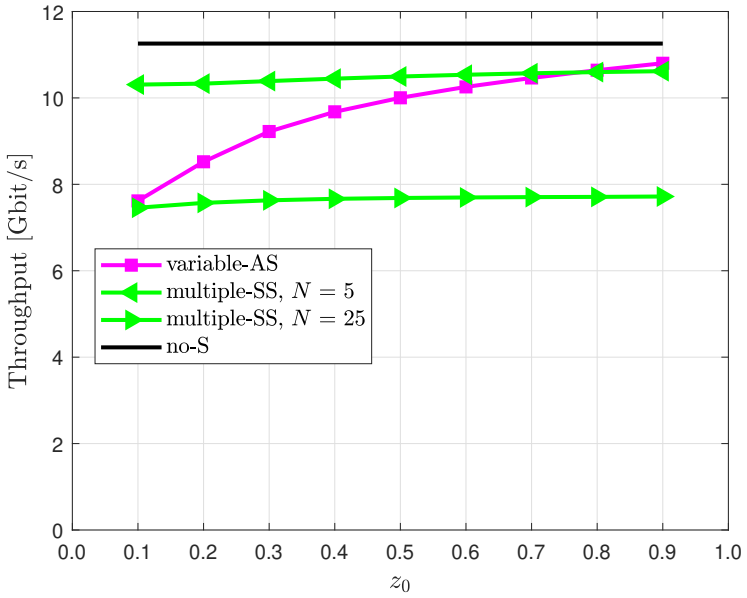

Figure 4.8 – Comparison among no-S, variable-AS and multiple-SS, regarding the throughput, as a function of the parameter z_0 of the algorithms 3.2 and 3.3; $K = 32$; ZF combiner.

Intuitively, increasing z_0 causes both algorithms to select more antennas to par-

ticipate in the signal detection of each user. Consequently, the total number of active antennas and the power consumption also increase with z_0, as depicted in Figures 4.7 and 4.10, respectively, as well as the total complexity (Figure 4.9) and the throughput (Figure 4.8).

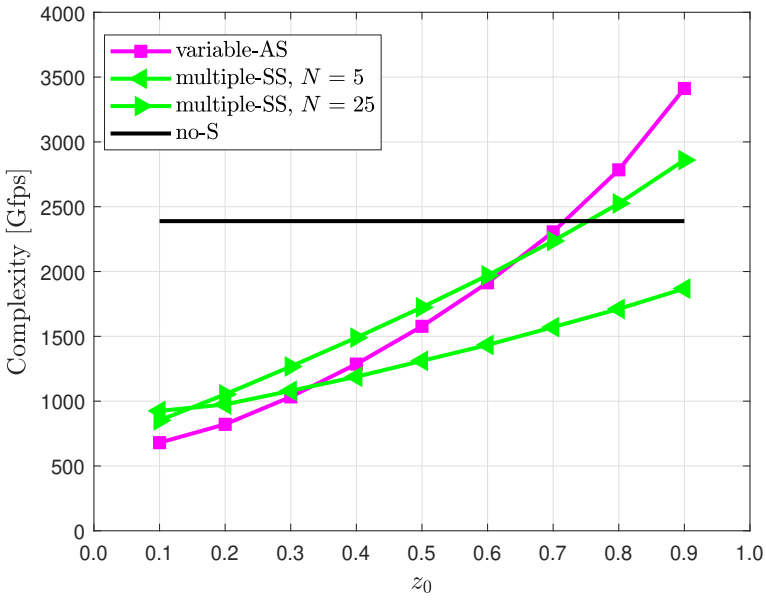

Figure 4.9 – Comparison among no-S, variable-AS and multiple-SS, regarding the complexity, as a function of the parameter z_0 of the algorithms 3.2 and 3.3; $K = 32$; ZF combiner.

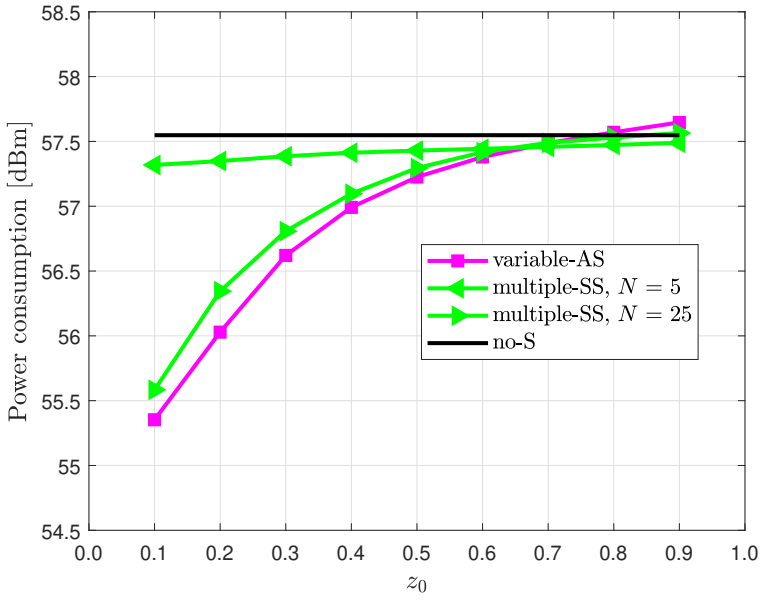

Figure 4.10 – Comparison among no-S, variable-AS and multiple-SS, regarding the total power consumption, as a function of the parameter z_0 of the algorithms 3.2 and 3.3; $K = 32$; ZF combiner.

Figure 4.11 shows the signal, interference and noise power as a function of z_0. See that, when employing multiple-SS, the ZF is more efficient at mitigating the interference if $N = 5$ than if $N = 25$, because the number of antennas per subarray is higher (200 instead of 40). Figure 4.8 shows that one can obtain a higher throughput when M_k is high, *i.e.*, when N is low (multiple-SS scheme) or $z_0 > 0.5$ (variable-AS scheme). However, choosing $z_0 < 0.5$ or a higher number of subarrays leads to a reduction in the number of active antennas without a big throughput decrease, saving energy and consequently improving the EE, according to Figure 4.12.

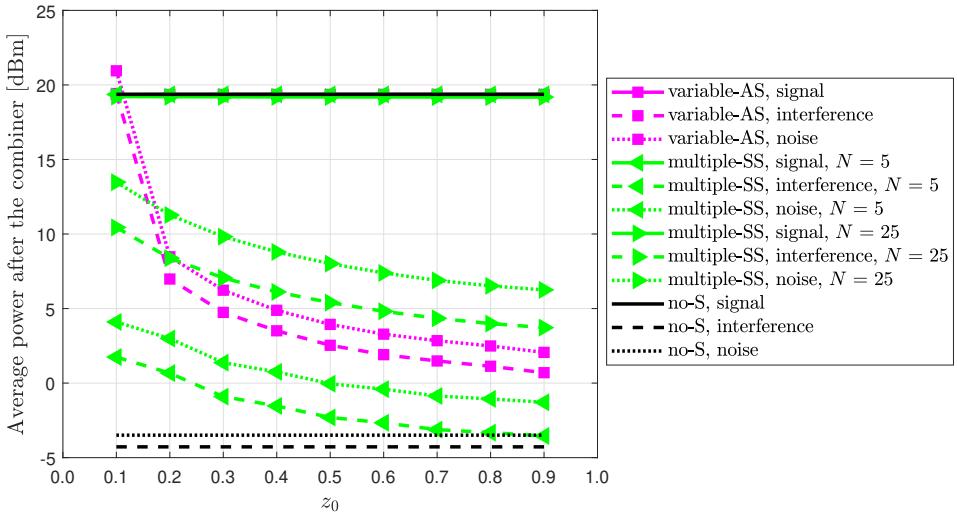

Figure 4.11 – Comparison among no-S, variable-AS and multiple-SS, regarding the average signal, interference and noise power, after the combiner, as a function of the parameter z_0 of the algorithms 3.2 and 3.3; $K = 32$; ZF combiner.

Finally, Figure 4.12 shows the dependency of the EE on z_0. Notice that, for $K = 32$ users, the EE can be improved by choosing an appropriate value for z_0 and N. Among the set of tested values for z_0, $z_0 = 0.1$ is the best choice regarding the EE when employing the variable-AS scheme: comparing to the no-S strategy, the EE raises from 19.9 Mbit/J to 22.9 Mbit/J (an increase of 15.2%). On the other side, the throughput drops from 11.3 Gbit/s to 8.6 Gbit/s (a decrease of 23.9%). However, there is a huge complexity reduction of 71.0% (from 2389 Gfps to 692 Gfps), and the power consumption also decreases considerably: from 57.5 dBm to 55.5 dBm (37.9%).

Among the set of tested values for z_0 and N, $z_0 = 0.1$ and $N = 25$ are the best choice regarding the EE when employing the multiple-SS scheme: when compared to the no-S strategy, the EE raises from 19.9 Mbit/J to 20.6 Mbit/J (an increase of 3.7%). On the other side, the throughput drops from 11.3 Gbit/s to 7.4 Gbit/s (a decrease of 34.4%). However, there is a huge complexity reduction of 64.4% (from 2389 Gfps to 851 Gfps), and the power consumption also decreases considerably: from 57.5 dBm to 55.6 dBm (36.1%).

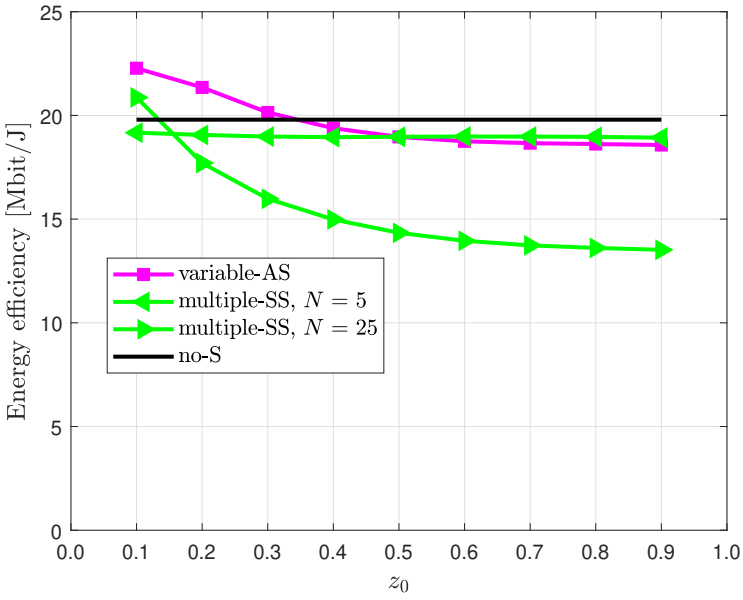

Figure 4.12 – Comparison among no-S, variable-AS and multiple-SS, regarding the energy efficiency, as a function of the parameter z_0 of the algorithms 3.2 and 3.3; $K = 32$; ZF combiner.

4.1.3 no-S x multiple-SS x single-SS

Single-SS scheme is a particular case of multiple-SS where only one subarray is selected for each user. Thus, its results are expected to be similar to the multiple-SS results when taking $z_0 \leq 0.1$. Figure 4.13 shows the influence of N in the average number of selected antennas per user and in the average number of active antennas. Four scenarios are considered: no-S, multiple-SS with $z_0 = 0.1$, multiple-SS with $z_0 = 0.5$ and single-SS.

As we already noticed in Figure 4.7, dividing the antenna array into as much as possible subarrays (recall the limitation $M/N \geq K$ associated to the ZF combining) is important to reduce the number of active antennas and consequently the complexity and the total power consumption, as shown in Figures 4.14 and 4.15, respectively. When employing the multiple-SS scheme, in particular, there is a value of N that minimizes the complexity. Notice that the single-SS scheme is specially good at reducing the complexity and the power consumption. The multiple-SS scheme has similar results when $z_0 = 0.1$.

Figure 4.16 shows the dependency of the average signal, interference and noise power on N. See that increasing the number of subarrays will diminish the number of antennas per subarray, reducing the efficiency of the ZF combining at mitigating the interference, and consequently reducing the throughput, according to Figure 4.17. When employing the multiple-SS scheme, the signals detected at each subarray are combined (with different weights), performining a precision detection, according to (3.16), and consequently the interference and noise powers are smaller than when employing single-SS. However, the throughput gain of multiple-SS compared to single-SS is very slight.

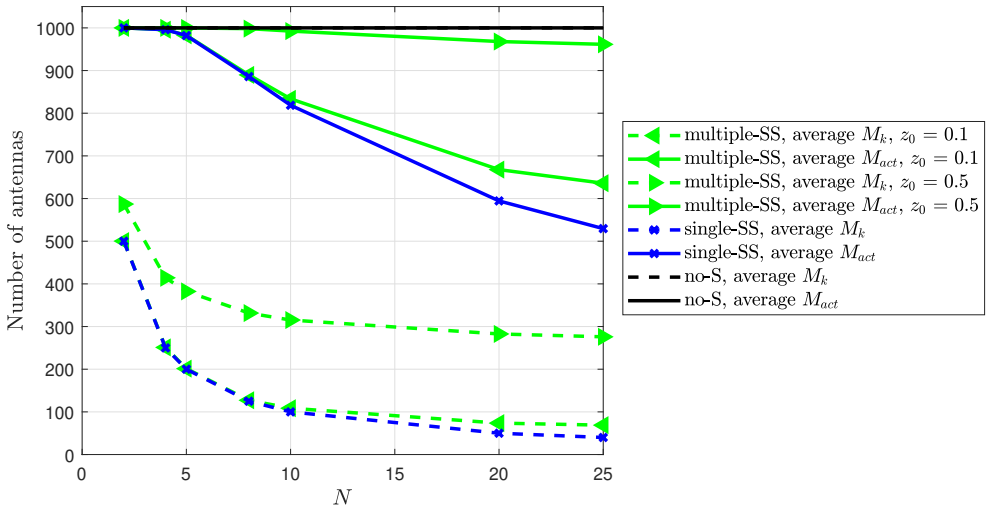

Figure 4.13 – Comparison among no-S, multiple-SS and single-SS, regarding the average number of selected antennas per user and the average number of active antennas, as a function of the parameter N of the algorithms 3.2 and 3.3; $K = 32$; ZF combiner.

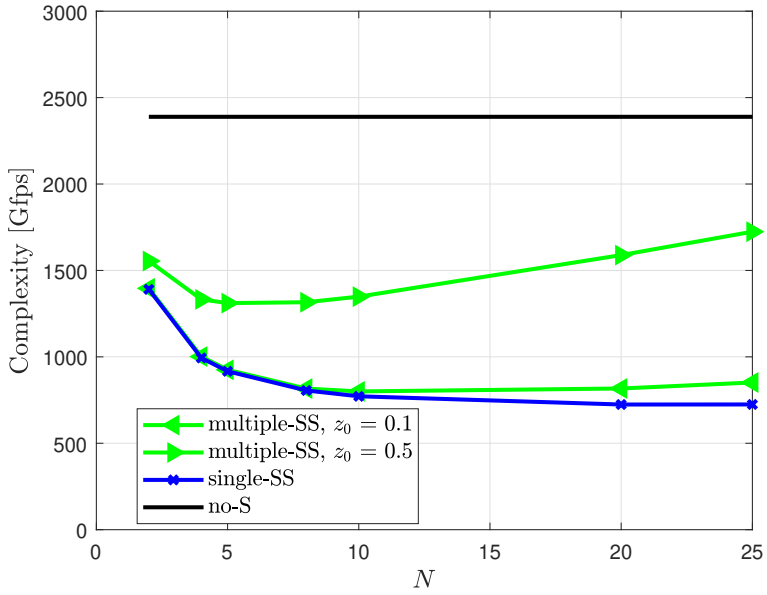

Figure 4.14 – Comparison among no-S, multiple-SS and single-SS, regarding the complexity, as a function of the parameter N of the algorithms 3.2 and 3.3; $K = 32$; ZF combiner.

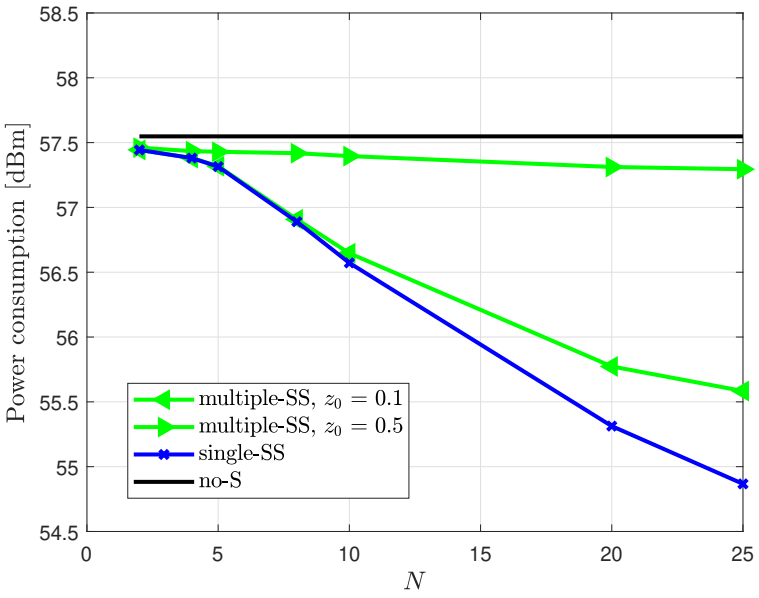

Figure 4.15 – Comparison among no-S, multiple-SS and single-SS, regarding the power consumption, as a function of the parameter N of the algorithms 3.2 and 3.3; $K = 32$; ZF combiner.

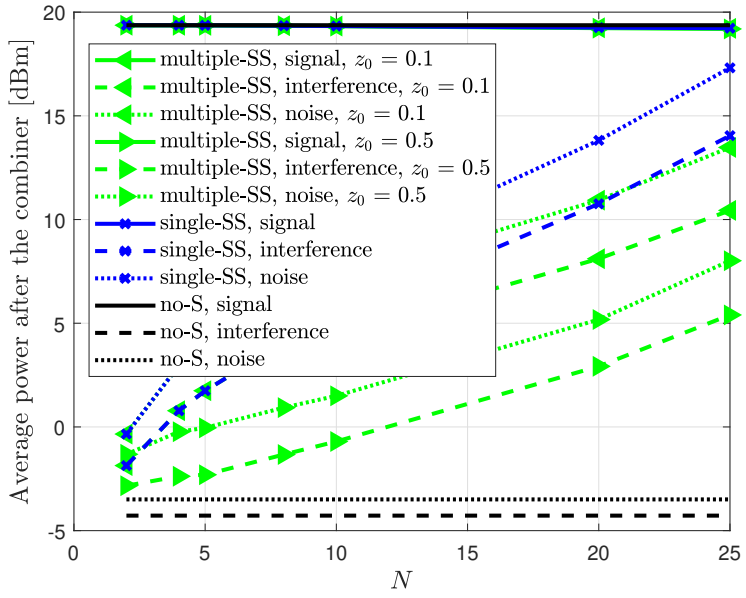

Figure 4.16 – Comparison among no-S, multiple-SS and single-SS, regarding the average signal, interference and noise power, after the combiner, as a function of the parameter N of the algorithms 3.2 and 3.3; $K = 32$; ZF combiner.

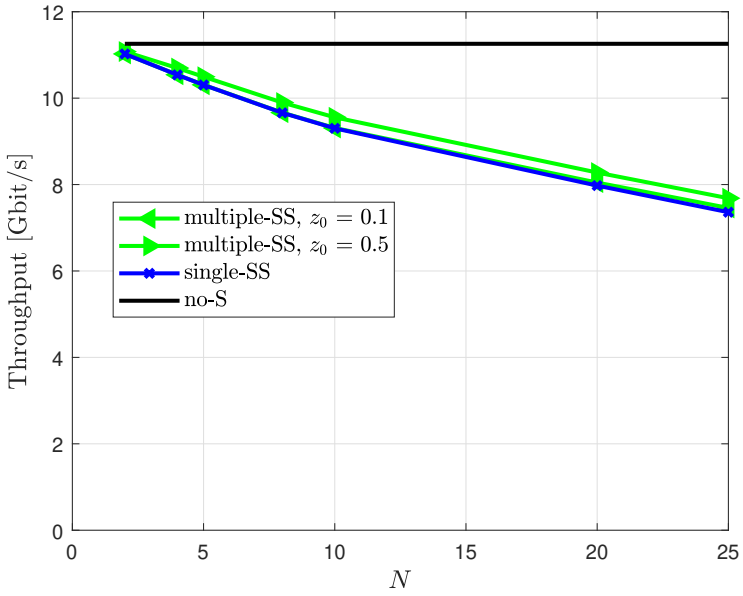

Figure 4.17 – Comparison among no-S, multiple-SS and single-SS, regarding the throughput, as a function of the parameter N of the algorithms 3.2 and 3.3; $K = 32$; ZF combiner.

Finally, Figure 4.18 shows the dependency of the EE on N. Notice that, for $K = 32$ users, the EE can be improved by choosing an appropriate value for z_0 and N. Among the set of tested values for N, $N = 25$ is the best choice regarding the EE when employing single-SS: comparing to the no-S strategy, the EE raises from 19.9 Mbit/J to 24.0 Mbit/J (an increase of 20.9%). On the other side, the throughput drops from 11.3 Gbit/s to 7.3 Gbit/s (a decrease of 35.3%). However, there is a huge complexity reduction of 69.7% (from 2389 Gfps to 725 Gfps), and the power consumption also decreases considerably: from 57.5 dBm to 54.9 dBm (45.8%).

Among the set of tested values for z_0 and N, $z_0 = 0.1$ and $N = 20$ are the best choice regarding the EE when employing the multiple-SS scheme: when compared to the no-S strategy, the EE raises from 19.9 Mbit/J to 21.2 Mbit/J (an increase of 7.1%). On the other side, the throughput drops from 11.3 Gbit/s to 8.0 Gbit/s (a decrease of 29.2%). However, there is a huge complexity reduction of 65.8% (from 2389 Gfps to 817 Gfps), and the power consumption also decreases considerably: from 57.5 dBm to 55.8 dBm (33.1%).

4.1.4 Fair-AS

Here, numerical results are presented to show how the arbitrarily defined number of active antennas (M_s) influences the system performance in terms of complexity, power consumption, throughput and energy efficiency. All results refer to example scenarios of $K = \{8, 32, 100\}$ users. Figure 4.19 shows the dependency of the throughput on M_s and confirms that the higher the number of active antennas, the higher the throughput. On

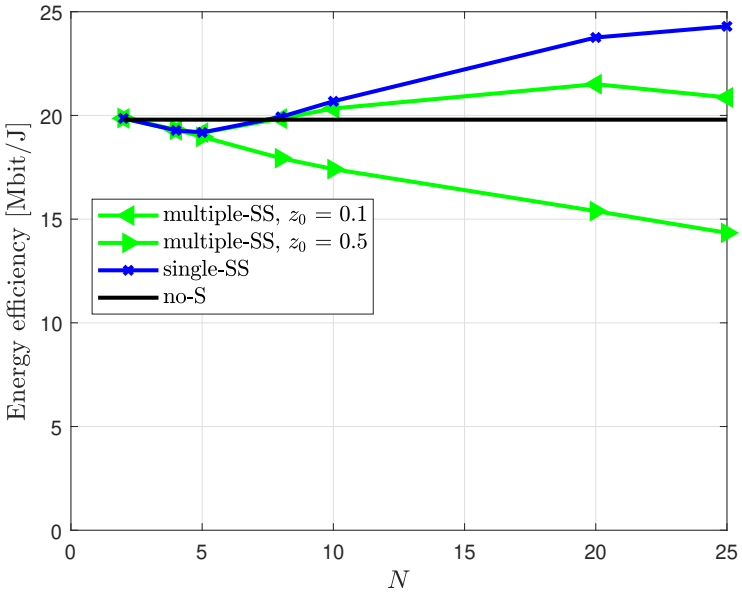

Figure 4.18 – Comparison among no-S, multiple-SS and single-SS, regarding the energy efficiency, as a function of the parameter N of the algorithms 3.2 and 3.3; $K = 32$; ZF combiner.

the other hand, the complexity and the power consumption also increases with M_s, as exposed by Figures 4.20 and 4.21. As a consequence, we can see in Figure 4.22 that there is an optimal value for M_s concerning the EE maximization, and that this value varies depending on the number of users.

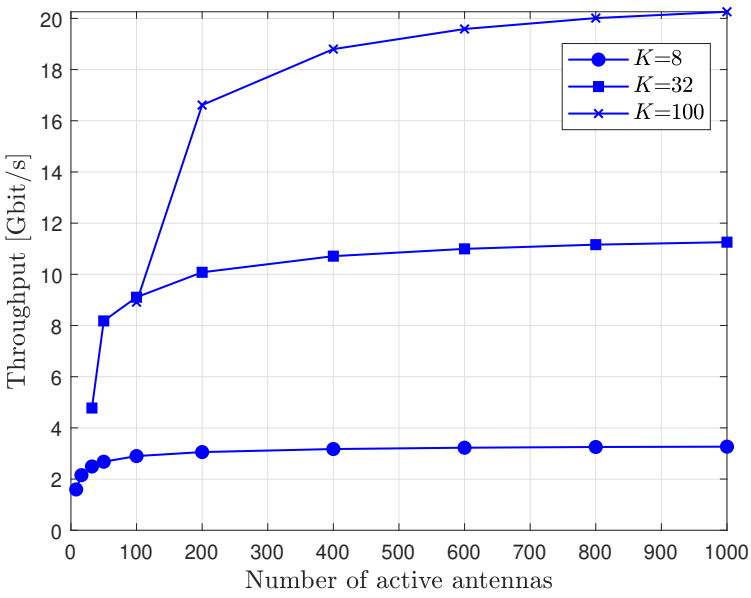

Figure 4.19 – Throughput as a function of the number of active antennas (the values of M_s that were tested are 8, 16, 32, 64, 100, 200, 400, 600, 800 and 1000), for different number of users. ZF combiner is employed.

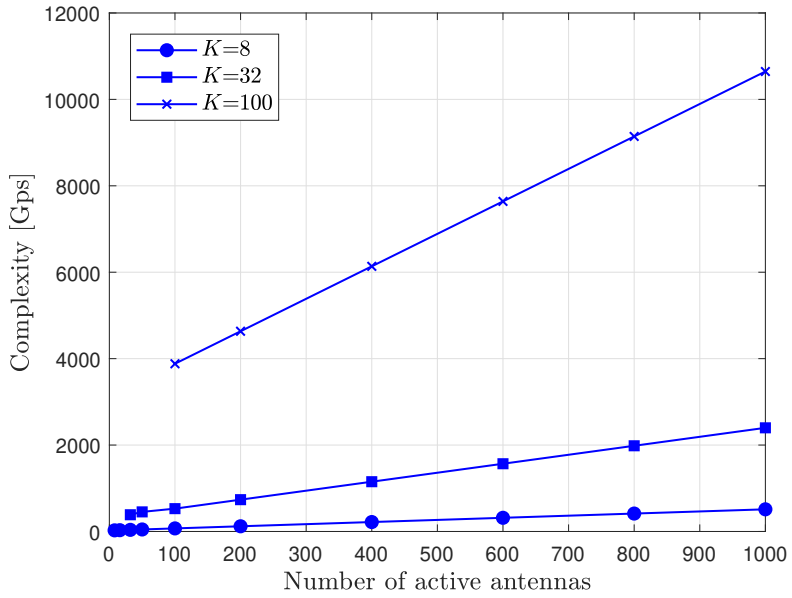

Figure 4.20 – Computational complexity as a function of the number of active antennas (the values of M_s that were tested are 8, 16, 32, 64, 100, 200, 400, 600, 800 and 1000), for different number of users. ZF combiner is employed.

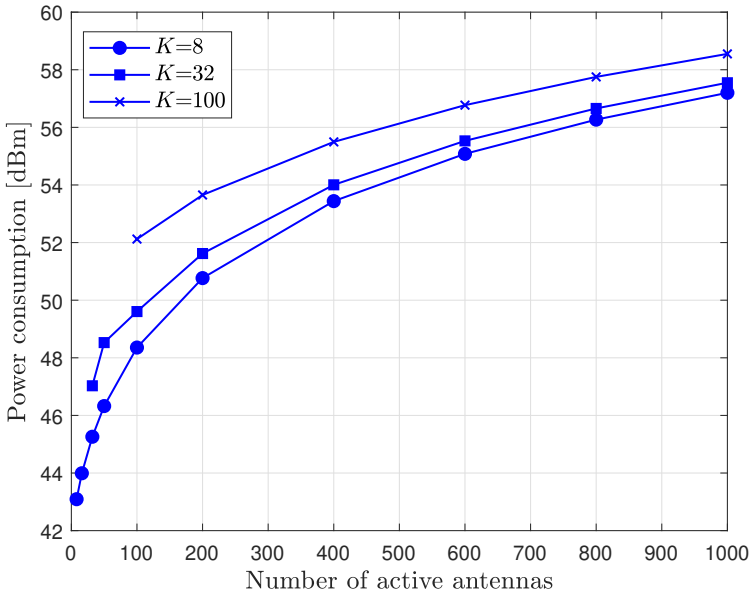

Figure 4.21 – Power consumption as a function of the number of active antennas (the values of M_s that were tested are 8, 16, 32, 64, 100, 200, 400, 600, 800 and 1000), for different number of users. ZF combiner is employed.

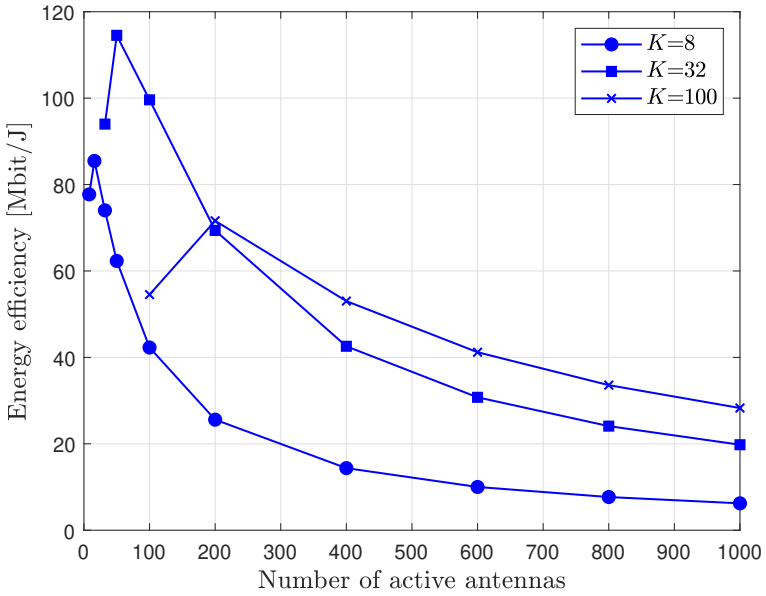

Figure 4.22 – Energy efficiency as a function of the number of active antennas (the values of M_s that were tested are 8, 16, 32, 64, 100, 200, 400, 600, 800 and 1000), for different number of users. ZF combiner is employed.

4.2 Optimizing the algorithm parameters to maximize the energy efficiency

In this section, the algorithm parameters are optimized in order to obtain the maximum energy efficiency that each selection scheme can provide in six different scenarios: $K = \{4, 8, 16, 32, 64, 100\}$. Table 4.3 shows: the optimal value of L that maximizes the EE in each scenario when employing fixed-AS; the optimal z_0 that maximizes the EE when employing variable-AS; the optimal pair (z_0, N) that maximizes the EE when employing multiple-SS; and the optimal N to maximize the EE with single-SS scheme. The table also shows the average number of selected antennas per user ($\mathbb{E}\{M_k\}$) resulting from setting $L = L^*$, $z_0 = z_0^*$ and $N = N^*$, as well as the average number of selected subarrays per user ($\mathbb{E}\{N_k\}$) when employing an SS scheme (multiple-SS or single-SS). The optimal inputs of the algorithms were found empirically, by varying incrementally their values and testing the resulting EE.

Figure 4.23 compares the average number of antennas selected per user and the average number of active antennas when employing each of the selection schemes, for different numbers of users, when using the optimal algorithm parameters (L, z_0 and N) in terms of maximizing the EE. Figures 4.24 and 4.25 show the average signal, interference (interf.) and noise power and the total power consumption, resulting from setting $L = L^*$, $z_0 = z_0^*$ and $N = N^*$. Figures 4.26a, 4.26b, 4.27a and 4.27b contain two graphics each: the left one refers to absolute values of the results of each selection scheme, while the right one refers to the absolute values normalized by the no-S results. These figures show,

Table 4.3 – Optimal values of L, z_0 and N for maximizing the EE when employing the proposed antennas/subarrays selection schemes, for different number of users, with $M = 1000$ antennas. The resulting $\mathbb{E}\{M_k\}$ and $\mathbb{E}\{M_{\text{act}}\}$, when setting $L = L^*$, $z_0 = z_0^*$ and $N = N^*$, are also presented.

	fixed-AS		variable-AS		multiple-SS				single-SS		
K	L^*	$\mathbb{E}\{M_k\}$	z_0^*	$\mathbb{E}\{M_k\}$	z_0^*	N^*	$\mathbb{E}\{N_k\}$	$\mathbb{E}\{M_k\}$	N^*	$\mathbb{E}\{N_k\}$	$\mathbb{E}\{M_k\}$
4	4	4	0.001	5.3	0.001	250	1.61	6.4	250	1	4
8	9	9	0.001	9.1	0.001	125	1.05	8.4	125	1	8
16	17	17	0.020	17.1	0.010	50	1.01	20.1	50	1	20
32	38	38	0.110	37.6	0.010	25	1.00	40.0	25	1	40
64	174	174	0.480	157.5	0.430	2	1.05	526.0	2	1	500
100	155	155	0.440	153.1	0.170	2	1.00	500.2	2	1	500

respectively, the behavior of the throughput, the average per user rate, the complexity and the EE depending on the number of users, when the algorithm parameters are set to maximize the EE.

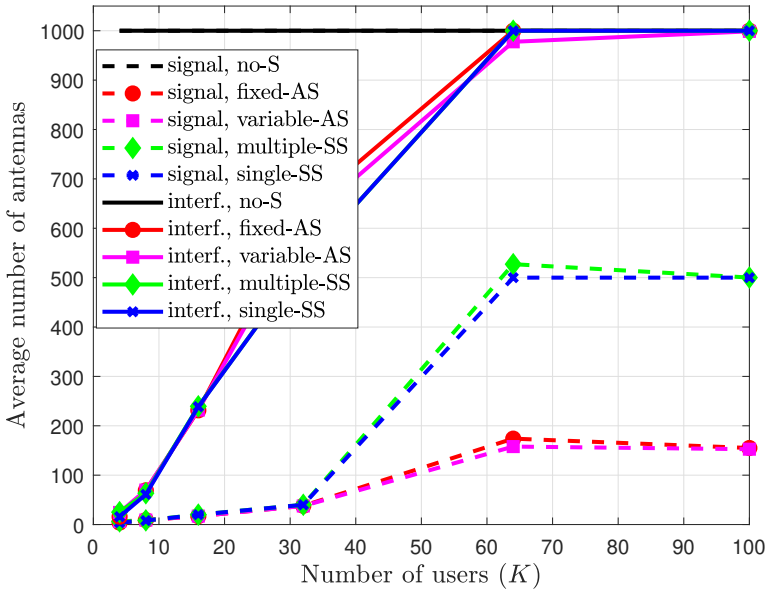

Figure 4.23 – Comparison between the five selection schemes (no-S, fixed-AS, variable-AS, multiple-SS and single-SS) in terms of the average number of selected antennas per user and average number of active antennas, as a function of the number of users (K), when the optimal values of L, z_0 and N are adopted to maximize the EE. ZF combiner is employed.

It is noticiable that the tested numbers of users can be divided in two groups, which we will call low user density (LUD) and high user density (HUD) scenarios, corresponding to $K = \{4, 8, 16, 32\}$ and $K = \{64, 100\}$, respectively.

In the LUD scenario, the average number of selected antennas per user resulting from setting $L = L^*$, $z_0 = z_0^*$ and $N = N^*$ is very low, nearly the minimum number of

antennas necessary to attend the constraint $M_k \geq K$ of the ZF combiner. In this scenario, all the proposed selection schemes (fixed-AS, variable-AS, multiple-SS and single-SS) cause a considerable reduction on the average number of active antennas, over the no-S scheme, according to Figure 4.23. Consequently, the transceiver chains power consumption (P_{TC}), which is proportional to M_{act}, gets quite lower (Figure 4.25). As $M_k << M$, there is also a very consistent complexity reduction, according to the results shown in Figure 4.27a. For instance, when $K = 4$ ($K = 32$), the complexity of the AS and SS schemes is about only 5% (30%) of the no-S complexity. As a consequence, the power consumption due to the signal processing ($P_{\mathrm{CE/SP}}$) also faces a huge reduction.

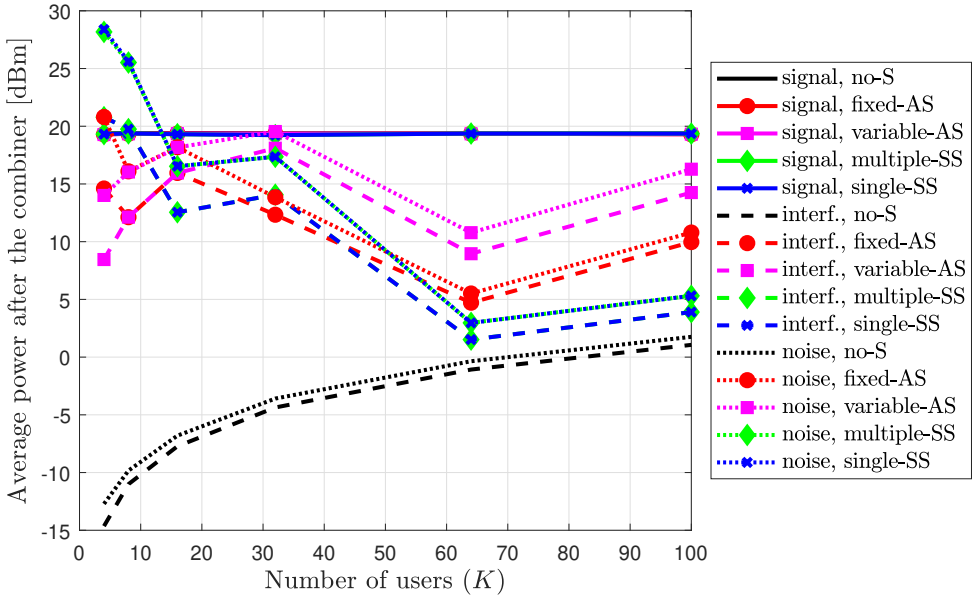

Figure 4.24 – Comparison between the five selection schemes (no-S, fixed-AS, variable-AS, multiple-SS and single-SS) in terms of the average signal, interference and noise power, after the receiver, as a function of the number of users (K), when the optimal values of L, z_0 and N are adopted to maximize the EE. ZF combiner is employed.

On the other side, as few antennas are used to perform ZF receive combining for each user, the interference and noise powers after the combiner increase when compared to the traditional strategy of using the whole antenna array (no-S scheme), according to Figure 4.24. Hence, the throughput is smaller, but it does not deteriorate as the antennas or subarrays are selected properly, following the criteria in (3.3) or (3.13), respectively. According to Figure 4.26a, the throughput is about 70% of the no-S throughput in the LUD scenario. Finally, as the power reduction is much more strong than the throughput reduction, the energy efficiency faces a huge increase: as Figure 4.27b shows, it about 1400% (250%) of the no-S EE when $K = 4$ ($K = 16$).

In the HUD scenario, the values of L, z_0 and N that maximize the EE leads to an increase in the number of selected antennas per user, in order to avoid a throughput

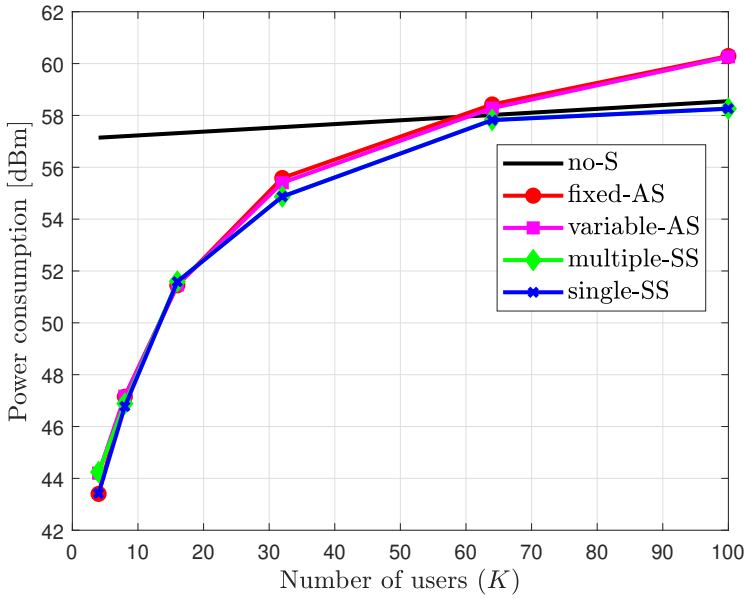

Figure 4.25 – Comparison between the five selection schemes (no-S, fixed-AS, variable-AS, multiple-SS and single-SS) in terms of power consumption, as a function of the number of users (K), when the optimal values of L, z_0 and N are adopted to maximize the EE. ZF combiner is employed.

deterioration as there is much more interference and ZF efficiency in mitigating interference depends on a great number of antennas. As a result, the computational complexity and the number of active antennas under fixed-AS, variable-AS, multiple-SS or single-SS increase when compared to the LUD scenario, causing the total power consumption also to increase.

Notice that, in the HUD scenario, $\mathbb{E}\{M_{\text{act}}\} \cong M$, which means that there will not be any power saving compared to no-S, as the most important portion of the power consumption comes from the activation of the BS antennas. Consequently, the selection schemes cannot provide an EE improvement when $K = 64$ or $K = 100$. Furthermore, with respect to fixed-AS and variable-AS, particularly, the EE decreases, because the complexity scales[1] and consequently the power consumption increases. In the LUD scenario, on the other hand, fixed-AS and variable-AS provide a complexity reduction in relation to no-S because the matrix to be inverted to compute the ZF combining vectors is $M_k \times K$ instead of $M \times K$, and in this scenario $M_k << M$.

As it selects only one subarray per user, single-SS was designed to provide lower complexity and power consumption than multiple-SS, in contrast to its possibly smaller throughput, as multiple-SS combines the signals received in each subarray after ZF combining to perform a precision detection. However, when optimizing the algorithm parameters to maximize the EE, we observed that multiple-SS and single-SS performed similarly. The reason is that the value of N that maximizes the EE is the same for both

[1] $C_{\text{C-UL}}^{\text{fixed-AS}}$ and $C_{\text{C-UL}}^{\text{variable-AS}}$ are proportional to K^4, while $C_{\text{C-UL}}^{\text{no-S}}$, $C_{\text{C-UL}}^{\text{multiple-SS}}$ and $C_{\text{C-UL}}^{\text{single-SS}}$ are proportional to K^3 (see Table 3.1).

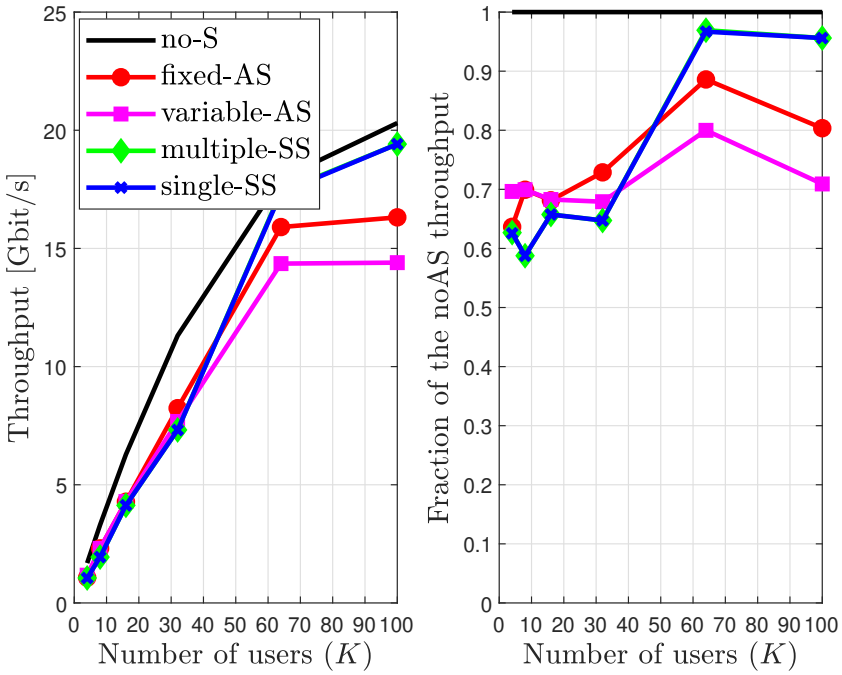

(a) Throughput

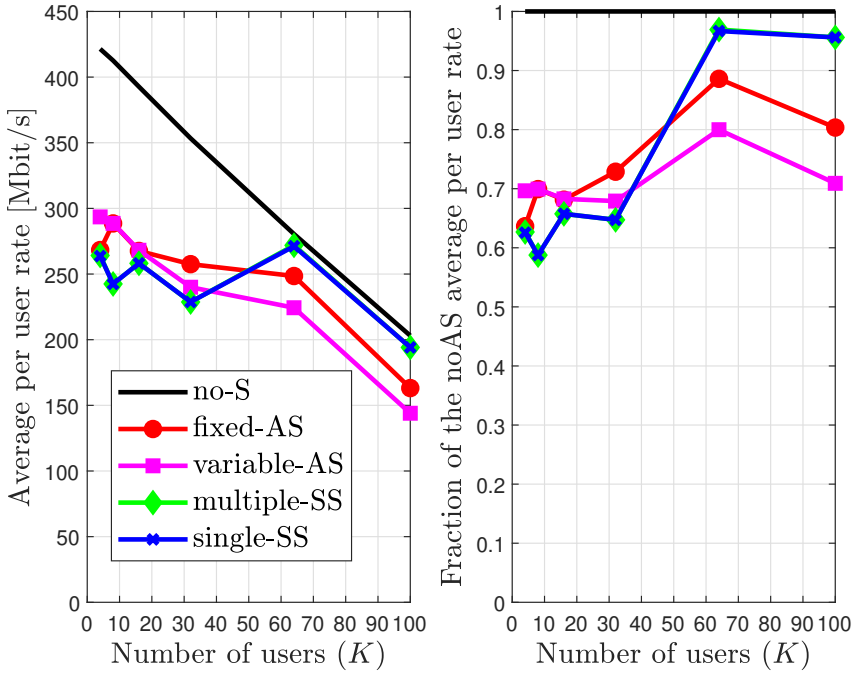

(b) Average per user rate

Figure 4.26 – Comparison between the five selection schemes (no-S, fixed-AS, variable-AS, multiple-SS and single-SS) regarding the throughput and the average per user rate, as a function of the number of users (K), when the optimal values of L, z_0 and N are adopted to maximize the EE. The left figures correspond to absolute values, while the data in the right figures are normalized by the results of the no-S scheme. ZF combiner is employed.

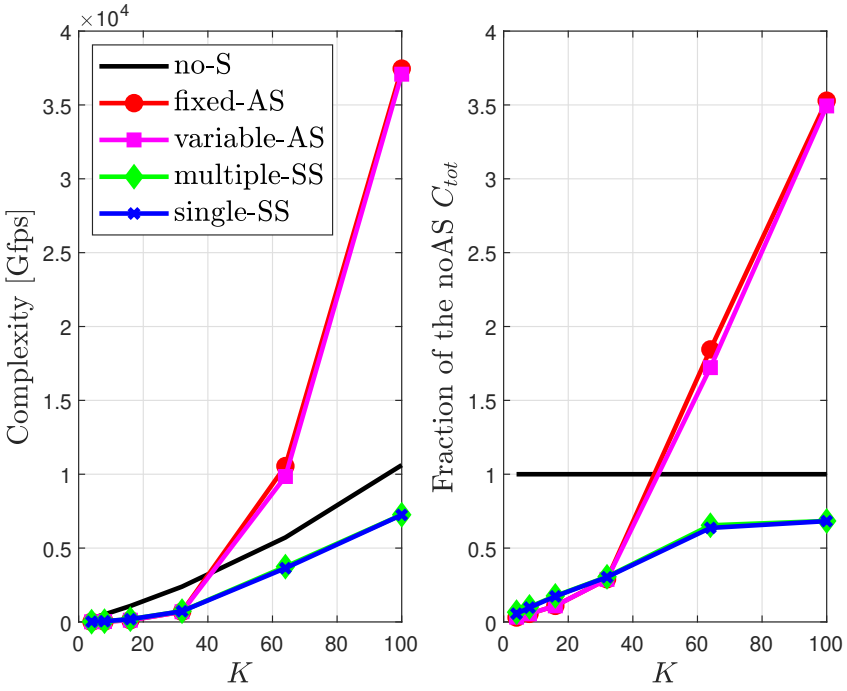

(a) Complexity

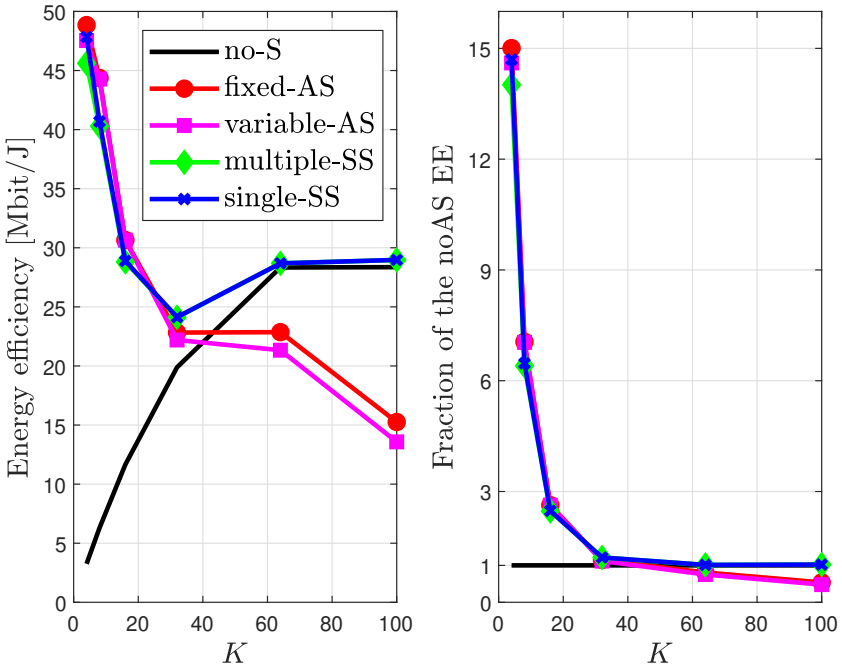

(b) Energy efficiency

Figure 4.27 – Comparison between the five selection schemes (no-S, fixed-AS, variable-AS, multiple-SS and single-SS) regarding the complexity and the energy efficiency, as a function of the number of users (K), when the optimal values of L, z_0 and N are adopted to maximize the EE. The left figures correspond to absolute values, while the data in the right figures are normalized by the results of the no-S scheme. ZF combiner is employed.

schemes in all tested number of users, while z_0^* of multiple-SS guarantees that most times only 1 subarray will be selected for each user.

With respect to fixed-AS and variable-AS, they provide similar perfomances, except regarding the throughput when $K = 32$, 64 or 100. One possible justificative for this result is the fact that variable-AS may select different number of antennas for each user, as long as the selected antennas contemplates at least a fraction z_0 of the total cumulative power of each user. Thus, some users may be given only K or a few more antennas (the minimum possible, due to ZF), and these users will have a lower throughput than if fixed-AS is utilized. Due to the relatively high number of users, the reduction in the number of selected antennas for some of these users will not prevent the whole antenna array to be activated. Consequently, EE is slightly worse when employing variable-AS than when employing fixed-AS if $K \geq 64$. However, the variable-AS philosophy of taking different number of antennas for each user has not necessarily been invalidated, as an antenna selection criterion other than the one described in Section 3.1 could be adopted in order to provide greater EE improvements than fixed-AS.

Finally, when $K \leq 32$, the four proposed selection schemes that were analyzed so far were successful at improving the EE and reducing the computational complexity and the power consumption, without considerably compromising the throughput. On the other hand, when $K \geq 64$, they could not improve the EE, as they could not prevent the whole antenna array from being active. Simultaneously, there is still a throughput reduction in relation to the no-S scheme, because each user is served by only some of the antenna elements. As the combining vectors of the K users are computed separately, the complexity scales in the HUD scenario, and consequently also does the power consumption. As a result, in this scenario, there is not benefit from employing fixed-AS or variable-AS, while multiple-SS and single-SS can still provide a complexity reduction. Thus, as multiple-SS and single-SS provided very similar performance, and single-SS has a simpler algorithm than multiple-SS, as only one subarray must be selected for each user, single-SS has demonstrated to be the most promising of all the four strategies that were proposed in Sections 3.1 and 3.2.

In the following, the results of fair-AS are compared to the ones obtained with single-SS (which has been demonstrated to be the most advantageous among the schemes proposed in Sections 3.1 and 3.2 and the no-S strategy. The algorithm inputs are optimized in order to obtain the maximum energy efficiency that each selection scheme can provide in six different scenarios: $K = \{4, 8, 16, 32, 64, 100\}$. Table 4.4 shows the optimal values of N and M_s that maximize the EE in each scenario when employing single-SS and fair-AS, respectively, as well as the energy efficiency resulting from adopting the optimized values of these inputs.

Table 4.4 shows that the optimal number of active antennas grows as the number of users grow. However, while single-SS achieves its highest EE when the whole array

Table 4.4 – Optimal values of N (single-SS) and M_s (fair-AS) for maximizing the EE, for different number of users, with $M = 1000$ antennas. The resulting EE is also presented.

	no-S		single-SS			fair-AS	
K	M_s	EE [Mbit/J]	N^*	$\mathbb{E}\{M_s\}$	EE [Mbit/J]	M_s^*	EE [Mbit/J]
4	1000	3.2	250	16	47.8	7	62.2
8	1000	6.3	125	61	40.6	12	86.1
16	1000	11.7	50	240	28.7	25	109.8
32	1000	19.9	25	531	24.1	46	118.5
64	1000	28.3	2	1000	28.8	92	103.1
100	1000	28.4	2	1000	29.0	141	75.8

is active, for K=64 or 100, fair-AS still maintain most part of the array inactive. As a consequence, it achieves the lowest throughput among no-S, single-SS and fair-AS schemes, according to results in Figure 4.28. On the other hand, it provides the lowest complexity and power consumption among the three schemes, according Figures 4.29 and 4.30. Finally, results in Figure 4.31 demonstrate that the fair-AS scheme attains much higher EE levels than single-SS. Furthermore, it improves the EE even when $K = 64$ or 100.

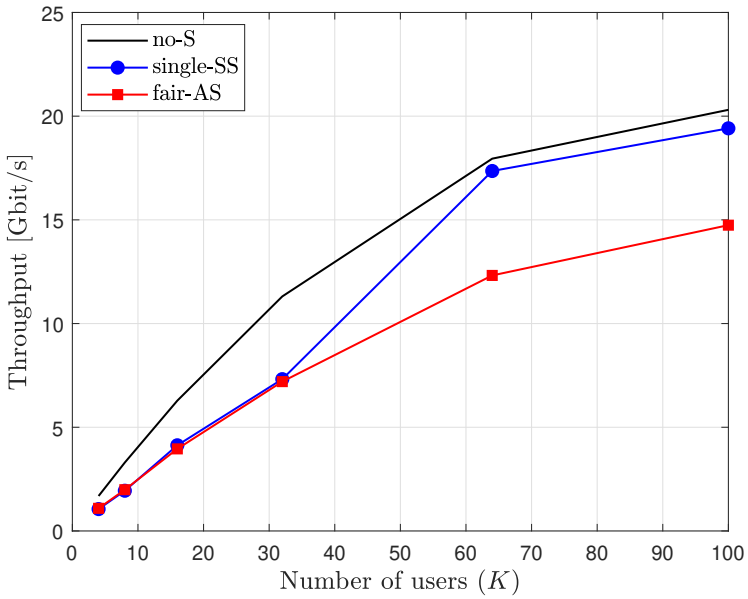

Figure 4.28 – Comparison between the no-S, single-SS and fair-AS schemes in terms of throughput, as a function of the number of users (K), when the optimal values of M_s and N are adopted to maximize the EE. ZF combiner is employed.

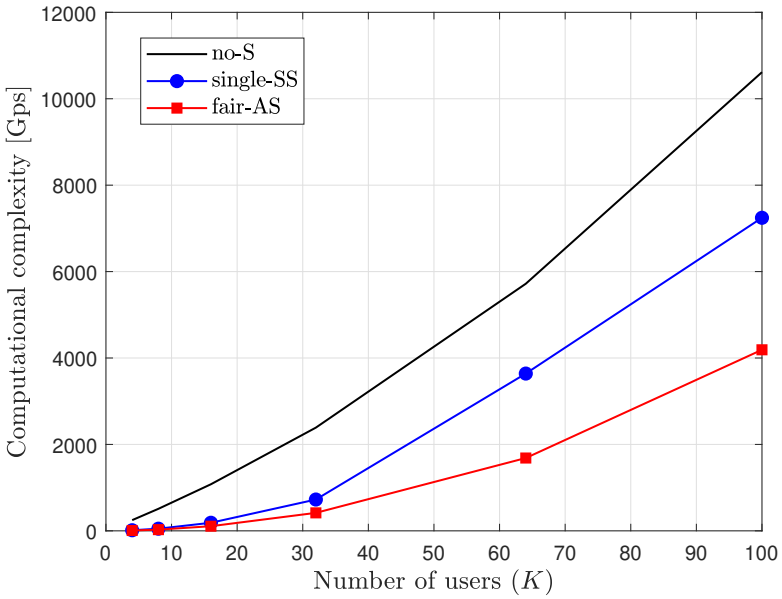

Figure 4.29 – Comparison between the no-S, single-SS and fair-AS schemes in terms of complexity, as a function of the number of users (K), when the optimal values of M_{s} and N are adopted to maximize the EE. ZF combiner is employed.

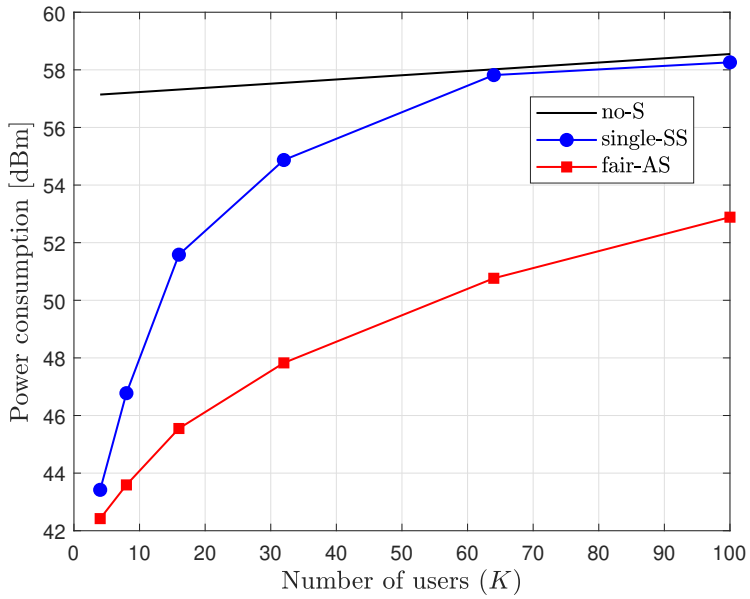

Figure 4.30 – Comparison between the no-S, single-SS and fair-AS schemes in terms of power consumption, as a function of the number of users (K), when the optimal values of M_{s} and N are adopted to maximize the EE. ZF combiner is employed.

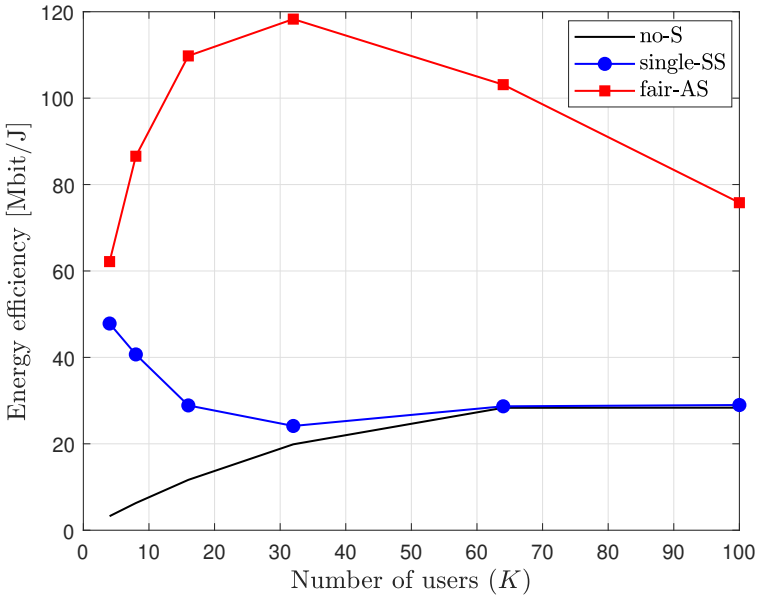

Figure 4.31 – Comparison between the no-S, single-SS and fair-AS schemes in terms of energy efficiency, as a function of the number of users (K), when the optimal values of M_s and N are adopted to maximize the EE. ZF combiner is employed.

4.3 Summary of the chapter

This chapter presents numerical results based on Monte-Carlo simulations demonstrating the performance of the selection schemes in the UL of an extra-large MIMO system using ZF receiver.

Section 4.1 shows how each of the five proposed selection schemes (fixed-AS, variable-AS, multiple-SS, single-SS and fair-AS) impacts the computational complexity, the power consumption, the throughput and the energy efficiency, depending on the algorithm inputs L (fixed-AS), z_0 (variable-AS and multiple-SS) and N (multiple-SS and single-SS), when $K = 32$. Results have demonstrated that, by choosing appropriate values of L, z_0, N and M_s, all the proposed schemes are successful at improving the EE and reducing the power consumption and the computational complexity over the no-S strategy, due to the considerable reduction in the number of antennas that are activated. As a counterpart, there is a little reduction in the system throughput.

In Section 4.2, the algorithm parameters are optimized in order to obtain the maximum energy efficiency that each selection scheme can provide in six different scenarios: $K = \{4, 8, 16, 32, 64, 100\}$. Results have demonstrated that, for $K = \{4, 8, 16, 32\}$, the selection schemes are efficient at reducing the number of active antennas. Consequently, the complexity and the power consumption decrease considerably while the throughput is only slightly affected, resulting in a great EE improvement. On the other hand, for $K = \{64, 100\}$, none of the proposed schemes is capable of reducing the number of active

antennas. As a result, there is no EE improvement. Furthermore, in this scenario, the subarray selection schemes (multiple-SS and single-SS) perform better than the first two AS schemes (fixed-AS and variable-AS), as their complexity does not scale so fast with K as when employing fixed-AS or variable-AS. Thus, as multiple-SS and single-SS provided very similar performance, and single-SS has a simpler algorithm than multiple-SS, as only one subarray must be selected for each user, single-SS has demonstrated to be the most promising of the four strategies that were proposed in Sections 3.1 and 3.2.

Finally, results demonstrate that fair-AS attains much higher EE levels than single-SS, as it is capable of maintaing the number of active antennas arbitrarily low without compromising the SE severely. Furthermore, it improves the EE even when $K = 64$ or 100.

5 Conclusions and Remarks

Increasing the number of antennas at the BS of a massive MIMO network is useful to provide higher data rates and energy efficiency. However, maintaining the antenna separation to at least half of the wavelength is fundamental to make real advantage from an array dimension of the order of hundreds or thousands of antennas. Consequently, the array length increases a lot and the channel spatial non-stationary properties appear, which means that the majority of the energy sent by a given user achieves only a small portion of the antenna array. Thus, selecting the antennas that will participate in the receive combining of the signal sent by each user, instead of using all the available antennas, may be a very useful strategy to reduce considerably the power consumption without degrading the throughput.

Numerical results shown that the selection schemes were capable of reducing the number of active antennas in the LUD scenario, therefore reducing the power consumption considerably. When assigning a small number of antennas to perform receive combining for each user, the complexity is also reduced in this scenario. The proposed algorithms select properly the antennas that are designated to each user, preferring the ones whose channel between them and the user is stronger and also considering the potential interference from the other users. Therefore, the throughput reduces only slightly, although ZF is more efficient at mitigating the interference when many antennas are used. As the power consumption decays much more than the throughput, the EE is dramatically improved in the LUD scenario.

On the other hand, in the HUD scenario, ZF needs more antennas being selected per user so that the throughput does not deteriorate. Consequently, it is not possible anymore to reduce the complexity and the number of active antennas when compared to the traditional strategy (no-S), and the power consumption is not reduced. Thus, the EE cannot be improved in this scenario.

The fair-AS scheme, on the side, was conceived to select just a predefined number of antennas to be active, which is a input of the algorithm. All the active antennas perform receive combining for all the users, which does not increase the interference levels significantly because ZF processing is used and because the adopted system model was assumed to have no pilot contamination. Results have shown that fair-AS improves the EE much further than the other methods, being able to increase the EE even in the HUD scenario.

Lastly, the XL-MIMO system, which itself is promising to achieve very high spectral and energy efficiencies, was demonstrated in this work to be even more energetically efficient in low or medium user-density scenarios, by utilizing an appropriate method for designating which antennas or subarrays will perform receive combining for each user,

instead of utilizing the whole antenna array.

5.1 Future Research Directions in AS XL-MIMO

Open research, solutions and hot issues in efficient antenna selection techniques and methods for XL-MIMO systems include:

1. Algorithm(s) to find analytically the optimal value of M_s in terms of maximizing the EE. For that propose, a procedure similar to the adopted in (Marinello et al., 2020) may be developed, considering the channel model described in this Dissertation text.

2. (Semi-)distributed processing techniques in massive MIMO antennas considering subarray switching aiming to improve energy efficiency of XL-MIMO systems.

3. Resource allocation procedures to perform joint antenna selection and power allocation aiming at maximizing the spectral efficiency of the XL-MIMO system.

4. Use of evolutionary meta-heuristic and machine learning procedures, such as genetic algorithm (GA), particle swarm optimization (PSO), ant colony optimization (ACO), deep learning for selecting antennas following some optimization criterion, such as EE or SE system maximization and so forth. In general quasi-distributed meta-heuristic-based procedures can result in excellent trade-off between performance, complexity and exchanged coordination data.

5. Extend the investigations on XL-MIMO systems to scenarios with higher number of users, where the number of orthogonal sequences is not sufficient to avoid pilot contamination. In this case, it may be convenient to consider combining/precoding schemes other than ZF, such as MMSE. A possible linear processing technique to improve the system performance in this scenario that could be implemented is based on the multicell-MMSE (M-MMSE) combiner described in (BJöRNSON et al., 2017). Other possible direction is to incorporate a pilot assignment scheme to minimize the coherent interference between users that were assigned the same pilot sequence.

Bibliography

Ali, A.; Carvalho, E. D.; Heath, R. W. Linear receivers in non-stationary massive mimo channels with visibility regions. *IEEE Wireless Communications Letters*, v. 8, n. 3, p. 885–888, June 2019. ISSN 2162-2345. Cited 2 times on page(s) 31 and 34.

Amiri, A.; Angjelichinoski, M.; de Carvalho, E.; Heath, R. W. Extremely large aperture massive mimo: Low complexity receiver architectures. In: *2018 IEEE Globecom Workshops (GC Wkshps)*. [S.l.: s.n.], 2018. p. 1–6. Cited 2 times on page(s) 31 and 34.

AMIRI, A.; MANCH'ON, C. N.; CARVALHO, E. de. *Deep Learning Based Spatial User Mapping on Extra Large MIMO Arrays*. 2020. Cited on page 34.

BJöRNSON, E.; HOYDIS, J.; SANGUINETTI, L. Massive MIMO networks: Spectral, energy, and hardware efficiency. *Foundations and Trends® in Signal Processing*, v. 11, n. 3-4, p. 154–655, 2017. ISSN 1932-8346. Disponível em: ⟨http://dx.doi.org/10.1561/2000000093⟩. Cited 7 times on page(s) 31, 43, 57, 61, 63, 65, and 92.

Björnson, E.; Sanguinetti, L.; Hoydis, J.; Debbah, M. Optimal design of energy-efficient multi-user mimo systems: Is massive mimo the answer? *IEEE Transactions on Wireless Communications*, v. 14, n. 6, p. 3059–3075, June 2015. ISSN 1558-2248. Cited on page 65.

Boccardi, F.; Heath, R. W.; Lozano, A.; Marzetta, T. L.; Popovski, P. Five disruptive technology directions for 5g. *IEEE Communications Magazine*, v. 52, n. 2, p. 74–80, 2014. Cited on page 31.

Bohagen, F.; Orten, P.; Oien, G. E. On spherical vs. plane wave modeling of line-of-sight mimo channels. *IEEE Transactions on Communications*, v. 57, n. 3, p. 841–849, 2009. Cited on page 33.

BOYD, S.; VANDENBERGHE, L. *Convex Optimization*. [S.l.]: Cambridge University Press, 2004. Cited on page 57.

Carvalho, E. D.; Ali, A.; Amiri, A.; Angjelichinoski, M.; Heath, R. W. Non-stationarities in extra-large-scale massive mimo. *IEEE Wireless Communications*, v. 27, n. 4, p. 74–80, 2020. Cited 2 times on page(s) 31 and 34.

Chen, J.; Wang, S.; Yin, X. A spherical-wavefront-based scatterer localization algorithm using large-scale antenna arrays. *IEEE Communications Letters*, v. 20, n. 9, p. 1796–1799, 2016. Cited on page 33.

Chen, J.; Yin, X.; Cai, X.; Wang, S. Measurement-based massive mimo channel modeling for outdoor los and nlos environments. *IEEE Access*, v. 5, p. 2126–2140, 2017. ISSN 2169-3536. Cited on page 31.

Flordelis, J.; Li, X.; Edfors, O.; Tufvesson, F. Massive mimo extensions to the cost 2100 channel model: Modeling and validation. *IEEE Transactions on Wireless Communications*, v. 19, n. 1, p. 380–394, 2020. Cited 2 times on page(s) 31 and 39.

Flordelis, J.; Rusek, F.; Tufvesson, F.; Larsson, E. G.; Edfors, O. Massive mimo performance - tdd versus fdd: What do measurements say? *IEEE Transactions on Wireless Communications*, v. 17, n. 4, p. 2247–2261, 2018. Cited on page 37.

Han, Y.; Jin, S.; Wen, C.; Ma, X. Channel estimation for extremely large-scale massive mimo systems. *IEEE Wireless Communications Letters*, p. 1–1, 2020. Cited 2 times on page(s) 31 and 39.

Hou, S.; Wang, Y.; Zeng, T.; Wu, S. Sparse channel estimation for spatial non-stationary massive mimo channels. *IEEE Communications Letters*, v. 24, n. 3, p. 681–684, 2020. Cited on page 31.

HUANG, Y.; HE, S.; WANG, J.; ZHU, J. Spectral and energy efficiency tradeoff for massive mimo systems. *IEEE Transactions on Vehicular Technology*, p. 1–1, 2018. ISSN 0018-9545. Cited on page 33.

Jeng-Shiann Jiang; Ingram, M. A. Spherical-wave model for short-range mimo. *IEEE Transactions on Communications*, v. 53, n. 9, p. 1534–1541, 2005. Cited on page 33.

KRAUS, J.; MARHEFKA, R. *Antennas for All Applications*. McGraw-Hill, 2002. (McGraw-Hill series in electrical engineering). ISBN 9780071232012. Disponível em: ⟨https://books.google.com.br/books?id=V6pSPgAACAAJ⟩. Cited on page 38.

Li, J.; Ai, B.; He, R.; Yang, M.; Zhong, Z.; Hao, Y.; Shi, G. The 3d spatial non-stationarity and spherical wavefront in massive mimo channel measurement. In: *2018 10th International Conference on Wireless Communications and Signal Processing (WCSP)*. [S.l.: s.n.], 2018. p. 1–6. Cited on page 31.

Marinello, J. C.; AbrÃ$o, T.; Amiri, A.; de Carvalho, E.; Popovski, P. Antenna selection for improving energy efficiency in xl-mimo systems. *IEEE Transactions on Vehicular Technology*, v. 69, n. 11, p. 13305–13318, 2020. Cited 2 times on page(s) 54 and 92.

Marinello, J. C.; Panazio, C.; Abrão, T.; Tomasin, S. Total energy efficiency of tr-mrc and fd-mrc receivers for massive mimo uplink. *IEEE Systems Journal*, v. 13, n. 3, p. 2285–2296, 2019. Cited 2 times on page(s) 63 and 65.

MARZETTA, T.; LARSSON, E.; YANG, H.; NGO, H. *Fundamentals of Massive MIMO*. Cambridge University Press, 2016. (Fundamentals of Massive MIMO). ISBN 9781107175570. Disponível em: ⟨https://books.google.com.br/books?id=IM0iDQAAQBAJ⟩. Cited on page 37.

MARZETTA, T. L. Noncooperative cellular wireless with unlimited numbers of base station antennas. *IEEE Transactions on Wireless Communications*, v. 9, n. 11, p. 3590–3600, November 2010. ISSN 1536-1276. Cited on page 37.

MOLISCH, A. F. *Wireless communications*. [S.l.]: John Wiley & Sons, 2012. v. 34. Cited on page 38.

UBIALI, G. A.; ABRÃO, T. Xl-mimo energy-efficient antenna selection under non-stationary channels. *Physical Communication*, v. 43, p. 101189, 2020. ISSN 1874-4907. Disponível em: ⟨http://www.sciencedirect.com/science/article/pii/S1874490720302664⟩. Cited 2 times on page(s) 63 and 65.

Wang, H.; Kosasih, A.; Wen, C.; Jin, S.; Hardjawana, W. Expectation propagation detector for extra-large scale massive mimo. *IEEE Transactions on Wireless Communications*, v. 19, n. 3, p. 2036–2051, 2020. Cited 3 times on page(s) 31, 32, and 34.

Yin, X.; Wang, S.; Zhang, N.; Ai, B. Scatterer localization using large-scale antenna arrays based on a spherical wave-front parametric model. *IEEE Transactions on Wireless Communications*, v. 16, n. 10, p. 6543–6556, 2017. Cited 2 times on page(s) 31 and 34.

Zhou, Z.; Gao, X.; Fang, J.; Chen, Z. Spherical wave channel and analysis for large linear array in los conditions. In: *2015 IEEE Globecom Workshops (GC Wkshps)*. [S.l.: s.n.], 2015. p. 1–6. Cited 2 times on page(s) 33 and 38.

Appendix

APPENDIX A – Full paper published in the journal "Physical Communication"

Physical Communication 43 (2020) 101189

Contents lists available at ScienceDirect

Physical Communication

journal homepage: www.elsevier.com/locate/phycom

Full length article

XL-MIMO energy-efficient antenna selection under non-stationary channels

Gabriel Avanzi Ubiali, Taufik Abrão *

Electrical Engineering Department, State University of Londrina (DEEL-UEL), Londrina, PR, Brazil

ARTICLE INFO

Article history:
Received 27 January 2020
Received in revised form 29 June 2020
Accepted 19 August 2020
Available online 26 August 2020

Keywords:
Extremely-large antenna regime
Non-stationary channels
Antenna selection
Energy efficiency
Spectral efficiency
Precoding
Combining

ABSTRACT

Massive multiple-input-multiple-output (M-MIMO) is a key technology for 5G networks. Within this research area, new types of deployment are arising, such as the extremely-large regime (XL-MIMO), where the antenna array at the base station (BS) has extreme dimensions. As a consequence, spatial non-stationary properties appear as the users see only a portion of the antenna array, which is called visibility region (VR). In this challenging transmission–reception scenario, an algorithm to select the appropriate antenna-elements for processing the received signal of a given user in the uplink (UL), as well as to transmit the signal of this user during downlink (DL) is proposed. The advantage of not using all the available antenna-elements at the BS is the computational burden and circuit power consumption reduction, improving the energy efficiency (EE) substantially. Numerical results demonstrate that one can increase the EE without compromising considerably the spectral efficiency (SE). Under few active users scenario, the performance of the XL-MIMO system shows that the EE is maximized using less than 20% of the antenna-elements of the array, without compromising the SE severely.

1. Introduction

Massive multiple-input-multiple-output (M-MIMO) is one of the key technologies for 5G networks [1], which permits that more than one single user transmits simultaneously with high spectral and energy efficiencies and using the same spectrum, *i.e.*, many antennas simultaneously serve many users using the same time–frequency resource [2]. In MIMO networks, the base station (BS) estimates the channel coefficients and employs a transmit precoding scheme in the downlink (DL) and a receive combining scheme in the uplink (UL), giving each user a different spatial signature [3,4]. M-MIMO wireless communication is a special case of MIMO systems using hundreds of antennas at the BS, providing sufficient spatial dimensions to uncover the fundamental properties of M-MIMO: channel hardening, large array gain and asymptotic inter-terminal channel orthogonality (favorable propagation) [5]. Thus, it can provide large improvements over traditional systems in both energy and spectral efficiencies.

As the number of BS antennas increases, it is possible to focus the transmission and reception of signal energy into ever-smaller regions of space, which brings huge improvements in throughput and EE. However, it may come with the computational complexity increasing, as well as with the increasing of implementation cost and power consumption, what advocates for new deployments that take real advantage from increasing the number of BS antennas to the order of hundreds or thousands, without severe problems due to the holdbacks above cited. Moreover, in order to make real advantage from the deployment of such a large number of antenna elements, it is desirable to distribute them over a substantially large area in order to increase the antenna separation and coverage [6]. One potential approach is the extremely-large MIMO (XL-MIMO) regime, where the antenna array is integrated into large building structures [5].

When a moderate number of (several tens of) antennas is compactly deployed in the BS, the entire array will receive approximately the same amount of energy from each user, *i.e.*, the channel is spatially stationary [7]. On the other hand, in the XL-MIMO regime, different parts of the array may observe the same propagation paths with varying power and phases or distinct propagation paths. Then, the majority of energy received from a specific user concentrates on small portions of the entire array, which is a channel property called spatial *non-stationarity*, which has been observed by recent channel measurements [8–10] and can be introduced in the channel model by using the concept of visibility region (VR) [5,11–13]. However, it is worth saying that the density of VRs influences on the size of the portion of the array that the user can see. For instance, if the VR density is

* Correspondence to: Rod. Celso Garcia Cid - PR445, s/n, Campus Universitário, Po. Box 10.011 86057-970, Londrina, PR, Brazil.
E-mail addresses: g.avanziubiali@gmail.com (G.A. Ubiali), taufik@uel.br (T. Abrão).

https://doi.org/10.1016/j.phycom.2020.101189
1874-4907/

sufficiently high, all portions of the array are able to receive some signal energy.

The conventional M-MIMO signal processing architecture is centralized at the BS, what means that the signals are received at the BS (UL) and transmitted by the BS (DL) deploying all elements of antennas. Then, the associated computational complexity becomes a challenge when employing extremely large arrays, specially in crowded scenarios, due to the need to transfer excessively large amounts of data received by the array to the processing unit [7]. A promising solution is to use only a portion of the whole element-antennas array to perform receive combining as well as the transmit precoding to each user.

Hence, by appropriately selecting a subset of BS antennas to communicate with each user, the receiver is able to capture almost the totality of the energy transmitted by that user, while reducing the interference coming from the other users and therefore potentially increasing the spectral efficiency (SE). Furthermore, by having higher SE and reduced power consumption, one can obtain higher EE. It is important to highlight that there is a growing concern about how to improve the EE in wireless communications, as the increasing data rates and the increasing number of users connected to the network increase substantially the overall energy consumption [14]. For this reason, in this work we take both SE and EE as performance metrics to be analyzed in Section 5. Finally, on can summarize the benefits of the VR-based subarray antenna selection architecture as: (a) computational complexity reduction; (b) overall energy saving by activating a reduced number of antenna-elements; (c) as a result an EE increasing; (d) while potentially improving the overall system SE by selecting appropriate antenna-elements associated to the each user VR.

Considering that the antenna array experiences spatial non-stationarities when using large-aperture arrays, in [15], authors propose two new channel estimation methods that, besides estimating the channel vector, obtains the position of the scatterers and the visibility regions, which may be useful for transceiver design. In [11], authors study the impact of spatial non-stationarity where the channel energy is concentrated on a portion of the array, *i.e.*, the VR, in terms of signal-to-interference-plus-noise ratio (SINR) performance. In [5], authors show that, when M-MIMO systems operate in extra-large scale regime, several important MIMO design aspects change, due to spatial non-stationarities, where the users see only a portion of the array and, inside the VR, different parts of the array see different propagation paths. Moreover, three low-complexity data detection algorithms are proposed in [12] as candidates for uplink communication in XL-MIMO systems.

In [7], authors designed an efficient detector for extra-large-scale massive MIMO systems with the subarray-based processing architecture, by extending the application of the expectation propagation principle. Their analysis is based on bit error rate (BER) performance. A different approach to the antenna selection methodology proposed herein, in [16], authors propose a design based on machine learning to select a small portion of the array that contains the beamforming energy to the user, aiming to overcome the prohibitive complexity of XL-MIMO systems. They provide numerical results in terms of sum-rate performance. To the best of author's knowledge, this is the first work addressing the subarray-based processing architecture, which remarkably provides huge reduction in the computational complexity, through the point of view of improving the overall system EE.

Contribution. We deal with an XL-MIMO system equipped with a subarray-based processing architecture, in order to reduce the overall system computational complexity. In such scenario, we propose a novel algorithm to judiciously select the antenna-elements subarray that will communicate with each user, aiming at obtaining higher EE while reducing the power consumption, when compared to the whole antenna array activation to communicate with every user. Thus, the *contribution* of this work can be summarized as: (***i***) we propose an antenna selection procedure to improve simultaneously the overall system EE by reducing the power consumption, taking into account the spatial non-stationarity assumption while taking advantage of the VRs features; (***ii***) the proposed algorithm also provides a considerable computational complexity reduction; (***iii***) a comprehensive analysis development on how the proposed procedure impacts the system performance is developed, highlighting and characterizing its benefits when comparing to the condition of using the entire antenna array to communicate with every user.

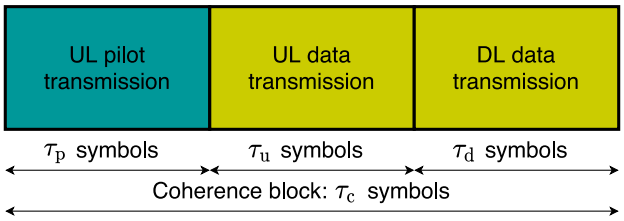

Fig. 1. Each coherence block is divided into the UL pilot transmission for channel estimation purpose, the UL data transmission, and the DL data transmission.

The remainder of the paper is organized as follows. The adopted XL-MIMO channel model and the channel estimation procedure is developed in Section 2; this section also provides the ergodic UL and DL spectral efficiencies expressions, based on the signal-to-interference-plus-noise ratio (SINR). Section 3 focuses on the proposed antenna selection procedure, as well as on the computational complexity aspects. The EE definition and a detailed circuit power model are discussed in Section 4. Section 5 examines numerical results corroborating our findings, while the main conclusions are presented in Section 6.

2. System model

We consider the UL and the DL of a single-cell multiuser XL-MIMO system with an M-antenna BS and K single-antenna users at each cell, operating over a bandwidth of B Hz. The channel estimates are acquired via UL synchronous pilot transmission. The time–division duplex (TDD) operation mode was chosen because of its advantages over the frequency–division duplex (FDD) mode. TDD does not require quantized channel state information (CSI) to be sent by the BS to the user via feedback, because of channel reciprocity, avoiding excessive overhead [3,17].

The channel coherence time (T_C) is divided into UL pilot, UL data and DL data transmission, as Fig. 1 shows. The number of symbols that fits in a channel coherence block is $\tau_c = T_C B_C$, being B_C the coherence bandwidth [2]. In order to estimate the channel, each of the K users of a given cell is assigned a different pilot sequence. There are τ_c symbols per coherence block, of which τ_p are dedicated to UL pilot transmission, $\tau_u = \epsilon_u \left(\tau_c - \tau_p\right)$ symbols are dedicated to UL data transmission and $\tau_d = \epsilon_d \left(\tau_c - \tau_p\right)$ symbols are dedicated to DL data transmission, where $\epsilon_u + \epsilon_d = 1$. The number of available orthogonal pilot sequences is equal to its length (τ_p). As we need K sequences, we can take $\tau_p = K$. Thus, the time required for pilots is proportional to the number of users served. The number of users that can be served is therefore limited by the coherence time, which itself depends on the mobility of the users [2].

The antenna-elements are uniformly spaced over a uniform linear L-length array containing M elements (M-ULA). The coordinates of the first and the Mth antennas are $(0, 0)$ and $(L, 0)$,

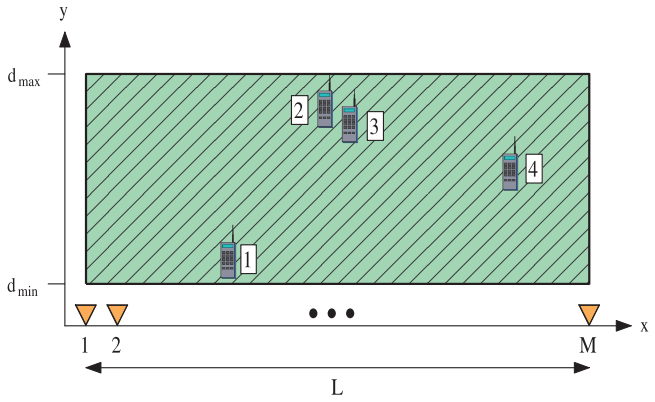

Fig. 2. Typical system spatial configuration.

respectively, which means that, when $M \geq 1$, the spacing between the antennas is $\frac{L}{M-1}$. The users are placed over a rectangle that extends along the antenna array in one dimension and between a minimum ($d_{\min}$) and a maximum distance ($d_{\max}$) in the other dimension, following a uniform distribution over this area. The coordinates of the mth antenna are denoted by $(a_m, 0)$, and its distance to the kth user is denoted by d_{mk}. A typical system configuration is represented by Fig. 2.

2.1. XL-MIMO channel model

In XL-MIMO systems, spatial non-stationarities occur frequently since typically $d_{\max} < L$, what means that a given user probably sees only a small part of the antenna array. The propagation environment contains numerous objects reflecting the signal, which are called scattering points. Each scattering point has an associated VR. Herein, we assume that each user can see the antenna array through N_c different VRs. The ith VR that is visible to the kth user extends from the c_{ik}th to the $(c_{ik} + N_{ik})$th antenna and is denoted by $\mathcal{C}_{ik} = \{c_{ik}\ ,\ c_{ik}+1\ ,\ \ldots\ ,\ c_{ik}+N_{ik}\}$. These VRs may overlap, and the set $\mathcal{C}_k = \mathcal{C}_{1,k} \cup \ldots \cup \mathcal{C}_{N_C,k}$ contains the indices of the antennas that are visible to the kth user. Considering that each user sees the antenna array through more than one VR, it is a way of taking into account that not only one subset of the array containing contiguous antenna elements may be visible. Indeed, the mobile user may see more than one portion of the array. For instance, if $M = 100$ in Fig. 2, it may see antennas 10 to 20 and 25 to 40, which means there is something in the propagation environment preventing the signal from reaching antennas 21 to 24.

In general, the distances between a given user and all the BS antennas are considered to be the same. However, in the XL-MIMO scenario, as the length of the antenna array is not negligible, the pathloss varies throughout the array, mainly when $d_{\max} \ll L$. The pathloss coefficient between the mth antenna and the kth user is given by:

$$b_{mk} = \frac{b_0}{(d_{mk})^{\gamma}} \tag{1}$$

where $\gamma \geq 2$ is the pathloss exponent and b_0 determines the median channel gain at a reference distance of 1 m [6]. The parameters b_0 and γ are functions of the carrier frequency, antenna gains, and vertical heights of the antennas, which are derived from fitting (1) to measurements [6]. Finally, the channel vector $\mathbf{h}_k = [h_{1k}\ \ldots\ h_{Mk}]^{\mathrm{T}}$ between the BS and the kth user is given by:

$$\mathbf{h}_k = \mathbf{a}_k \odot \sqrt{\mathbf{b}_k} \odot \overline{\mathbf{h}}_k \tag{2}$$

where $\mathbf{b}_k$ is a vector whose mth element is b_{mk}, and $\overline{\mathbf{h}}_k$ is the independent Rayleigh fading component, which accounts for the short-scale fading and follows a complex-Gaussian distribution $\overline{\mathbf{h}}_k \sim \mathcal{CN}(\mathbf{0}_M, \mathbf{I}_M)$. The coefficient $a_{mk} = [\mathbf{a}_k]_m$ indicates whether the mth antenna is visible to the kth user ($a_{mk} = 1$) or not ($a_{mk} = 0$), and is given by:

$$a_{mk} = \begin{cases} 1 & m \in \mathcal{C}_k \\ 0 & \text{otherwise.} \end{cases} \tag{3}$$

2.2. UL pilot transmission

We assume the channel is estimated via UL synchronous pilot transmission, which means that all users simultaneously send pilot sequences from the same pilot codebook. They have length τ_{p} and form an orthogonal set. Herein, it is assumed that each user is assigned a different pilot sequence. Then, the pilot sequences' set is $\boldsymbol{\Psi} = [\boldsymbol{\psi}_1 \ldots \boldsymbol{\psi}_K] \in \mathbb{C}^{\tau_{\mathrm{p}} \times K}$ and the orthogonality condition states that $\boldsymbol{\Psi}^{\mathrm{H}}\boldsymbol{\Psi} = \tau_{\mathrm{p}}\mathbf{I}_{\tau_{\mathrm{p}}}$, *i.e.*:

$$\boldsymbol{\psi}_i^{\mathrm{H}}\boldsymbol{\psi}_k = \begin{cases} \tau_{\mathrm{p}} & i = k, \\ 0 & i \neq k. \end{cases} \tag{4}$$

During the UL pilot transmission, the kth user transmits the pilot sequence $\boldsymbol{\psi}_k \in \mathbb{C}^{\tau_{\mathrm{p}}}$, with transmit power p_{p}. The elements of $\boldsymbol{\psi}_k$ are scaled by $\sqrt{p_{\mathrm{p}}}$, forming the signal $\mathbf{s}_k = \sqrt{p_{\mathrm{p}}}\boldsymbol{\psi}_k^{\mathrm{H}}$, to be transmitted over τ_{p} UL samples. As a result, the BS receives the signal $\mathbf{Y}^{\mathrm{p}} \in \mathbb{C}^{M \times \tau_{\mathrm{p}}}$:

$$\mathbf{Y}^{\mathrm{p}} = \sum_{i=1}^{K} \sqrt{p_{\mathrm{p}}}\mathbf{h}_i\boldsymbol{\psi}_i^{\mathrm{H}} + \mathbf{N}^{\mathrm{p}} \tag{5}$$

where $\mathbf{N}^{\mathrm{p}} \in \mathbb{C}^{M \times \tau_{\mathrm{p}}}$ is the noise matrix at the receiver of the BS with i.i.d. entries following a complex normal distribution with zero mean and variance σ_{UL}^2.

As the information about which antennas are visible for each user is unknown, it might be necessary to consider obtaining the channel estimates by using estimators that require no prior statistical information, such as the least-squares (LS). Moreover, as we consider that each user is assigned a different pilot sequence and these sequences are mutually orthogonal, there is no pilot contamination. Hence, the imperfections on the channel estimates are just due to the noise power at the BS antennas during the UL pilot transmission. It advocates for using LS channel estimation rather than MMSE. The LS estimate of $\mathbf{h}_k$ is attained by [6]:

$$\hat{\mathbf{h}}_k = \frac{1}{\tau_{\mathrm{p}}\sqrt{p_{\mathrm{p}}}}\mathbf{Y}^{\mathrm{p}}\boldsymbol{\psi}_k \tag{6a}$$

$$= \mathbf{h}_k + \frac{1}{\tau_{\mathrm{p}}\sqrt{p_{\mathrm{p}}}}\mathbf{N}^{\mathrm{p}}\boldsymbol{\psi}_k \tag{6b}$$

The last term in (6b) is the equivalent noise vector, which adds imperfections to the channel estimates and follows a complex normal distribution: $\mathbf{N}^{\mathrm{p}}\boldsymbol{\psi}_k \sim \mathcal{CN}(\mathbf{0}_M, \tau_{\mathrm{p}}\sigma_{\mathrm{UL}}^2\mathbf{I}_M)$. Finally, the estimated channel matrix is $\hat{\mathbf{H}} = [\hat{\mathbf{h}}_1\ \ldots\ \hat{\mathbf{h}}_K]$, while $\mathbf{H} = [\mathbf{h}_1\ \cdots\ \mathbf{h}_K] \in \mathbb{C}^{M \times K}$ is the true channel matrix. According to Eq. (6a), the channel estimation process corresponds to the inner product of M complex vectors of length τ_{p}, requiring $M\tau_{\mathrm{p}}$ multiplications between complex numbers (or $3M\tau_{\mathrm{p}}$ multiplications between real numbers[1]) to estimate the channel vector of each of the K users. Herein, we consider that both multiplication

[1] Consider $x = a + jb$ and $y = c + jd$. The hardware implementation of the complex multiplication $xy = ac - bd + j[(a + b)(c + d) - ac - bd]$ involves 3 real multiplications and 5 real sums. Only those will be considered, due to their very greater hardware complexity compared to the real sum operation.

and division between real numbers correspond to 1 floating-point operation (flop). As the channel estimation process is performed once per coherence block, its computational complexity, defined in number of flops per coherence block [fpcb], is:

$$C_{\text{CE}} = 3MK\tau_{\text{p}} \qquad \text{[fpcb]} \tag{7}$$

2.3. UL data transmission

The received signal $\mathbf{r} \in \mathbb{C}^M$ at the BS during the UL data transmission is:

$$\mathbf{r} = \sum_{k=1}^{K} \mathbf{h}_k x_k + \mathbf{n} \tag{8}$$

where x_k is the signal sent by the kth user and $\mathbf{n} \sim \mathcal{CN}(\mathbf{0}_M, \sigma_{\text{UL}}^2 \mathbf{I}_M)$ contains the noise received at the BS antennas. By utilizing a suitable combining vector, $\mathbf{v}_k \in \mathbb{C}^M$, the BS detects the kth user's signal as follows:

$$y_k = \mathbf{v}_k^{\text{H}} \mathbf{r} \tag{9}$$

Herein we consider the two simplest types of linear processing for receive combining: zero-forcing (ZF) and maximum-ratio (MR), which are respectively defined by:

$$\mathbf{V} = \hat{\mathbf{H}}(\hat{\mathbf{H}}^{\text{H}}\hat{\mathbf{H}})^{-1} \tag{10}$$

and

$$\mathbf{V} = \hat{\mathbf{H}} \tag{11}$$

where the matrix $\mathbf{V} = [\mathbf{v}_1 \dots \mathbf{v}_K]$ is the collection of the combining vectors. ZF induces considerably smaller intra-cell interference than MR, yielding significantly better performance under interference-limited conditions, which is normally the case. On the other hand, it increases computational complexity significantly when employing large antenna arrays, due to multiplications of complex numbers, and when serving a great number of users, due to the size of the $K \times K$ matrix that is inverted [3,6]. Due to these particularities, it is interesting to compare the system performance in terms of SE and EE considering such linear processing techniques.

The channels are practically constant within a coherence block, while the signals and noise take new realization at every sample. Then, the instantaneous SINR is actually an expectation over one coherence block, what means that $p_k^{\text{UL}} = \mathbb{E}\{|x_k|^2\}$ – which is the UL transmit power of the kth user – and σ_{UL}^2 will be taken instead of the instantaneous values of $|x_k|^2$ and $|n_k|^2$, respectively. Thus, one can define the SINR of the kth user during the UL data transmission as

$$\gamma_k^{\text{UL}} = \frac{p_k^{\text{UL}} |\mathbf{v}_k^{\text{H}} \mathbf{h}_k|^2}{\sum_{\substack{i=1 \\ i \neq k}}^{K} p_i^{\text{UL}} |\mathbf{v}_k^{\text{H}} \mathbf{h}_i|^2 + \sigma_{\text{UL}}^2 \|\mathbf{v}_k\|^2} \tag{12}$$

As a result, the UL ergodic spectral efficiency is defined by [6]:

$$\text{SE}_{\text{UL}} = \frac{\tau_{\text{u}}}{\tau_{\text{c}}} \sum_{k=1}^{K} \mathbb{E}\{\log_2(1 + \gamma_k^{\text{UL}})\} \tag{13}$$

2.4. DL data transmission

In the DL, the information to be transmitted by the BS to the kth user, x_k, needs to be precoded, by using the precoding vector $\mathbf{w}_k$. The signal to be transmitted, denoted by $\mathbf{s} \in \mathbb{C}^M$, is generated as:

$$\mathbf{s} = \sum_{k=1}^{K} \mathbf{w}_k x_k \tag{14}$$

We denote the matrix containing the collection of the precoding vectors by $\mathbf{W} = [\mathbf{w}_1 \ \cdots \ \mathbf{w}_K] \in \mathbb{C}^{M \times K}$. The UL–DL duality motivates a simple precoding design principle: selecting the DL precoding vectors as the normalized version of their respective combining vectors [6]:

$$\mathbf{w}_k = \frac{\mathbf{v}_k^*}{\|\mathbf{v}_k\|} \tag{15}$$

Assuming no receive combining, user k receives the signal:

$$y_k = \mathbf{h}_k^{\text{T}} \mathbf{s} + n_k \tag{16}$$

where the received noise follows the distribution $n_k \sim \mathcal{CN}(0, \sigma_{\text{DL}}^2)$. Analogously to (12) for the UL, the SINR of the kth user in the DL data transmission is defined as:

$$\gamma_k^{\text{DL}} = \frac{p_k^{\text{DL}} |\mathbf{h}_k^{\text{T}} \mathbf{w}_k|^2}{\sum_{\substack{i=1 \\ i \neq k}}^{K} p_i^{\text{DL}} |\mathbf{h}_k^{\text{T}} \mathbf{w}_i|^2 + \sigma_{\text{DL}}^2} \tag{17}$$

where p_k^{DL} is the downlink transmit power assigned for user k, i.e., $\sqrt{p_k^{\text{DL}}}$ scales the vector $\mathbf{w}_k$, which has unit norm. Finally, the DL ergodic spectral efficiency is given by [6]:

$$\text{SE}_{\text{DL}} = \frac{\tau_{\text{d}}}{\tau_{\text{c}}} \sum_{k=1}^{K} \mathbb{E}\{\log_2(1 + \gamma_k^{\text{DL}})\} \tag{18}$$

3. Antenna selection for combining and precoding in XL-MIMO

In this section, we propose an algorithm to select the antenna-elements in an XL-MIMO system for received signal processing (combiner) of a given user during the UL and transmit the signal (precoder) of this user during the DL. One advantage of not using all the M available antennas is the reduction of the computational complexity and the circuit power consumption (Tx and Rx operations), as less antennas are active at the same time. Furthermore, the throughput potentially increases, because the interference power at the receivers decreases since each antenna individually does not serve all the K users simultaneously.

3.1. HRNP-based antenna selection criterion and algorithm

First, Algorithm 1 computes the vector $\boldsymbol{\theta}_k \in \mathbb{C}^M$, which is a quantitative indicator of the quality of the channel between the kth user and each of the M antennas as:

$$\theta_{mk} = \frac{|\hat{h}_{mk}|^2}{\sum_{\substack{i=1 \\ i \neq k}}^{K} |\hat{h}_{mi}|^2}, \qquad m = 1, 2, \dots, M \tag{19}$$

where $\hat{h}_{mk} = [\hat{\mathbf{h}}_k]_m$ and $\theta_{mk} = [\boldsymbol{\theta}_k]_m$. A high signal intensity may be obtained when $|\hat{h}_{mk}|^2$ is strong. Selecting the N strongest θ_{mk} values among $m = 1, \dots, M$ in (19) for each user, provides the *highest received normalized power* (HRNP) antenna selection criterion. On the other hand, the terms $|\hat{h}_{mi}|^2$, $i \neq k$, are related to the interference intensity. Higher θ_{mk} values are therefore associated to higher SINRs on the signal detection, as defined by the Eqs. (12) and (17), and consequently higher SE and EE.

Second, the Algorithm 1 obtains the set $\mathcal{D}_k$ (lines 5–10), which contains the indices of the N antennas with the highest θ_{mk} values. Only these N antenna-elements are activated for user k. Lastly, Algorithm 1 computes the receive combining and the transmit precoding vectors of the kth user (lines 11–14) based on the matrix $\hat{\mathbf{H}}_k \in \mathbb{C}^{N \times K}$, which contains all the columns of the estimated channel $\hat{\mathbf{H}}$ but only the rows corresponding to the elements of the set $\mathcal{D}_k$.

As the set $\mathcal{D}_k$ contains the indices of the antennas that are active for the kth user, the superset $\mathcal{D} = \mathcal{D}_1 \cup \dots \cup \mathcal{D}_K$ contains

all the indices of the antennas that are active for any user. The number of elements in $\mathcal{D}$, denoted by N_{act}, corresponds to the total number of active elements of antenna. Notice that the rows of the combining and the precoding matrices corresponding to the antennas whose indices are not in the set $\mathcal{D}_k$ are set equal zero.

Algorithm 1 Antenna selection (AS) for receive combining and transmit precoding

Input: M, N, K, $\hat{\mathbf{H}}$
Output: $\mathbf{V}$, $\mathbf{W}$

1: Initialize the combining matrix $\mathbf{V}$ with $\mathbf{0}_{M\times K}$
2: **for** $k = 1$ to K **do**
3: Compute vector $\boldsymbol{\theta}_k$ via Eq. (19)
4: Reinitialize the set of the indices of the antennas: $\mathcal{M} = \{1, \ldots, M\}$
5: Initialize $\mathcal{D}_k = \emptyset$
6: **for** $n = 1$ to N **do**
7: find $m^* = \underset{m\in\mathcal{M}}{\text{argmax}}\ \theta_{mk}$
8: $\mathcal{M} = \mathcal{M}\backslash m^*$
9: $\mathcal{D}_k = \mathcal{D}_k \cup \{m^*\}$
10: **end for**
11: $\hat{\mathbf{H}}_k = \hat{\mathbf{H}}(\mathcal{D}_k, :)$
12: If MR is selected: $\mathbf{V}_{\text{MR}}(\mathcal{D}_k, k) = \hat{\mathbf{H}}_k(:, k)$
13: If ZF is selected: $\mathbf{V}_{\text{ZF}}(\mathcal{D}_k, k) = [\hat{\mathbf{H}}_k(\hat{\mathbf{H}}_k^{\text{H}}\hat{\mathbf{H}}_k)^{-1}]_{(:,k)}$
14: $\mathbf{W}(:, k) = \frac{\mathbf{V}(:,k)^*}{||\mathbf{V}(:,k)||}$
15: **end for**

3.2. Computational complexity

We first address the complexity of computing the ZF combining vectors (line 13, Algorithm 1). Recalling that $\hat{\mathbf{H}}_k \in \mathbb{C}^{N\times K}$, the multiplication of $\hat{\mathbf{H}}_k^{\text{H}}$ by $\hat{\mathbf{H}}_k$ requires $\frac{K^2+K}{2}N$ complex multiplications,[2] using the Hermitian symmetry. When the inverse of a matrix is multiplied by another matrix, the $\mathbf{LDL}^{\text{H}}$ decomposition can be used to achieve an efficient hardware implementation [6]. The decomposition of $\hat{\mathbf{H}}_k^{\text{H}}\hat{\mathbf{H}}_k$ requires $\frac{K^3-K}{3}$ complex multiplications [6]. Finally, we need to multiply the matrix $\hat{\mathbf{H}}_k$ by the kth column of the matrix $(\hat{\mathbf{H}}_k^{\text{H}}\hat{\mathbf{H}}_k)^{-1}$, which requires KN complex multiplications plus K complex divisions to compute $\mathbf{D}^{-1}$ [6,18]. Considering complex multiplications and complex divisions to correspond to 3 and 7 flops,[3] respectively, the computation of the combining vector $\mathbf{v}_k$ has a complexity of $3\left(\frac{K^2+K}{2}N + \frac{K^3-K}{3} + KN\right) + 7K$ flops per coherence block. Thus, the computational complexity to obtain the whole combining matrix $\mathbf{V}$ is given by:

$$C_{\text{SP-C}}^{\text{UL-ZF}} = K^4 + \frac{3}{2}K^3N + \frac{9}{2}K^2N + 6K^2 \qquad \text{[fpcb]} \tag{20}$$

As defined in (11), MR combining does not require multiplications or divisions, because it is given directly from the channel estimates (from Algorithm 1, one can see that the kth column of the MR combining matrix is simply a copy of the kth column of $\hat{\mathbf{H}}_k$). However, in practical implementations, we typically normalize the combining vector such that $\mathbf{v}_k^{\text{H}}\mathbf{h}_k$ in front of the desired signal x_k is close to one. Thus, this normalization requires 1 complex division per user [6], resulting in a total of $7K$ flops per coherence block. Finally, the complexity of computing the MR combining matrix is given by:

$$C_{\text{SP-C}}^{\text{UL-MR}} = 7K \qquad \text{[fpcb]} \tag{21}$$

The precoding vectors ($\mathbf{w}_k$) are chosen as the normalized versions of the combining vectors ($\mathbf{v}_k$), as described in Eq. (15). The computation of $\|\mathbf{v}_k\|$ requires $2N$ real multiplications[4] and the division of $\mathbf{v}_k$ by $\|\mathbf{v}_k\|$ also requires $2N$ real divisions,[5] resulting in a total of $4N$ flops. Thus, the computation of the precoding matrix has a complexity of:

$$C_{\text{SP-C}}^{\text{DL}} = 4KN \qquad \text{[fpcb]} \tag{22}$$

Notice that the rows of the combining and the precoding vectors of the user k that correspond to the antennas whose indices are not in the set $\mathcal{D}_k$ are set equal zero. It reduces the complexity to obtain y_k, as in (9), because the BS will use N elements of the vectors $\mathbf{v}_k$ and $\mathbf{r}$, instead of M elements, resulting in $3N$ flops. This procedure is repeated τ_{u} times per coherence block. Similarly, the complexity to precode the information during DL, $\mathbf{w}_k x_k$, following (14), is reduced since the BS only uses N elements of the vector $\mathbf{w}_k$, also resulting in $3N$ flops. This task is performed τ_{d} times per coherence block. Finally, the computational complexity associated to the reception and transmission of the information, in number of flops per coherence block, is:

$$C_{\text{SP-R/T}} = 3(\tau_{\text{u}} + \tau_{\text{d}})KN \qquad \text{[fpcb]} \tag{23}$$

To obtain θ_{mk} in (19), the BS computes $2K$ real multiplications and 1 real division. As there are M antennas and K users, the associated complexity is:

$$C_{\text{SP},\theta} = (2K + 1)MK \qquad \text{[fpcb]} \tag{24}$$

Finally, the *total signal processing computational complexity*, in flops per coherence block, when employing MR and ZF processing in the context of XL-MIMO antenna selection is given respectively by:

$$C_{\text{TSP}} = C_{\text{SP-C}}^{\text{UL-MR}} + C_{\text{SP-C}}^{\text{DL}} + C_{\text{SP-R/T}} + C_{\text{SP},\theta} \quad \text{[fpcb]} \tag{25}$$

and

$$C_{\text{TSP}} = C_{\text{SP-C}}^{\text{UL-ZF}} + C_{\text{SP-C}}^{\text{DL}} + C_{\text{SP-R/T}} + C_{\text{SP},\theta} \quad \text{[fpcb]} \tag{26}$$

Hence, if antenna selection (AS) procedure is not applied, the complexities given in (20), (22) and (23) will be higher, since all the M antennas always will be active for all the K users, *i.e.*, $N = M$.

4. SE and EE in XL-MIMO systems

The SE is defined as the sum-rate in bits per channel use [bpcu] achieved in the UL + DL, expressed as:

$$\text{SE} = \text{SE}_{\text{UL}} + \text{SE}_{\text{DL}} \qquad \text{[bpcu]} \tag{27}$$

The overall network EE can be defined as the number of bits that can be reliably transmitted per unit of energy, which is the same as the throughput per unit of power $\left[\frac{\text{bit/s}}{\text{W}}\right]$, given by:

$$\text{EE} = \frac{B\cdot\text{SE}}{P_{\text{TX}}^{\text{UL}} + P_{\text{TX}}^{\text{DL}} + P_{\text{TX}}^{\text{tr}} + P_{\text{CP}}} \qquad \left[\frac{\text{bit}}{\text{J}}\right] \tag{28}$$

[2] Being $\mathbf{A} \in \mathbb{C}^{a\times b}$ and $\mathbf{B} \in \mathbb{C}^{b\times c}$, the multiplication $\mathbf{AB}$ requires ac inner products between b-length vector, what corresponds to abc complex multiplications. However, if $\mathbf{B} = \mathbf{A}^{\text{H}}$, the Hermitian symmetry is utilized. Thus, only the a diagonal elements of $\mathbf{A}\cdot\mathbf{B}$ and half of the $a^2 - a$ off-diagonal elements need to be computed, what gives $\frac{a^2+a}{2}b$ complex multiplications [6].

[3] Considering $x = a + jb$ and $y = c + jd$, then $\frac{x}{y} = \frac{xy^*}{yy^*} = \frac{xy^*}{|y|^2}$, while the computation of xy^* requires 3 real multiplications. The computation of $|y|^2 = c^2 + d^2$ requires 2 real multiplications. Finally, the complex division $\frac{xy^*}{|y|^2}$ corresponds to 2 real divisions, making a total of 7 real operations.

[4] Consider the complex vector $\mathbf{x} = [x_1, \ldots, x_N]$. The computation of $\|\mathbf{x}\| = \sqrt{\sum_{n=1}^{N}|x_n|^2}$ depends on previously obtaining $|x_m|^2$. Being $x_n = a_n + jb_n$ a complex scalar, $|x_n|^2 = a_n^2 + b_n^2$ requires 2 real multiplications and 1 real sum. Therefore, the computation of $\|\mathbf{x}_k\|$ requires $2N$ real multiplications.

[5] The division of a complex scalar $x = a + jb$ by a real scalar c requires 2 real divisions. Therefore, the division of $\mathbf{x}$ by $\|\mathbf{x}\|$ requires $2N$ real divisions.

where the denominator includes all power consumption terms required to make the wireless communication system operational. Hence, the term

$$P_{\mathrm{TX}}^{\mathrm{tr}} = \frac{\tau_{\mathrm{p}}}{\tau_{\mathrm{c}}} \frac{1}{\eta^{\mathrm{UL}}} K p_{\mathrm{p}} \tag{29}$$

accounts for the total power consumed by the power amplifiers during the UL pilot transmission, while

$$P_{\mathrm{TX}}^{\mathrm{UL}} = \frac{\tau_{\mathrm{u}}}{\tau_{\mathrm{c}}} \frac{1}{\eta^{\mathrm{UL}}} \sum_{k=1}^{K} p_k^{\mathrm{UL}} \tag{30}$$

and

$$P_{\mathrm{TX}}^{\mathrm{DL}} = \frac{\tau_{\mathrm{d}}}{\tau_{\mathrm{c}}} \frac{1}{\eta^{\mathrm{DL}}} \sum_{k=1}^{K} p_k^{\mathrm{DL}} \tag{31}$$

refers to the UL and DL power consumed for data transmission, respectively, being η^{UL} and η^{DL} the power amplifier efficiency at the BS and at the users, respectively. P_{CP} represents the circuit power consumption. A detailed model for P_{CP} is discussed in the sequel.

4.1. Circuit power model

The following circuit power consumption model based on [6] is adopted in this work:

$$P_{\mathrm{CP}} = P_{\mathrm{FIX}} + P_{\mathrm{TC}} + P_{\mathrm{CE}} + P_{\mathrm{C/D}} + P_{\mathrm{BH}} + P_{\mathrm{SP}} \tag{32}$$

where P_{FIX} is a constant quantity. It accounts for the power consumption required for site-cooling, control signaling and load-independent power of backhaul infrastructure and baseband processors. The power consumed by the backhaul is commonly modeled as the sum of two parts: load-independent and load-dependent. The last one will be included in P_{BH}, and is typically the least significant part (around 20%) [6].

The other terms of the model represented in (32) account for the power consumption of the transceiver chains (P_{TC}), the channel estimation process (P_{CE}), the channel coding and decoding units ($P_{\mathrm{C/D}}$), the load-dependent backhaul (P_{BH}) and the linear processing at the BS (P_{LP}). Each of these terms depends on at least one of the main system parameters: M, K and the ergodic spectral efficiency (SE).

The power consumption of the transceiver chains (P_{TC}) involves the power consumed by the BS local oscillator (P_{LO}), the power required by the circuit components (converters, mixers and filters) of each BS antenna (P_{BS}) and the power necessary to run the circuit components (mixers, filters, amplifiers and oscillator) of each single-antenna user (P_{UE}), as described by the equation

$$P_{\mathrm{TC}} = P_{\mathrm{LO}} + N_{\mathrm{act}} P_{\mathrm{BS}} + K P_{\mathrm{UE}} \tag{33}$$

The computational complexity associated to the channel estimation process is given by Eq. (7). Hence, the resulting power consumption is given by[6]:

$$P_{\mathrm{CE}} = \frac{B C_{\mathrm{CE}}}{\tau_{\mathrm{c}} L_{\mathrm{BS}}} \tag{34}$$

[6] As each coherence block contains τ_{c} symbols per second, B/τ_{c} is the number of coherence blocks per second. If a given signal processing has a computational complexity denoted by C, representing the number of flops per coherence block, and L is the computational efficiency, representing the number of flops per Joule of energy, then $\frac{C}{L}$ represents the energy consumption per coherence block. Therefore, the associated power consumption is $\frac{BC}{\tau_{\mathrm{c}} L}$.

Table 1
Summary of system and channel adopted parameter values, similar to those adopted in [6,19,20].

Parameter	Value
Pathloss attenuation exponent: γ	2.5
Median channel gain at a distance of 1 m: b_0	$2.95 \cdot 10^{-4}$
Number of NLoS VRs for each user: N_{C}	3
Antenna array length: L	60 m
Number of BS antennas (ULA), M	100
Number of mobile users, K	{4; 40}
Minimum distance ($d_{\min}$)	5 m
Maximum distance ($d_{\max}$)	30 m
Number of Monte Carlo realizations: $\mathcal{T}$	1000
Transmission bandwidth: B	20 MHz
Channel coherence bandwidth: B_{C}	100 kHz
Channel coherence time: T_{C}	2 ms
Total UL noise power: σ^2_{UL}	−100 dBm
Total DL noise power: σ^2_{DL}	−80 dBm
UL pilot transmit power per user: p_{P}	0.1 W
UL data transmit power per user: p_{UL}	0.1 W
Total DL data transmit power: P_{DL}	1.0 W
Fraction of UL transmission: ϵ_{u}	0.4
Fraction of DL transmission: ϵ_{d}	0.6
Power amplifier efficiency at the users: η^{UL}	0.5
Power amplifier efficiency at the BSs: η^{DL}	0.4
Computational efficiency at the BS: L_{BS}	75 $\left[\frac{\mathrm{Gflop/s}}{\mathrm{W}}\right]$
Fixed power consumption: P_{FIX}	10 W
Power consumed by local oscillators at BS: P_{SYN}	0.2 W
Power consumed by circuit components at BS: P_{BS}	0.2 W
Power consumed by circuit components at UE: P_{UE}	0.2 W
Power density for coding of data signals: $\mathcal{P}_{\mathrm{COD}}$	0.1 $\left[\frac{\mathrm{W}}{\mathrm{Gb/s}}\right]$
Power density for decoding of data signals: $\mathcal{P}_{\mathrm{DEC}}$	0.8 $\left[\frac{\mathrm{W}}{\mathrm{Gb/s}}\right]$
Power density for backhaul traffic: $\mathcal{P}_{\mathrm{BT}}$	0.25 $\left[\frac{\mathrm{W}}{\mathrm{Gb/s}}\right]$

where L_{BS} is the computational efficiency at the BS, in [flop/s W]. Similarly, the total signal power consumption is given by:

$$P_{\mathrm{SP}} = \frac{B C_{\mathrm{TSP}}}{\tau_{\mathrm{c}} L_{\mathrm{BS}}} \tag{35}$$

The power consumed by the channel coding and decoding units is defined as

$$P_{\mathrm{C/D}} = B \ \mathrm{SE} \ (\mathcal{P}_{\mathrm{COD}} + \mathcal{P}_{\mathrm{DEC}}) \tag{36}$$

which increases linearly with the actual rates. $\mathcal{P}_{\mathrm{COD}}$ and $\mathcal{P}_{\mathrm{DEC}}$ are the coding and decoding power densities, respectively, in $\left[\frac{\mathrm{W}}{\mathrm{bit/s}}\right]$. For simplicity, $\mathcal{P}_{\mathrm{COD}}$ and $\mathcal{P}_{\mathrm{DEC}}$ are assumed to be the same in both UL and DL.

The load-dependent backhaul power consumption, necessary for the UL and DL data transmission between the BS and the core network, is modeled as

$$P_{\mathrm{BH}} = B \ \mathrm{SE} \ \mathcal{P}_{\mathrm{BT}} \tag{37}$$

where $\mathcal{P}_{\mathrm{BT}}$ is the backhaul traffic power density, in $\left[\frac{\mathrm{W}}{\mathrm{bit/s}}\right]$. There is also a load-independent backhaul power consumption, which can be included in P_{FIX}.

5. Numerical results

In the sequel we present numerical results based on Monte Carlo simulations with the objective to demonstrate that the proposed algorithm provides an EE increase while reducing considerably the computational complexity and the power consumption in the context of XL-MIMO systems. Table 1 contains a list of the main deployed parameter values, similar to those adopted in [6,19,20].

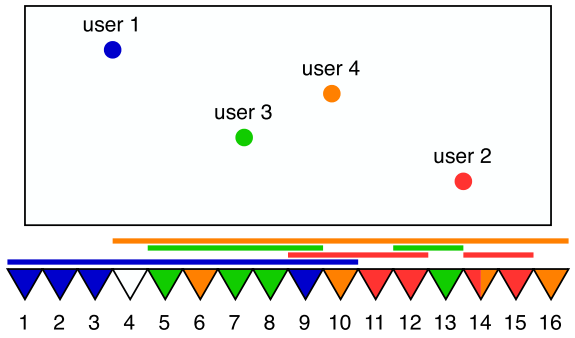

Fig. 3. Example of a XL-MIMO system, with 4 users being served by a BS equipped with a 16-antenna linear antenna array. The figure illustrates each user's VR and the antennas that the proposed algorithm designates to communicate with each user. (For interpretation of the references to color in this figure legend, the reader is referred to the web version of this article.)

Table 2
Definitions considered in Fig. 4, in [dBm].

Definition 1: UL average received signal power: $\mathcal{S}_{\text{UL}} = 10 \cdot \log_{10}\left(\frac{1}{K}\sum_{k=1}^{K}\mathbb{E}\{p_k^{\text{UL}}\lvert\mathbf{v}_k^{\text{H}}\mathbf{h}_k\rvert^2\}\right) + 30$
Definition 2: UL average received interference power $\mathcal{I}_{\text{UL}} = 10 \cdot \log_{10}\left(\frac{1}{K}\sum_{k=1}^{K}\sum_{\substack{i=1\\ i\neq k}}^{K}\mathbb{E}\{p_i^{\text{UL}}\lvert\mathbf{v}_k^{\text{H}}\mathbf{h}_i\rvert^2\}\right) + 30$
Definition 3: UL average received noise power $\mathcal{N}_{\text{UL}} = 10 \cdot \log_{10}\left(\frac{\sigma_{\text{UL}}^2}{K}\sum_{k=1}^{K}\mathbb{E}\{\lVert\mathbf{v}_k\rVert^2\}\right) + 30$
Definition 4: DL average received signal power $\mathcal{S}_{\text{DL}} = 10 \cdot \log_{10}\left(\frac{1}{K}\sum_{k=1}^{K}\mathbb{E}\{p_k^{\text{DL}}\lvert\mathbf{h}_k^{\text{H}}\mathbf{w}_k\rvert^2\}\right) + 30$
Definition 5: DL average received interference power $\mathcal{I}_{\text{DL}} = 10 \cdot \log_{10}\left(\frac{1}{K}\sum_{k=1}^{K}\sum_{\substack{i=1\\ i\neq k}}^{K}\mathbb{E}\{p_i^{\text{DL}}\lvert\mathbf{h}_k^{\text{H}}\mathbf{w}_i\rvert^2\}\right) + 30$
Definition 6: DL average received noise power $\mathcal{N}_{\text{DL}} = 10 \cdot \log_{10}\left(\sigma_{\text{DL}}^2\right) + 30$

5.1. Simulation setup and system configuration

In our simulations, the antenna array contains $M = 100$ antenna elements and each user sees the array through 3 different VRs, *i.e.*, $N_c = 3$. Furthermore, N_{ik} is taken as a uniform random variable distribution over the interval $[0.1M, 0.3M]$, while the index of the first antenna that is inside this VR, denoted by c_{ik}, follows a uniform distribution in the interval $[1, M - N_{ik}]$.

The set $\mathcal{C}_k = \mathcal{C}_{1,k} \cup \ldots \cup \mathcal{C}_{N_c,k}$ contains the indices of the antennas that sees the kth user. Thus, the number of elements in $\mathcal{C}_k$ corresponds to the total number of antennas seen by user k. We obtained this value numerically from our simulations. As well as the other numerical results presented in the paper, this value was averaged out of 1000 random realizations, obtaining the average number of active antennas for the k-user as $|\mathcal{C}| = 55.8$. It means that approximately 56 antennas are seen by each user, on average. Also from our simulations, we found that, when $K = 4$, each antenna sees an average of 2.23 users, while for $K = 40$ this number goes to 22.3, resulting in higher interference levels.

Moreover, we assume equal power allocation (EPA), what means the transmit power is the same for all users. Hence, during the UL data transmission, $p_k^{\text{UL}} = p_{\text{UL}}$, while during the DL data transmission, the total available transmit power at the BS, P_{DL}, is equally divided among the K users, so that the power allocated to the kth user is $p_k^{\text{DL}} = P_{\text{DL}}/K$. We have adopted $p_{\text{P}} = p_{\text{UL}} = 0.1$ W and $P_{\text{DL}} = 1$ W. Although the position of the users (and consequently the pathloss), the short-scale fading and the VRs are random variables, the numerical results are statically relevant because they represent an average over 1000 realizations.

Fig. 3 shows an example of the XL-MIMO system user spatial distribution, where $K = 4$ and $M = 16$, for simplicity. Each triangle represents one of the 16 BS antennas, while each colored circle represents one of the 4 mobile users, which are randomly distributed over a rectangular area. Taking a random channel realization, the portion of the array that each user sees is indicated by the horizontal line with its correspondent color. User 1, for example, sees the antennas 1 to 10, while user 2 sees the antennas 9 to 15, excepting the antenna 13. This fragmentation of the VR into two parts may occur if any object is blocking the signal in that region.

In this example, the algorithm was set up to define $N = 4$ antennas to communicate with each user. In the figure, the triangle that represents a given antenna m is painted with the user k color if user k sees antenna m. For example, antennas 1, 2, 3 and 9, which are in blue, were designated to communicate with user 1. Notice that all these 4 antennas are part of the VR of user 1. Although the signal from user 1 probably achieves the antennas 4 to 8 with higher intensity than antenna 9, choosing one of these antennas would increase the received interference power, mainly due to user 3. Observe that antenna 4 is not active, while antenna 14 serves users 2 and 4, simultaneously. Therefore, considering that only one antenna was designated to communicate with 2 users at the same time, we can say that the algorithm succeeded in avoiding the interference from other users to affect the SINR while reducing the computational complexity.

5.2. Dependency of the system performance on N

In the following, we present numerical results demonstrating how the number of active antennas per user (N) influences the system performance, in terms of throughput and EE, and the resource consumption, in terms of computational complexity and power consumption. From these results, we can see the advantages of appropriately selecting the antennas subset (AS strategy) against utilizing the whole antenna array strategy to serve all users at the same time (no-AS strategy). To refine the comprehension upon these results, which depend on the processing scheme (MR or ZF), Fig. 4 provides, for two different scenarios ($K = 4$ and $K = 40$), valuable insights on how N influences the received signal, interference and noise power, during the UL and during the DL, which are given by the definitions in Table 2.

Figs. 4a and 4b compare the UL signal, interference and noise power, as given by the definitions Def. 1 to 3, when the number of users is 4 and 40, respectively. When $N < K$, it is not possible to execute ZF, due to singularity problems with the matrix $\hat{\mathbf{H}}^{\text{H}}\hat{\mathbf{H}}$. First, one can see that the received power levels of ZF are higher than of MR. The reason is that ZF receive combining is the pseudoinverse of $\hat{\mathbf{H}}$ (recall that the elements of the channel matrix include the pathloss effect), while MR combining is simply a copy of $\hat{\mathbf{H}}$. Second, by comparing Figs. 4a and 4b, one can observe that,as expected, when $K = 40$, the received interference power ($\mathcal{I}_{\text{UL}}$) is higher than when $K = 4$, because the selectivity of the receive combining deteriorates. Third, looking at the MR curves, one can verify that, by selecting more antennas to be active for each user, the received signal power increases, but so does the interference and noise power. It does not occur when employing ZF combining. By increasing N, ZF performs better at reducing the interference and noise power, because the receive combining becomes more selective. Fourth, if the channel estimates are reliable, ZF combining will force the average received signal power ($\mathcal{S}_{\text{UL}}$) to p_{UL}, as $|\mathbf{v}_k^{\text{H}}\mathbf{h}_k|^2 = 1$, from the definition of ZF combining.

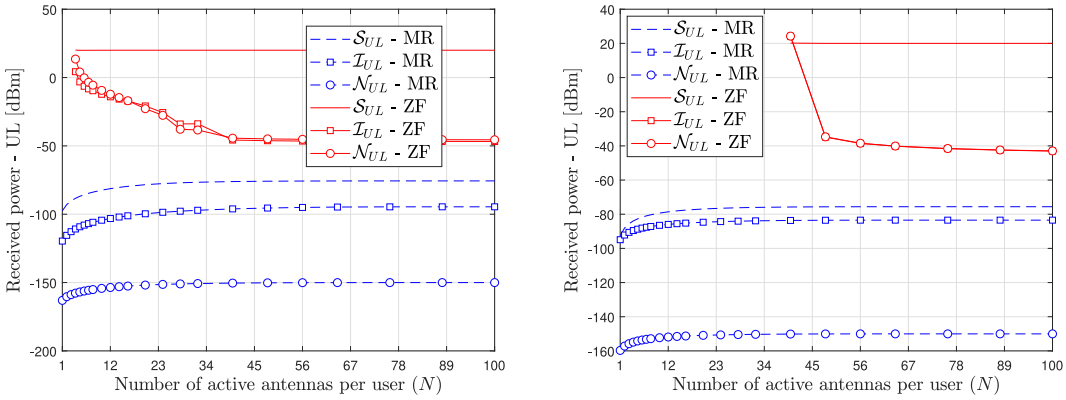

(a) UL received power, $K = 4$

(b) UL received power, $K = 40$

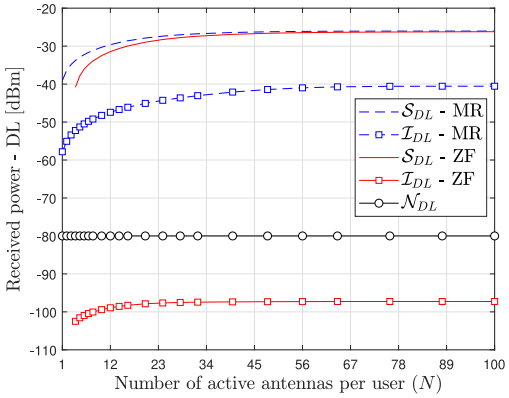

(c) DL received power, $K = 4$

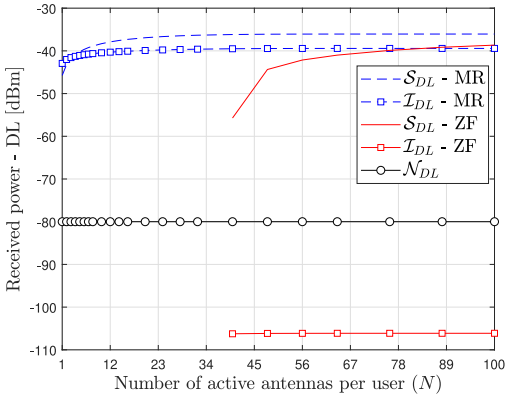

(d) DL received power, $K = 40$

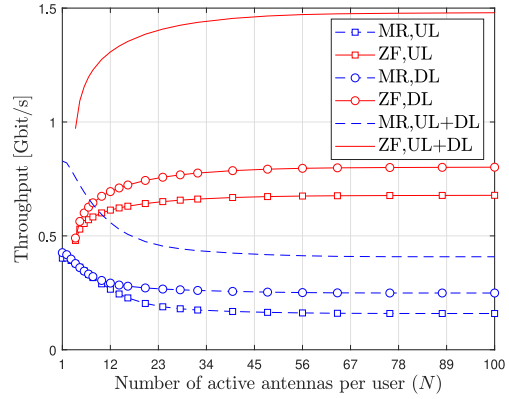

(e) Throughput, $K = 4$

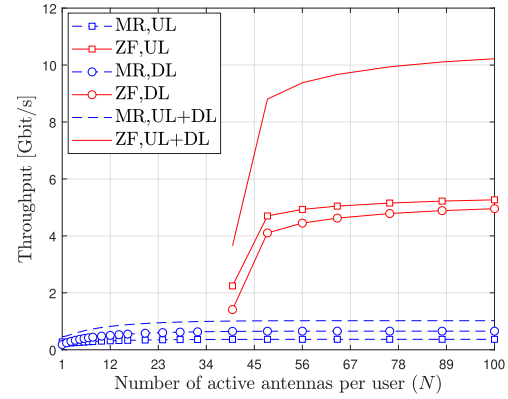

(f) Throughput, $K = 40$

Fig. 4. Average received power of the desired signal, undesired signal (interference) and noise as given by Def. 1 to 6), as well as the system throughput, during the UL and the DL data transmission. Two scenarios are considered: $K = 4$ and $K = 40$ users.

It can be observed in the figure, what attests that the channel estimation predicted by Eq. (6a) provides good estimates.

Unlike the UL case, during the DL (see Figs. 4c and 4d), the average received noise, $\mathcal{N}_{\text{DL}}$, does not depend on the precoding scheme (compare Def. 3 and 6). Another important point is that the desired signal power ($\mathcal{S}_{\text{DL}}$) is the same magnitude order for both MR and ZF, because the precoding vectors are normalized, unlike the combining vectors. Finally, as the total available DL transmit power (P_{DL}) is distributed among the K users, the individual DL transmit power (p_k^{DL}) is inversely proportional to K. That is why the average signal and interference power are smaller in Fig. 4d than in Fig. 4c. The exception is $\mathcal{I}_{\text{DL}}$ when employing MR precoding, which is less efficient than ZF at eliminating the interference.

Figs. 4e and 4f depict the UL, DL and UL + DL throughput, given by $B{\cdot}\text{SE}_{\text{UL}}$, $B{\cdot}\text{SE}_{\text{DL}}$ and $B{\cdot}\text{SE}$, respectively. The throughput resulting from the no-AS strategy can be obtained in the point $N = 100$. Thus, we can see that in a scenario with few active users, the AS strategy improves considerably the system throughput when using MR. On the other side, considering the $K = 40$ scenario, the high interference levels deteriorate the selectivity of MR combining and precoding, and the AS strategy cannot improve the throughput. The same behavior is observed with ZF processing, independently of the number of users. However, as the array is physically large and the users have a VR corresponding to around 50% of the array, on average (as discussed in the beginning of Section 5.1), increasing N beyond $M/2$ can barely improves the throughput. Thus, by taking N close to $M/2$, we can obtain almost the same throughput achieved with the no-AS strategy, as shown

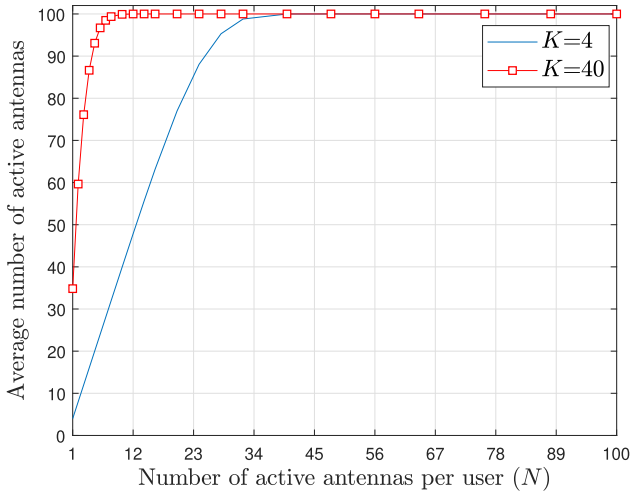

Fig. 5. Average number of active antennas per user (N) *versus* the total number of active BS antennas (N_{act}).

in Figs. 4e and 4f, while benefiting from lower computational complexity and consequently lower power consumption.

5.3. Computational complexity

While $\mathcal{D}_k$ contains the indices of the N antennas that are active for user k, the set $\mathcal{D}$ contains the indices of antennas N_{act} that are active for any of the K users. Fig. 5 addresses the dependency of N_{act} on N. In the scenario with 4 users, the whole antenna array is expected to be active when $N \geq 34$, approximately. When $K = 40$, N_{act} scales faster than when $K = 4$, and reaches the limit of 100 when $N \approx 8$. If a small N is sufficient to substantially increase the EE or throughput, one will benefit from the reduced circuit power consumption, as P_{TC} is proportional to N_{act}, according to (33). It can be evidenced by Figs. 6c and 6d that with small values of N, the AS strategy provides considerable reduction on the power consumption comparing to the entire antenna array activation (no-AS strategy).

Table 3 provides a quantitative analysis of the impact of the proposed HRNP-based AS scheme on the overall XL-MIMO computational complexity, given by $C = C_{\text{CE}} + C_{\text{TSP}}$. The complexity associated to the no-AS strategy can be obtained from (20), (21), (22) and (23) by simply replacing N with M in these equations, and canceling $C_{\text{SP},\theta}$ out in (25) and (26). The complexities are in the unit of [flop/s], which is given by BC/τ_c, recalling that C is measured in flop per coherence block [fpcb]. The first three columns of the table define four scenarios, with different values of M, N and K. The other columns contain the complexity associated to each processing scheme (MR and ZF), when using or not the AS algorithm. Notice that the algorithm yields very lower complexities, which is particularly advantageous in high system dimensions (many BS antennas and many users). Also, although providing lower throughput than ZF, one can benefit from using MR due to its much smaller complexity. However, in the fourth scenario, the AS's complexity surpasses the no-AS's when employing MR, because $C_{\text{SP},\theta}$ is the only term of C_{TSP} that is proportional to K^2. It does not occur with ZF, as the term $C_{\text{SP-C}}^{\text{UL-ZF}}$ is much more significative than $C_{\text{SP},\theta}$.

Fig. 6a shows the linear dependency of the computational complexity on N and the remarkable computational complexity reduction provided by the adopted AS strategy. As a consequence, there is also a reduction in the total power consumption, defined as $P_{\text{tot}} = P_{\text{TX}}^{\text{UL}} + P_{\text{TX}}^{\text{DL}} + P_{\text{TX}}^{\text{tr}} + P_{\text{CP}}$, as depicted in Fig. 6c. Moreover, Fig. 6b reveals a significant complexity increase when the number of active users grows from 4 to 40. Furthermore, by avoiding all antennas to be simultaneously active, the adopted HRNP-AS strategy in Eq. (19) reduces the transceiver chains power consumption,[7] and consequently the total power consumption, as indicated in Figs. 6c and 6d. As a final remark on the advantage in adopting the HRNP-AS strategy is the operation point where the AS power consumption curves meet the no-AS curves is very close to the point where the average number of active antennas meet M in Fig. 5.

Table 3
AS computational complexity in [Gflop/s], discriminated by processing scheme.

M	N	K	no-AS MR	AS MR	no-AS ZF	AS ZF
32	4	2	4	1	4	1
128	16	8	62	12	76	14
512	64	32	990	369	3,848	819
2048	256	128	15,834	17,551	702,031	126,822

Table 4
Optimal number of selected antennas for maximizing the EE (N^*) *versus* the number of active users.

	K	2	4	**6**	8	10	12	16	**20**	24	32	40	50
N^*	MR	3	1	1	1	1	1	1	**1**	48	48	48	47
	ZF	5	6	**8**	64	62	60	58	57	57	60	65	75

5.4. Energy efficiency

Fig. 7 confirms the EE improvement when AS strategy based on highest received power is adopted. Under reduced loading scenario ($K = 4$), the EE is maximized when $N = 6$ and $N = 1$ for ZF and MR, respectively. It demonstrates that the HRNP-AS strategy can guarantee huge EE improvements in a scenario with few users, while reducing considerably the power consumption and the computational burden, as discussed above. On the other hand, results in Fig. 7b demonstrate that, the AS strategy cannot improve the EE considerably when XL-MIMO operates under high loading scenarios ($K = 40$). However, the HRNP-based AS strategy is still advantageous over the no-AS strategy, as it still provides a considerable complexity reduction. Thus, regardless of the number of users, it is not reasonable to use the whole antenna array to serve all users if about half of the antennas is sufficient to achieve a remarkable EE increasing with a lower computational complexity.

5.5. Overall XL-MIMO performance comparison

Table 4 shows the optimal number of selected antennas (N^*) that maximizes the EE, when employing both linear MR or ZF filtering. According to the data, N^* is strongly influenced by the number of active users K. As a rule of thumb, when the number of active users is up to a limit, namely $K_{\max}$, the EE is maximized when the AS algorithm selects less than 10% of the antenna array to communicate with each user, *i.e.*, $N^* \leq M/10$. From the data in Table 4, we see that $K_{\max} = 20$ for MR and $K_{\max} = 6$ for ZF.

Figs. 8a, 8b, 8c and 8d depict the EE, throughput, power consumption and computational complexity, respectively, for the proposed HRNP-AS and no-AS strategy assuming $N = N^*$. If the system operates under the bound $K \leq K_{\max}$, the HRNP-AS strategy provides an increasing in the EE and simultaneously reduces the power consumption and the computational burden, while the throughput is very close to the obtained with the no-AS strategy.

[7] Notice that from (33), power consumption is linearly dependent on N_{act}.

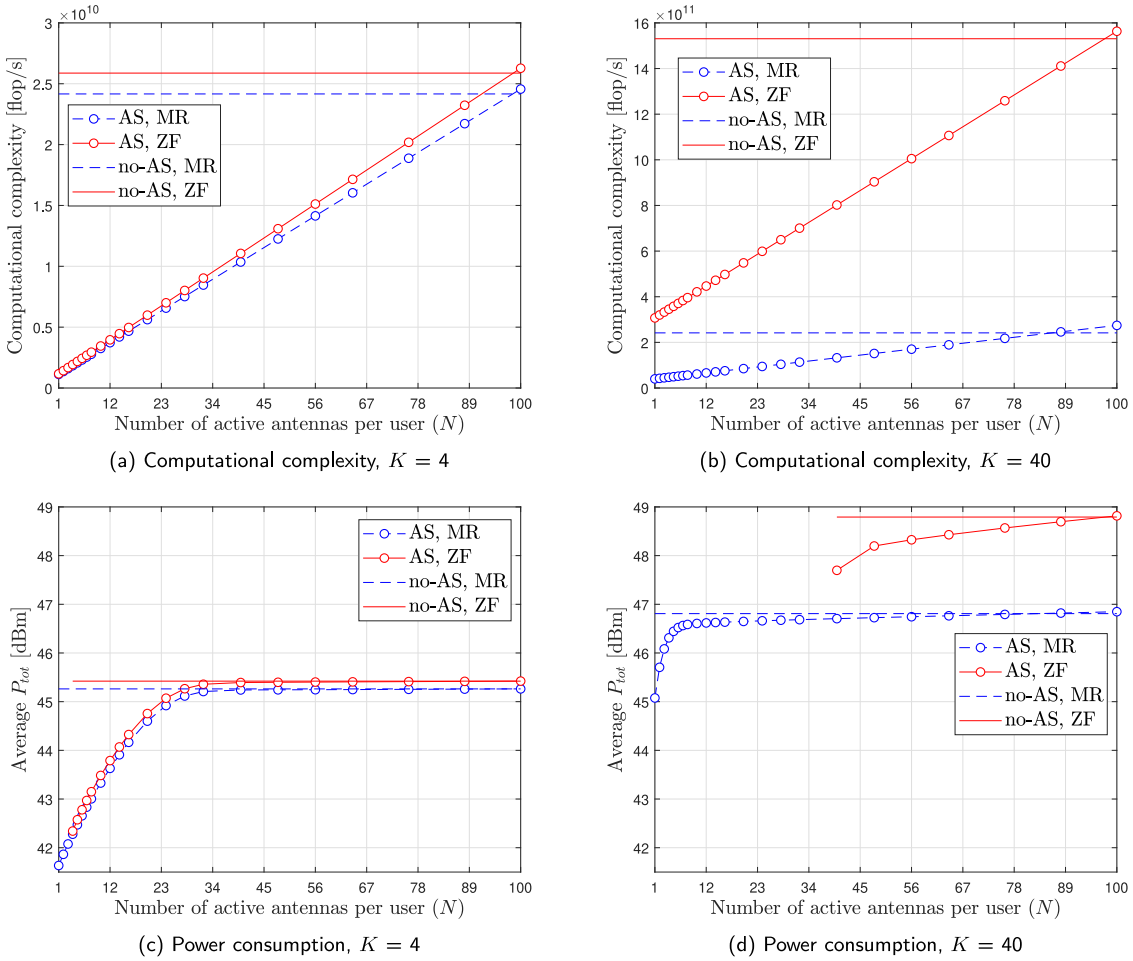

(a) Computational complexity, $K = 4$ (b) Computational complexity, $K = 40$

(c) Power consumption, $K = 4$ (d) Power consumption, $K = 40$

Fig. 6. The average consumption of computational and power resources raises when increasing N, while depends on the adopted AS strategy.

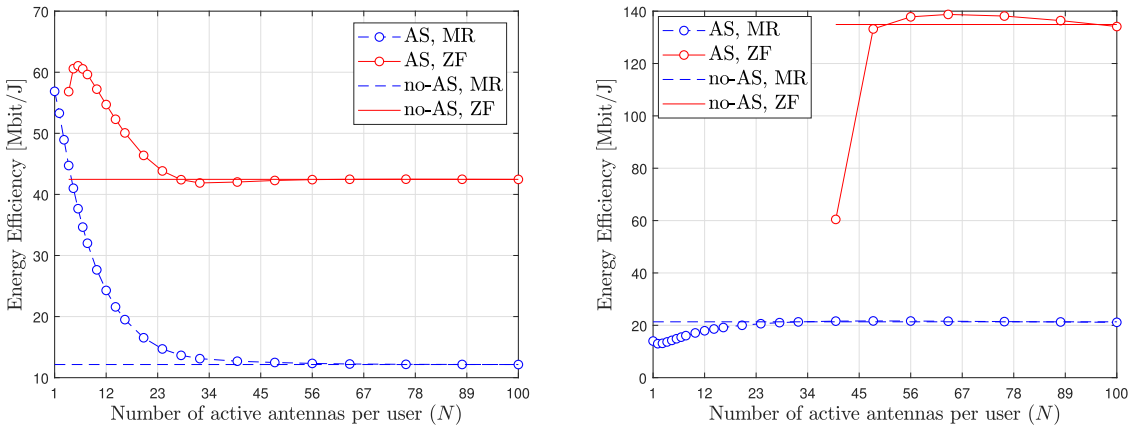

(a) $K = 4$ (b) $K = 40$

Fig. 7. Energy efficiency as a function of N, in both low and high loading scenarios: $K = 4$ and $K = 40$.

Besides, when increasing K until it is close to $K_{\max}$, the EE gradually decreases until it meets the no-AS strategy EE curve. It occurs because taking $N \leq M/10$ is no longer enough to mitigate the interference. Besides, from the point $K = K_{\max}$, N^* suddenly jumps to about 50 or 60% of the ULA array size, $M = 100$. Finally, when the XL-MIMO system operates over the maximum number of user bound, $K > K_{\max}$, the AS-strategy is no longer able to improve the EE and simultaneously reduce the power consumption considerably. However, it is still advantageous when compared to the all-antennas activation strategy, as it is still able to reduce the computational burden.

6. Conclusion

In XL-MIMO systems operating under non-stationary channels, the users see only a portion of the antenna array and the majority of the energy sent by the users is concentrated on this part of the array. Therefore, by appropriately selecting a

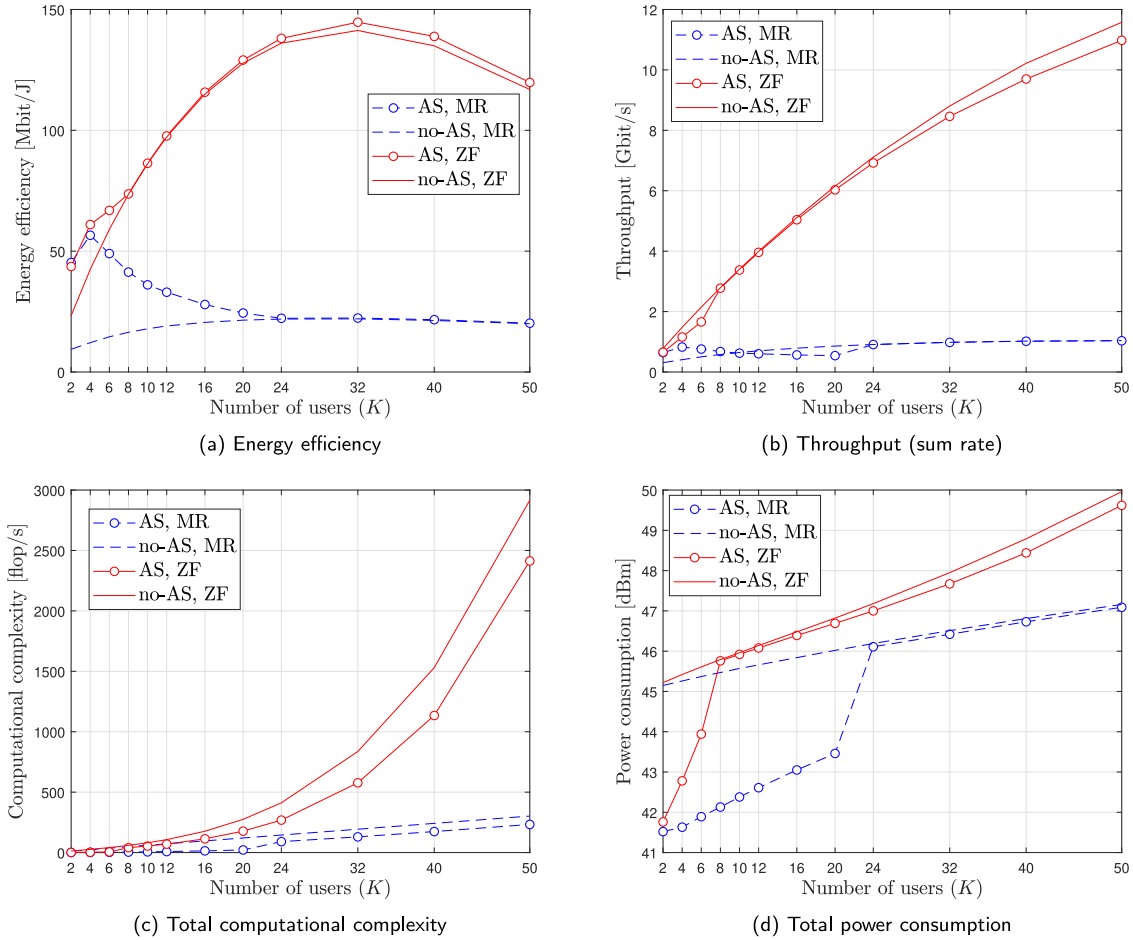

(a) Energy efficiency

(b) Throughput (sum rate)

(c) Total computational complexity

(d) Total power consumption

Fig. 8. EE, throughput, power consumption and computational complexity for the HRNP-AS and no-AS strategies taking $N = N^*$.

subset of antennas that communicate to each user, it can be guaranteed to capture almost the totality of the incident energy from that user, while reducing substantially the interference coming from the other $(K - 1)$ users. As corroborated by extensive numerical results, the HRNP antenna selection criterion reduces considerably the complexity of computing the combiners and precoders and consequently reducing the power consumption also. Furthermore, when the AS-HRNP algorithm is set to select only a few N antennas per user, there may be several antennas which are not activated, reducing the transceiver chains power consumption. As the HRNP-based AS strategy results in almost the same spectral efficiency as the no-AS strategy and a considerable substantial power consumption reduction, as a result, the EE is increased significantly. Furthermore, the extensive numerical results demonstrated the existence of an optimal value of N in terms of maximizing the EE, which depends on the number of users and array size. Also, it is not even advantageous to increase N beyond this optimal value, since neither the throughput nor the EE would be considerably improved while computational burden and energy consumption increases remarkably.

CRediT authorship contribution statement

Gabriel Avanzi Ubiali: Conception and design of study, Acquisition of data, Analysis and/or interpretation of data, Drafting the manuscript, Revising the manuscript, Approval of the version of the manuscript to be published. **Taufik Abrão:** Conception and design of study, Acquisition of data, Analysis and/or interpretation of data, Drafting the manuscript, Revising the manuscript, Approval of the version of the manuscript to be published.

Declaration of competing interest

The authors declare that they have no known competing financial interests or personal relationships that could have appeared to influence the work reported in this paper.

Acknowledgments

This study was financed in part by the Coordenacão de Aperfeicoamento de Pessoal de Nível Superior – Brazil (CAPES) – Finance Code 001; in part it was supported by the National Council for Scientific and Technological Development (CNPq) of Brazil under Grants 304066/2015-0 and 404079/2016-4; in part by Londrina State University, Paraná State Government (UEL).

References

[1] F. Boccardi, R.W. Heath, A. Lozano, T.L. Marzetta, P. Popovski, Five disruptive technology directions for 5g, IEEE Commun. Mag. 52 (2) (2014) 74–80.

[2] T.L. Marzetta, Noncooperative cellular wireless with unlimited numbers of base station antennas, IEEE Trans. Wireless Commun. 9 (11) (2010) 3590–3600.

[3] T. Marzetta, E. Larsson, H. Yang, H. Ngo, Fundamentals of Massive MIMO, in: Fundamentals of Massive MIMO, Cambridge University Press, 2016, [Online]. Available: https://books.google.com.br/books?id=IM0iDQAAQBAJ.

[4] A. Chockalingam, B.S. Rajan, Large MIMO Systems, Cambridge University Press, 2014.

[5] E. de Carvalho, A. Ali, A. Amiri, M. Angjelichinoski, R.W.H. Jr., Non-stationarities in extra-large scale massive MIMO, 2019, CoRR abs/1903.03085, [Online]. Available: http://arxiv.org/abs/1903.03085.

[6] E. Björnson, J. Hoydis, L. Sanguinetti, Massive MIMO networks: Spectral, energy, and hardware efficiency, Found. Trends Signal Process. 11 (3–4) (2017) 154–655, [Online]. Available: http://dx.doi.org/10.1561/2000000093.
[7] H. Wang, A. Kosasih, C. Wen, S. Jin, W. Hardjawana, Expectation propagation detector for extra-large scale massive mimo, IEEE Trans. Wireless Commun. 19 (3) (2020) 2036–2051.
[8] S. Hou, Y. Wang, T. Zeng, S. Wu, Sparse channel estimation for spatial non-stationary massive mimo channels, IEEE Commun. Lett. 24 (3) (2020) 681–684.
[9] J. Li, B. Ai, R. He, M. Yang, Z. Zhong, Y. Hao, G. Shi, The 3d spatial non-stationarity and spherical wavefront in massive mimo channel measurement, in: 2018 10th International Conference on Wireless Communications and Signal Processing (WCSP), 2018, pp. 1–6.
[10] J. Chen, X. Yin, X. Cai, S. Wang, Measurement-based massive mimo channel modeling for outdoor los and nlos environments, IEEE Access 5 (2017) 2126–2140.
[11] A. Ali, E.D. Carvalho, R.W. Heath, Linear receivers in non-stationary massive mimo channels with visibility regions, IEEE Wirel. Commun. Lett. 8 (3) (2019) 885–888.
[12] A. Amiri, M. Angjelichinoski, E. de Carvalho, R.W. Heath, Extremely large aperture massive mimo: Low complexity receiver architectures, in: 2018 IEEE Globecom Workshops (GC Wkshps), 2018, pp. 1–6.
[13] J. Flordelis, X. Li, O. Edfors, F. Tufvesson, Massive mimo extensions to the cost 2100 channel model: Modeling and validation, IEEE Trans. Wireless Commun. 19 (1) (2020) 380–394.
[14] Y. Huang, S. He, J. Wang, J. Zhu, Spectral and energy efficiency tradeoff for massive mimo systems, IEEE Trans. Veh. Technol. (2018) 1.
[15] Y. Han, S. Jin, C. Wen, X. Ma, Channel estimation for extremely large-scale massive mimo systems, IEEE Wirel. Commun. Lett. (2020) 1.
[16] A. Amiri, C.N. Manch'on, E. de Carvalho, Deep learning based spatial user mapping on extra large mimo arrays, 2020.
[17] J. Flordelis, F. Rusek, F. Tufvesson, E.G. Larsson, O. Edfors, Massive mimo performance—tdd versus fdd: What do measurements say?, IEEE Trans. Wireless Commun. 17 (4) (2018) 2247–2261.
[18] S. Boyd, L. Vandenberghe, Convex Optimization, Cambridge University Press, 2004.
[19] E. Björnson, L. Sanguinetti, J. Hoydis, M. Debbah, Optimal design of energy-efficient multi-user mimo systems: Is massive mimo the answer?, IEEE Trans. Wireless Commun. 14 (6) (2015) 3059–3075.
[20] J.C.M. Filho, C. Panazio, T. Abrão, S. Tomasin, Total energy efficiency of tr-mrc and fd-mrc receivers for massive mimo uplink, IEEE Syst. J. 13 (3) (2019) 2285–2296.

Gabriel Avanzi Ubiali received the B.S. in electrical engineering from the Londrina State University, Parana, Brazil in 2017 and M.S. degree in electrical engineering from the same university, in 2020. He is currently pursuing his Ph.D. Degree in Electrical Engineering at the doctorate program Londrina State University (UEL)/UTFPR-CP association, Brazil. His research interest includes optimization wireless communication aspects involving resource allocation and energy efficiency. Besides, it has been dealing with the concept and implementation of new heuristic methods based on artificial intelligence.

Taufik Abrão (IEEE-SM'12, SM-SBrT) received the B.S., M.Sc., and Ph.D. degrees in electrical engineering from the Polytechnic School of the University of São Paulo, Brazil, in 1992, 1996, and 2001, respectively. Since March 1997, he has been with the Communications Group, Department of Electrical Engineering, Londrina State University, Londrina, Brazil, where he is currently an Associate Professor of Communications Engineering and the head of the Telecommunication and Signal Processing Group. He has been a Guest Researcher in the Connectivity Group at Aalborg University, DK (July–Oct. 2018). In 2012, he was an Academic Visitor with the Communications, Signal Processing, and Control Research Group, University of Southampton, Southampton, U.K. From 2007 to 2008 he was a Postdoctoral Researcher with the Department of Signal Theory and Communications, Polytechnic University of Catalonia (TSC/UPC), Barcelona, Spain. He has participated in several projects funded by government agencies and industrial companies. He has supervised 24 M.Sc., five Ph.D. students, and two postdocs. He has co-authored 11 book chapters on mobile radio communications He is involved in editorial board activities of six journals in the wireless communication area, and he has served as TCP member in several symposium and conferences. He has been served as an Editor for the IEEE Communications Surveys & Tutorials since 2013, IET Journal of Engineering since 2014, and IEEE Access since 2016 and Transactions on Emerging Telecommunications Technologies (ETT-Wiley) since 2018. He is a senior member of IEEE and SBrT-Brazil. His current research interests include communications and signal processing, especially in massive MIMO multiuser detection and estimation, ultra-reliable low latency communications (URLLC), machine-type communication (MTC), resource allocation, as well as heuristic and convex optimization aspects of 4G and 5G wireless systems. He has co-authored +240 research papers published in specialized/international journals and conferences.

APPENDIX B – Full paper published in the journal "International Journal of Electronics and Communications"

Int. J. Electron. Commun. (AEÜ) 130 (2021) 153568

Contents lists available at ScienceDirect

International Journal of Electronics and Communications

journal homepage: www.elsevier.com/locate/aeue

Regular paper

Energy-efficient flexible and fixed antenna selection methods for XL-MIMO systems

Gabriel Avanzi Ubiali [a], José Carlos Marinello [b], Taufik Abrão [a,*]

[a] Electrical Engineering Department, State University of Londrina, PR, Brazil
[b] Electrical Engineering Department, Federal University of Technology PR, Cornélio Procópio, PR CEP: 86300-000, Brazil

ARTICLE INFO

Keywords:
Extra-large-scale antenna array
Non-stationary channels
Near-field propagation
Spherical wavefront
Energy efficiency
Spectral efficiency

ABSTRACT

Massive multiple-input multiple-output (M-MIMO) is a key technology for 5G networks which consists on equipping the base station (BS) with hundreds or thousands of antennas. Increasing the antenna separation is paramount in order to make real advantage from an array dimension of the order of thousands of antennas. One potential approach is the integration of the antenna array into large structures, which is referred to as extra-large-scale MIMO (XL-MIMO). However, when employing extremely large arrays, centralized processing architectures face a challenging complexity. A promising solution is to divide the antenna array into disjoint units, referred to as subarrays, with individual processing units. In this paper, we modify the M-MIMO channel model aiming to take two implications of the extreme array dimensions into account: the spherical wavefronts, which is called near-field propagation, and the concentration of the majority of energy received from a specific user on a small portion of the array, namely spatial non-stationarity. Considering the latter, it is not efficient from an energy perspective to activate the antennas with lower channel gains to transmit/receive the signal to/from a given user. Thus, antenna selection methods are quite important in the considered scenario. Two antenna selection (AS) methods for XL-MIMO are proposed in this paper: the adjustable-flexible antenna selection (FAS), and the fixed subarray selection (FSS). Numerical results demonstrate that, by judiciously selecting the antennas subset used to detect the signal of each user in the uplink (UL), the number of active antennas can be reduced considerably in a scenario with up to 64 active users, reducing the power consumption without compromising the throughput. The EE is hugely increased in such scenario. Finally, the FSS scheme achieved the same performance of FAS, while having a simpler hardware implementation.

1. Introduction

Mobile networks have expanded recently with the objective of improving capacity and providing ubiquitous connectivity. Multiple-input multiple-output (MIMO) antenna systems permit multiple users to transmit simultaneously in the same bandwidth, avoiding the addition of extra resources to the network, such as spectrum and energy [1]. This is possible as each mobile user equipment (UE) is given a different spatial signature [2]. During the uplink (UL), a combining technique is employed by the base station (BS) to coherently receive the signal sent by each user. During the downlink (DL) the information to be transmitted is precoded, so that the multipath components of the transmitted signal combine coherently at the users [1].

Massive MIMO (M-MIMO) is considered a crucial component for fulfilling the demands of the fifth generation (5G) wireless communication standard and beyond [3]. The M-MIMO base station is equipped with tens or hundreds of antennas, which is central to provide sufficient spatial dimensions to uncover the M-MIMO fundamental properties: channel hardening, large array gain and asymptotic inter-terminal channel orthogonality [4]. Specifically, having an order of thousands or more antenna elements provides extreme spatial resolution that can be used to boost both capacity and energy efficiency (EE).

However, practical challenges appear when the array dimension is increased to the order of thousands or more, such as the size and weight of the array [5], as current cellular networks deploy compact and colocated antenna array, with antenna separation in the order of the wavelength. Moreover, in order to make real advantage from the deployment of such a large number of antenna elements, a proper antenna separation is important to achieve great spatial resolution [6]. These difficulties advocate for distributing the antennas over a

* Corresponding author.
E-mail addresses: g.avanziubiali@gmail.com (G.A. Ubiali), jcmarinello@utfpr.edu.br (J.C. Marinello), taufik@uel.br (T. Abrão).

https://doi.org/10.1016/j.aeue.2020.153568
Received 27 September 2020; Accepted 26 November 2020
Available online 23 December 2020

substantially large area. One potential approach is to divide the antenna array into disjoint subsets of antennas and distributing them over a large area, coordinated by a central processing unit (CPU), which is known as distributed M-MIMO [5]. Another approach, called extra-large-scale M-MIMO (XL-MIMO), is the integration of the antenna array into large structures, such as the facades of buildings, shopping malls or stadiums [4]. In this work, we stick to the latter.

When a moderate number of antennas is compactly deployed in the BS, the wavefront from a far user signal can be reasonably approximated as planar wavefront, while the channel is spatially stationary, which means that the entire array receives approximately the same amount of energy from each user [7]. On the other hand, an antenna array with extreme dimensions yields different channel conditions. As the availability of sufficiently accurate propagation channel models is of critical importance to the design and evaluation of new wireless systems [8], one must take such conditions into account in order to define a consistent channel model. First, due to the use of large aperture arrays and the close distance between the array and the users' antenna, the BS antenna array will experience spherical wavefronts instead of planar wavefronts [9], which is called *near-field propagation*.

Second, in large aperture arrays, different parts of the array might observe the same propagation paths with varying power or distinct propagation paths [4]. Consequently, the majority of energy received from a specific user concentrates on small portions of the antenna array [10,11], according to recent channel measurements [12–14]. It is called spatial *non-stationarity*, and such channel property can be introduced in the M-MIMO and XL-MIMO channel modelling by defining the concept of *visibility region* (VR). In the sequel, we discuss these two additional aspects on the propagation pattern and the concept of VR, specifically in Section 2, where we modify the traditional M-MIMO channel model in order to aggregate the spherical wavefront and the spatial non-stationarity assumptions.

When employing extremely large arrays, saying a thousands of antenna-elements, the computational complexity for signal processing becomes a bottleneck if a centralized processing architecture is implemented, specially in crowded scenarios, due to the excessively large amounts of data being transferred from the array and the processing unit [5]. A promising solution is to divide the antenna array into subarrays, which are disjoint units with individual processing units that accesses only its locally received signals to estimate them [5] , consequently reducing the complexity. The number and size of subarrays may be fixed, when they correspond to separate hardware entities, or adjustable, when they correspond to software-defined logical interconnections between different antenna elements [5].

Numerous benefits arise from the subarray-based processing architecture, including: **a**) *Simplification of the channel acquisition:* as the channel of each subarray individually can be approximated as stationary, one can simply apply MMSE channel estimation, which is known to provide very good channel estimation quality in stationary channels. Furthermore, as the channel matrix is divided into multiple submatrices and each one is estimated individually, the associated computational complexity is reduced. **b**) *Computational complexity reduction:* due to the spatial non-stationarities along the array, the energy received from each user is mostly concentrated in small portions of the array. Thus, the majority of the energy coming from that user can be received by using only a few antennas, instead of the whole antenna array. Hence, the complexity associated to computing the combining matrix, as well as the complexity associated to the UL reception and DL transmission, decreases. **c**) *Energy saving:* the channel estimation and signal processing power consumption decreases, due to the reduction in the computational complexity associated to tasks such as signal processing and channel estimation.

By appropriately selecting a subset of BS antennas to communicate to each user, the BS may receive almost the totality of the energy transmitted by a specific user, while reducing the interference coming from the other users. Consequently, although less antennas participate in the signal detection, the SE is not compromised, while the power consumption considerably decreases. As a result, such AS configuration attains higher EE. Aside the necessity of improving SE, minimizing the power consumption is a growing concern in the XL-MIMO implementation systems, including green communication technologies issues [15]. The EE is a performance metric that can manage both objectives. For this reason, the numerical results in Section 5 discuss both SE and EE. Finally, one can summarise the aforementioned benefits from the subarray-based architecture and a judicious antenna selection as: 1) simplification of the channel acquisition; 2) computational complexity reduction; 3) energy saving; and increased; 4) SE; and (5) EE.

1.1. Contribution and related works

This work deals with XL-MIMO systems with subarray-based processing architecture, in order to reduce the overall computational complexity while ensuring increasing EE and SE. We propose two novel algorithms to judiciously select the BS antennas that communicate with each user, aiming at obtaining higher SE and EE and reducing the power, when compared to the whole antenna array to communicate to every user. The *flexible antenna selection* (FAS) algorithm assigns the BS subset of antennas to perform receive combining and transmit precoding to each user. The *fixed subarray selection* (FSS) algorithm divides the antenna array into a number of fixed-size subarrays, which can be implemented in a distributed way, as separate hardware entities, while selecting one of the subarrays to communicate with each user. The FAS algorithm is expected to achieve higher SE and EE than the FSS algorithm, since there are more freedom degrees. However, FSS ensures smaller computational complexity and a simpler hardware implementation.

Related works. The spatial non-stationarity impact on the SINR performance is analysed in [10]. In [4], authors show that, when M-MIMO systems operate in extra-large scale regime, several important MIMO design aspects change, due to spatial non-stationarities. In [11], three low-complexity data detection algorithms are proposed for uplink communication in XL-MIMO systems. Efficient detector for XL-MIMO systems based on the subarray processing architecture is proposed in [5], by extending the application of the expectation propagation principle to each subarray. A different approach to the AS in XL-MIMO is proposed in [16], which is based on machine learning to select a small portion of the array that contains a considerable portion of beamforming energy, aiming at overcoming the prohibitive antenna activation consumption/complexity in conventional XL-MIMO systems.

Differently of our previous work in [17], herein the FAS and FSS schemes does not select a fixed number of antennas for every user. Thus, such AS schemes proceed with a flexible antenna selection based on cumulative power receiver signal, being able to provide a higher EE increase over antenna selection strategy suggested in [17]. The proposed FAS and FSS schemes may select only a few antennas (flexible) if the energy coming from an individual user signal is concentrated over a small portion of the array, for example. Also, herein we adopt a more realistic XL-MIMO channel model, considering a much larger number of antennas (1000 instead of 100 adopted in [17]). Moreover, the numerical results discussed herein cannot be directly compared to the ones in [17], as the system parameters configuration are quite different, including number of antennas, array length, antenna separation and channel model.

Contributions. The contributions of this work are threefold: *i*) we propose two novel antenna selection procedures to improve SE and EE of XL-MIMO systems while reduce the computational complexity and the power consumption, using a detailed circuit power consumption model. *ii*) we also propose a simplified but consistent XL-MIMO channel model that takes into account the spatial non-stationarity and the near-field propagation assumptions. *iii*) we have developed a comprehensive analysis on how each proposed AS algorithm impacts on the system performance, highlighting the benefits arising from the algorithms

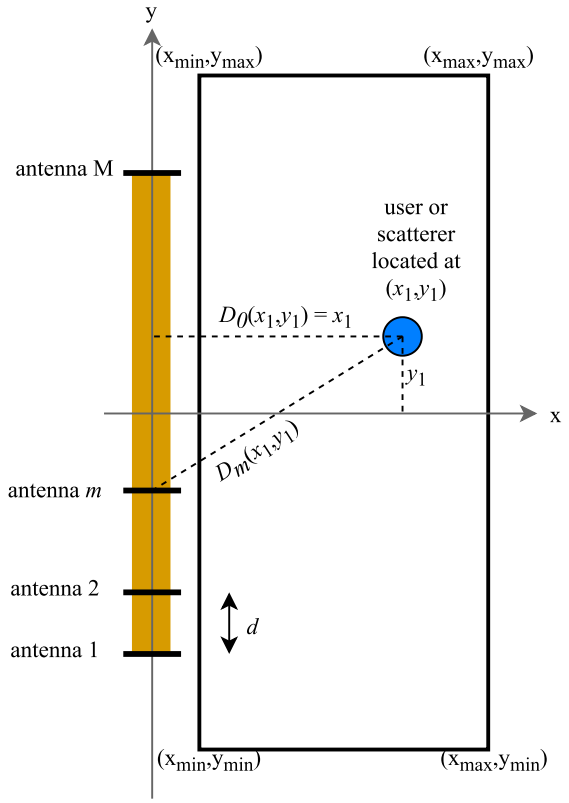

Fig. 1. XL-MIMO system representation: xy-coordinates, with the ULA situated over the y-axis and the user located inside a rectangular cell, positioned in (x_1, y_1). $D_0(x,y)$ is the distance between the user and the array; $D_m(x,y)$ is the distance between the user and the m-th antenna element, while d denotes the antenna separation.

compared to the case of using the whole antenna array to communicate to every user.

The next sections are organized as follows. The system model for the TDD XL-MIMO system is developed in Section 2, which describes the proposed channel model, the channel estimation process and the adopted power consumption model. The proposed flexible antenna selection and fixed subarray selection algorithms are presented in the Sections 3.1 and 3.2, respectively. Computational complexity corresponding to each algorithm is discussed in Section 4. Numerical results corroborating our findings are presented in Section 5 and Section 6 shows the head conclusions.

Notations. Throughout the paper, boldface lowercase letters, boldface uppercase letters and calligraphic letters represent, respectively, column vectors, matrices and sets, while $(.)^{\mathrm{T}}$ and $(.)^{\mathrm{H}}$ denote the transpose and conjugate transpose (Hermitian) operators, respectively. $\mathbf{I}$ and $\mathbf{A}^{-1}$ denote the identity matrix and the inverse of matrix $\mathbf{A}$, respectively, while $\|\mathbf{a}\|$ represents the norm-2 of the vector $\mathbf{a}$ and both a_i and $[\mathbf{a}]_i$ correspond to its i-th element. The (i,j)-th element of the matrix $\mathbf{A}$ is denoted by a_{ij}, the k-th row of $\mathbf{A}$ is denoted by $\mathbf{A}_{(k,:)}$, and the k-th column of $\mathbf{A}$ is denoted by both $\mathbf{A}_{(:,k)}$ and $\mathbf{a}_k$. We denote the submatrix of A containing only the rows (columns) whose indices are in the set $\mathcal{D}$ by $\mathbf{A}_{(\mathcal{D},:)}$ ($\mathbf{A}_{(:,\mathcal{D})}$). Finally, $|\mathcal{D}|$, $\mathbb{E}\{\cdot\}$ and $\odot$ stand for the cardinality of the set $\mathcal{D}$, the expectation operator and the element-wise matrix product.

2. System model

We consider the UL of a single-cell multiuser XL-MIMO system with M-antenna BS and K single-antenna users, operating over a bandwidth of B Hz in the time-division duplex (TDD) operation mode. Due to channel reciprocity, TDD mode does not require CSI to be sent from the UEs to the BS via feedback, avoiding excessive overhead [18,19]. Channel state information (CSI) is acquired via UL synchronous pilot transmission, and the pilot sequences are taken from the same pilot codebook. Their length is denoted by τ_{p} and they form an orthogonal set. Herein, it is assumed that each user uses a different pilot sequence. Then, the pilot sequences' set is $\mathbf{\Psi} = [\boldsymbol{\psi}_1 \ldots \boldsymbol{\psi}_K] \in \mathbb{C}^{\tau_{\mathrm{p}} \times K}$ and the orthogonality condition states that $\mathbf{\Psi}^{\mathrm{H}}\mathbf{\Psi} = \tau_{\mathrm{p}}\mathbf{I}_{\tau_{\mathrm{p}}}$, *i.e.*:

$$\boldsymbol{\psi}_i^{\mathrm{H}}\boldsymbol{\psi}_k = \begin{cases} \tau_{\mathrm{p}} & i = k, \\ 0 & i \neq k. \end{cases} \tag{1}$$

The channel coherence time (T_{C}) is divided into UL pilot and UL data transmission. Being B_{C} the coherence bandwidth, the number of symbols that fits in a channel coherence block is determined by $\tau_{\mathrm{c}} = T_{\mathrm{C}}B_{\mathrm{C}}$, in which τ_{p} symbols are dedicated to UL pilot transmission and $\tau_{\mathrm{u}} = \tau_{\mathrm{c}} - \tau_{\mathrm{p}}$ symbols are dedicated to UL data transmission [1]. During the UL pilot transmission, a different pilot sequence is assigned to each user. The number of available orthogonal pilot sequences is equal their length (τ_{p}). As we need K sequences, we can take $\tau_{\mathrm{p}} = K$, which means that the time required for pilots is proportional to K. Thus, the number of users that can be served is limited by the coherence time, which itself depends on the mobility of the users [1].

We consider a BS equipped with an M antenna elements uniformly and linearly arranged (ULA array). The distance between two adjacent ULA elements is d. Fig. 1 depicts the ULA lying along the y-axis of an xy coordinate system and centered at its origin. Therefore, the m-th antenna is located at $\left[0,\ \left(m - \frac{M+1}{2}\right)d\right]$. Users are located in the positive x-axis region, inside the rectangular cell defined by $\mathrm{x_{min}} \leqslant x \leqslant \mathrm{x_{max}}$, $x > 0$, and $\mathrm{y_{min}} \leqslant y \leqslant \mathrm{y_{max}}$, being (x,y) the coordinates of the user. The distance between any point (x,y) and the antenna array is $D_0(x,y) = x$ and the distance to the m-th antenna is

$$D_m\left(x,y\right) = \sqrt{x^2 + \left(y - d\left(m - \frac{M+1}{2}\right)\right)^2} \tag{2}$$

2.1. XL-MIMO channel

The XL-MIMO channel model takes into consideration the spherical wavefront assumption and the spatial non-stationarities.

Near-field propagation. The spherical wavefront causes the signal to arrive with different angles along the antenna array, and consequently with different intensities. Furthermore, the distance between a scatterer or user located at the point (x,y) and the antenna array varies significantly on the antenna index. We can model these properties associated with spherical wavefront assumption deploying the *array response* vector $\mathbf{a}(x,y) \in \mathbb{C}^{M\times 1}$, which is excited by the scatterer located at (x,y), whose m-th entry can be expressed as [7]:

$$[\mathbf{a}(x,y)]_m = \frac{D_0(x,y)}{D_m(x,y)} e^{j2\pi D_m(x,y)} \tag{3}$$

Spatial non-stationarities. In [8], authors propose the notion of BS-side visibility region (BS-VR) and UE-side visibility region (UE-VR) to model spatial non-stationarities. Throughout this paper, when we say that the k-th user "sees" the m-th antenna, it means that the m-th antenna receives the signal transmitted by the k-th user with non-zero energy.

The transmitted signal interacts with the objects in the environment such as building facades, trees and street furniture, in outdoor environments, or inner walls, pillars and office equipment, in indoor settings. Interactions happen at so-called scattering points [8]. The signal may travel from the user to the BS or from the BS to the user through a line-of-sight (LoS) or through the interactions with the scattering points, *i.e.*, non-LoS (NLoS) propagation configurations. If there is no obstacle in the straight line between the k-th user and the m-th antenna, then there is a LoS propagation and we say that the m-th antenna is located in the k-

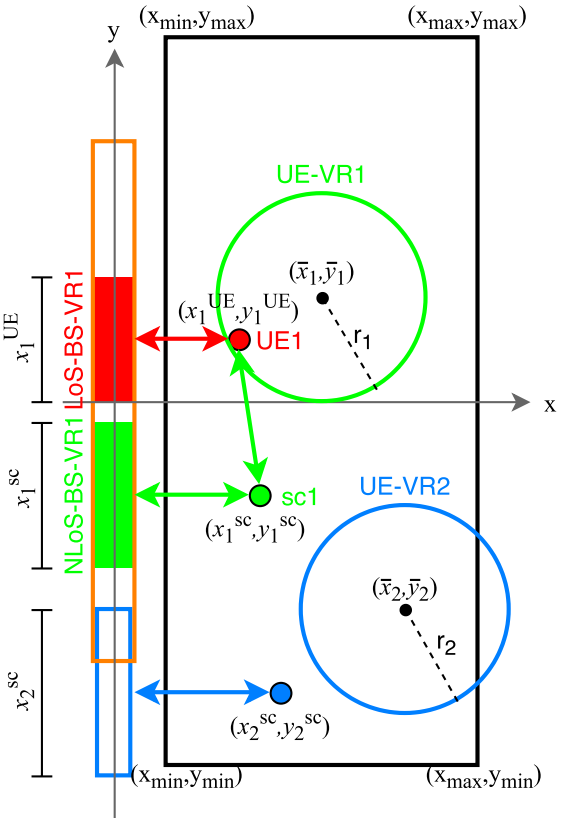

Fig. 2. Simplified example of an XL-MIMO system, with 1 user (UE 1) and two scatterers (sc1, sc2). The user sees a portion of the array through a LoS propagation and other portion of the linear array through a NLoS propagation via scatterer sc1.

th user's LoS-BS-VR. The set containing the antennas that are seen by the k-th user through LoS propagation is denoted by Ξ_k.

Each scatterer $s \in \{1, 2, \ldots, S\}$ has an associated UE-VR and an associate BS-VR. The UE-VR of the s-th scatterer is a circle centered in $(\bar{x}_s, \bar{y}_s)$, whose radius is denoted by r_s. The scatterers and the associated UE-VR centers are uniformly distributed over the cell area. The set containing the antennas that are in the BS-VR of the s-th scatterer is denoted by $\mathbf{\Phi}_s$. We considered, for simplification, a binary case where, if the k-th user is located inside the UE-VR of the s-th scatterer, it will see the antennas that are inside the BS-VR of the s-th scatterer. Otherwise, the k-th user it will not see these antennas.

Fig. 2 illustrates a scenario with one user (UE1) and two scattering points, denoted by sc1 and sc2. The UE1 sees a portion of the array through LoS propagation. We say that this portion of the array is inside the BS-VR associated to the line-of-sight of UE1, which is denoted by LoS-BS-VR1. However, UE1 may also see other portions of the array, through NLoS propagation. In the case represented by Fig. 2, UE1 is inside the UE-VR of sc1, namely, UE-VR1, what means that it sees the portion of the array that is inside the BS-VR of sc1, namely, NLoS-BS-VR1. Then, the portion of the array seen by UE1 corresponds to the union of the regions LoS-BS-VR1 and NLoS-BS-VR1. The antennas that are not inside any of these two BS-VRs are assumed to receive zero energy from UE1, and the signal transmitted by these antennas will not achieve UE1 as well.

Modeling the XL-MIMO Channel. In this paper, we model the XL-MIMO channel as a sum of the LoS component and a number ($\leqslant S$) of NLoS components. The considered model embraces the pathloss, the small-scale fading, the spherical wavefront and spatial non-stationarity. The channel vector between the BS and the k-th user is defined by both LoS and NLoS terms:

$$\mathbf{h}_k = \mathbf{h}_k^{\mathrm{LoS}} + \sum_{s=1}^{S} \mathbf{h}_{ks}^{\mathrm{NLoS}} \alpha_{ks} \tag{4}$$

with the LoS component defined as:

$$\mathbf{h}_k^{\mathrm{LoS}} = \sqrt{\mathbf{b}_k^{\mathrm{LoS}}} \odot \mathbf{a}\left(x_k^{\mathrm{UE}}, y_k^{\mathrm{UE}}\right) \odot \mathbf{q}\left(\Xi_k\right) \tag{5}$$

and the NLoS components associated to S scatterers:

$$\mathbf{h}_{ks}^{\mathrm{NLoS}} = \sqrt{\mathbf{b}_{ks}^{\mathrm{NLoS}}} \odot \bar{\mathbf{h}}_{ks} \odot \mathbf{a}\left(x_s^{\mathrm{sc}}, y_s^{\mathrm{sc}}\right) \odot \mathbf{q}\left(\mathbf{\Phi}_s\right) \tag{6}$$

where $(x_k^{\mathrm{UE}}, y_k^{\mathrm{UE}})$ and $(x_s^{\mathrm{sc}}, y_s^{\mathrm{sc}})$ are the position of the k-th user and the s-th scatterer, respectively; $\mathbf{\Phi}_s$ is the set containing the indices of the antennas that see the s-th scatterer, while

$$[\mathbf{q}(\mathbf{\Phi})]_m = \begin{cases} 1 & \text{if } m \in \mathbf{\Phi}, \\ 0 & \text{otherwise.} \end{cases} \tag{7}$$

indicates whether the m-th antenna is in the BS-VR associated to the generic set $\mathbf{\Phi}$ or not, and α_{ks} indicates if the k-th user is located inside the UE-VR associated to the s-th scatterer. Then,

$$\alpha_{ks} = \begin{cases} 1 & \text{if } d_{ks} \leqslant r_s, \\ 0 & \text{otherwise.} \end{cases} \tag{8}$$

where $d_{ks} = \sqrt{(x_k^{\mathrm{UE}} - \bar{x}_s)^2 + (y_k^{\mathrm{UE}} - \bar{y}_s)^2}$ is the distance between the k-th user and center of the UE-VR associated to the s-th scatterer.

The vector $\mathbf{b}_k^{\mathrm{LoS}} = [\beta_{1k}^{\mathrm{LoS}}, \ldots, \beta_{Mk}^{\mathrm{LoS}}]^{\mathrm{T}}$ groups the pathloss coefficients from the k-th user to each of the M antennas, in the case of the LoS channel. Considering that $D_{mk}^{\mathrm{UE}} = D_m(x_k^{\mathrm{UE}}, y_k^{\mathrm{UE}})$ is the distance between the k-th user and the m-th antenna, according to Eq. (2), the LoS propagation has a pathloss determined by:

$$\beta_{mk}^{\mathrm{LoS}} = \beta_0 \left(\frac{D_{mk}^{\mathrm{UE}}}{1\mathrm{m}}\right)^{-\gamma} \tag{9}$$

where β_0 defines the *median channel gain* for the *reference distance* $d_0 = 1\mathrm{m}$, and $\gamma \geqslant 2$ is the pathloss exponent. The parameter β_0 and γ values are functions of the propagation environment, the carrier frequency, the antenna gains, and the vertical heights of the antennas, which can be obtained from fitting (9) and (10) to measurements [6].

The vector $\mathbf{b}_{ks}^{\mathrm{NLoS}} = [\beta_{1ks}^{\mathrm{NLoS}}, \ldots, \beta_{Mks}^{\mathrm{NLoS}}]^{\mathrm{T}}$ groups the pathloss coefficients in the case of NLoS propagation, when the signal travels from the user to the scatterer and then from the scatterer to the BS. Defining $D_{ks} = \sqrt{(x_k^{\mathrm{UE}} - x_s^{\mathrm{sc}})^2 + (y_k^{\mathrm{UE}} - y_s^{\mathrm{sc}})^2}$ the distance between the k-th user and the s-th scatterer, and $D_{ms}^{\mathrm{sc}} = D_m(x_s^{\mathrm{sc}}, y_s^{\mathrm{sc}})$ the distance between the s-th user and the m-th antenna; hence, the NLoS pathloss is ready determined as:

$$\beta_{mks}^{\mathrm{NLoS}} = \beta_0 \left(\frac{D_{ms}^{\mathrm{sc}} + D_{ks}}{1\mathrm{m}}\right)^{-\gamma} \tag{10}$$

In the NLoS propagation scenarios, the transmitted signal interacts with the objects in the environment, what changes its module and phase. This is the small-scale fading, which can be modeled as an independent Rayleigh fading; hence, in (6), the vector $\bar{\mathbf{h}}_{ks}$ can be modeled as complex Gaussian distribution with zero mean and unity variance, $\bar{\mathbf{h}}_{ks} \sim \mathcal{CN}(\mathbf{0}, \mathbf{I}_M)$.

2.2. Channel estimates in XL-MIMO

During the UL pilot transmission, the BS estimates the channel matrix, $\widehat{\mathbf{H}} = [\widehat{\mathbf{h}}_1 \ldots \widehat{\mathbf{h}}_K]$. The true channel matrix is expressed as $\mathbf{H} = [\mathbf{h}_1 \cdots \mathbf{h}_K] \in \mathbb{C}^{M \times K}$. The k-th user transmits the pilot sequence $\boldsymbol{\psi}_k$, with power p_{p}. The elements of $\boldsymbol{\psi}_k$ are scaled by $\sqrt{p_{\mathrm{p}}}$, forming the signal $\mathbf{s}_k =$

$\sqrt{p_\mathrm{p}}\boldsymbol{\psi}_k^\mathrm{H}$, to be transmitted over τ_p UL symbols. As a result, the BS receives the signal $\mathbf{Y}^\mathrm{p} \in \mathbb{C}^{M\times\tau_\mathrm{p}}$:

$$\mathbf{Y}^\mathrm{p} = \sum_{i=1}^{K} \sqrt{p_\mathrm{p}}\mathbf{h}_i\boldsymbol{\psi}_i^\mathrm{H} + \mathbf{N}^\mathrm{p} \tag{11}$$

where $\mathbf{N}^\mathrm{p} \in \mathbb{C}^{M\times\tau_\mathrm{p}}$ is the noise matrix at the receiver of the BS with i.i.d. elements following a complex normal distribution with zero mean and variance σ_n^2.

As the information about which antennas are visible for each user is unknown, it might be necessary to consider obtaining the channel estimates by using estimators that require no prior statistical information, such as the *Least-Squares* (LS). The LS estimate of $\mathbf{h}_k$ is attained by [6]:

$$\widehat{\mathbf{h}}_k = \frac{1}{\tau_\mathrm{p}\sqrt{p_\mathrm{p}}}\mathbf{Y}^\mathrm{p}\boldsymbol{\psi}_k \tag{12a}$$

$$= \mathbf{h}_k + \frac{1}{\tau_\mathrm{p}\sqrt{p_\mathrm{p}}}\mathbf{N}^\mathrm{p}\boldsymbol{\psi}_k \tag{12b}$$

where the second term in (12b) is the equivalent noise vector, defined as $\mathbf{N}^\mathrm{p}\boldsymbol{\psi}_k \sim \mathcal{CN}(\mathbf{0}_M, \tau_\mathrm{p}\sigma_\mathrm{n}^2\mathbf{I}_M)$.

LS Channel Estimate (CE) Complexity According to (12a), the channel estimation process corresponds to the inner product of M complex vectors of length τ_p, requiring $M\tau_\mathrm{p}$ multiplications between complex numbers to estimate the channel vector of each of the K UEs. Each complex multiplication corresponds to 3 real multiplications.[1] Herein, we consider that both multiplication and division between real numbers correspond to 1 floating-point operation (flop). The channel estimation (CE) process is performed once per coherence block, and the associated complexity, defined in number of flops per coherence block [fpcb], is given by:

$$C_\mathrm{CE} = 3MK\tau_\mathrm{p} \ \ [\mathrm{fpcb}] \tag{13}$$

3. Antenna selection methods for XL-MIMO

In this section, we propose two procedures for smart, flexible antenna-elements selection in the XL-MIMO systems, namely FAS and FSS procedures, to be used to detect the signal sent by each of the K users during the UL communication stage.

3.1. Flexible antenna selection (FAS)

The algorithm returns the subset $\mathcal{D}_k$, for each $k \in \{1, \ldots, K\}$ user, which contains the indices of the antennas that will be active for user k. One advantage of using $M_k = |\mathcal{D}_k| < M$ antennas instead of all the M available antennas is the reduction of the computational complexity, as the combining vector for a given user will be based only on the rows of the estimated channel matrix corresponding to the antennas that the algorithm designated to be active for that user, instead of the full estimated channel matrix. As less antennas are activated at the same time, and also due to the complexity reduction, the power consumption is considerably reduced. Besides, by properly selecting the antennas, the throughput will not deteriorate, because the interference power received at the BS antennas decreases. Consequently, the EE increases.

In the sequel, we discuss how the UL data transmission structure in TDD XL-MIMO operates, as well as we discuss the FAS algorithm itself.

3.1.1. UL data transmission

The received signal $\mathbf{r} \in \mathbb{C}^M$ at the BS during the UL data transmission is:

$$\mathbf{r} = \sum_{k=1}^{K} \mathbf{h}_k x_k + \mathbf{n} \tag{14}$$

where x_k is the signal sent by the k-th user and $\mathbf{n} \sim \mathcal{CN}(\mathbf{0}_M, \sigma_\mathrm{n}^2\mathbf{I}_M)$ contains the noise received at the BS antennas. The detected signal for the user k after the combiner is given by:

$$y_k = \mathbf{v}_k^\mathrm{H}\mathbf{r} \tag{15}$$

where $\mathbf{v}_k \in \mathbb{C}^M$ is the k-th user receive combining vector and its m-th entry is given by:

$$[\mathbf{v}_k]_m = \begin{cases} \widehat{h}_{mk} & \text{if } m \in \mathcal{D}_k, \\ 0 & \text{otherwise.} \end{cases} \tag{16}$$

or:

$$[\mathbf{v}_k]_m = \begin{cases} \widehat{\mathbf{H}}_{(m,:)}\left(\left[\widehat{\mathbf{H}}_{(\mathcal{D}_k,:)}^\mathrm{H}\widehat{\mathbf{H}}_{(\mathcal{D}_k,:)}\right]^{-1}\right)_{(:,k)} & \text{if } m \in \mathcal{D}_k, \\ 0 & \text{otherwise,} \end{cases} \tag{17}$$

depending on whether maximum-ratio (MR) or zero-forcing (ZF) combining is chosen, respectively. As defined in (16) and (17), the combiner v_k has $M - M_k$ zero entries, reducing the complexity. The matrix $\mathbf{V} = [\mathbf{v}_1 \ldots \mathbf{v}_K]$ is the collection of the combining vectors for all the K users.

Assuming the channels are constant within the coherence block, while the signals and noise take new realization at every sample, the instantaneous signal-to-interference-plus-noise ratio (SINR) is actually an expectation over one coherence block. Thus, the average UL transmit power of the k-th user, $p_k = \mathbb{E}\{|x_k|^2\}$, and the average noise power, σ_n^2, will be taken rather than the instantaneous values $|x_k|^2$ and $|n_k|^2$, respectively. Thus, one can define the SINR of the k-th user during the UL data transmission as

$$\gamma_k = \frac{p_k|\mathbf{v}_k^\mathrm{H}\mathbf{h}_k|^2}{\sum\limits_{\substack{i=1 \\ i\neq k}}^{K} p_i|\mathbf{v}_k^\mathrm{H}\mathbf{h}_i|^2 + \sigma_\mathrm{n}^2\|\mathbf{v}_k\|^2} \tag{18}$$

3.1.2. FAS algorithm

In this subsection, we propose a procedure to select the most suitable antenna-elements inside of the k-th user's VR. First, Algorithm 1 computes the vector $\boldsymbol{\theta}_k = [\theta_{1k}, \theta_{2k}, \ldots, \theta_{Mk}] \in \mathbb{C}^{M\times 1}$, which is a quantitative indicator of the quality of the channel between the k-th user and each of the M antennas. It is defined by:

$$\theta_{mk} = \frac{|\widehat{h}_{mk}|^2}{\sum\limits_{\substack{i=1 \\ i\neq k}}^{K} |\widehat{h}_{mi}|^2} \tag{19}$$

where $\widehat{h}_{mk} = [\widehat{\mathbf{h}}_k]_m$. A high signal intensity may be obtained when $|\widehat{h}_{mk}|^2$ is strong. On the other hand, the terms $|\widehat{h}_{mi}|^2, i \neq k$, are related to the interference intensity. Higher θ_{mk} values are therefore associated to higher SINRs on the signal detection, as defined by Eq. (18), and consequently higher spectral and energy efficiencies.

After that, Algorithm 1 obtains the suitable subset $\mathcal{D}_k$, containing the indices of the $M_k \leqslant M$ antennas with the highest θ_{mk} values. These antennas will be designated to process the signals of the k-th UE. Being θ_{m_ik}

[1] The multiplication between two complex numbers, $x = a + jb$ and $y = c + jd$, may be implemented in a way that involves only 3 real floating-point multiplications: $xy = ac - bd + j[(a + b)(c + d) - ac - bd]$. 5 real sums are also necessary, but will not be taken into account, due to their very lower hardware complexity compared to the real multiplication operation [6].

the i-th highest element of the vector θ_k, M_k is the minimum number of antennas that satisfies

$$\sum_{i=1}^{M_k} |\widehat{h}_{m_{ik}k}|^2 \geqslant z_0 Z_k \tag{20}$$

where $0 \leqslant z_0 \leq 1$, and Z_k is the total cumulative power associated to the k-th user, defined as:

$$Z_k = \sum_{m=1}^{M} |\widehat{h}_{mk}|^2 \tag{21}$$

Indeed, $z_0 Z_k$ represents a fraction of the total cumulative power for the kth user. For instance, setting $z_0 = 0.9$ represents 90% of the total cumulative power. Hence, setting $z_0 = 1$ corresponds to using all the M antennas to process the signal of the k-th user. In practice, it is the same as not applying antenna selection procedure for that user. On the other hand, setting $z_0 = 0$ will simply force the BS to ignore that user. Finally, setting z_0 as low values implies that the main concern is reduce the power consumption.

In case the ZF combiner is chosen, there is an additional condition to guarantee that the matrix to be inverted in (17) is not singular, $M_k \geqslant K$, which is attended in line 13 of Algorithm 1.

Algorithm 1. FAS for combining in XL-MIMO systems

Input: $M, K, \widehat{\mathbf{H}}, z_0$
1: **for** $k = 1$ to K **do**
2: Reinitialize the set containing the indices of the M antennas: $\mathcal{M} = \{1, \ldots, M\}$
3: Initialize the set containing the indices of the antennas that will communicate with the user k : $\mathcal{D}_k = \varnothing$
4: Compute $\boldsymbol{\theta}_k$, according to (19)
5: Compute Z_k, according to (21)
6: Initialize $z_k = 0$
7: **while** $z_k < z_0 Z_k$ **do**
8: $m^* = \text{argmax}_{m \in \mathcal{M}} \theta_{mk}$
9: $z_k = z_k + |\widehat{h}_{m^*k}|^2$
10: $\mathcal{D}_k = \mathcal{D}_k \cup \{m^*\}$
11: $\mathcal{M} = \mathcal{M} \backslash m^*$
12: **end while**
13: for ZF combiner, repeat lines 8–11 until $|\mathcal{D}_k| \geqslant K$.
14: **end for**
Output: $\mathcal{D}_k, k = 1, \ldots, K$

As the set $\mathcal{D}_k$ contains the indices of the antennas that are active for the k-th user, the superset $\mathcal{D} = \mathcal{D}_1 \cup \ldots \cup \mathcal{D}_K$ contains all the indices of the antennas that are active for some user. $M_{\text{act}} = |\mathcal{D}|$ is the number of antennas that are activated.

3.2. Fixed Subarray Selection (FSS)

In the Fixed Subarray Selection (FSS) method, the antenna array is divided into subarrays, which can be implemented as separate hardware entities. It is an advantage over the FAS approach, as the implementation complexity is reduced. The number of subarrays (N) is fixed, as well as their size. We considered the specific case where all the subarrays have the same number of antennas (M/N). In case ZF combining is adopted, the number of antennas per subarray needs to be at least equal to the number of users, *i.e.*, $M/N \geqslant K$. In other words, $N \leqslant M/K$ is a condition that must be attended when defining the number of subarrays. The antennas in subarray n form the set $\mathcal{M}_n = \left\{ \frac{M}{N}\left(n-1\right) + 1, \ \ldots, \ \frac{M}{N} n \right\}$. For instance, considering a ULA with $M = 100$ antennas, if we want to divide it into $N = 10$ subarrays of the same size, then each one will have $M_i = 10$ antennas $i = 1, \ldots, N$, and subarray 1 corresponds to the antennas 1 to 10.

The objective of Algorithm 2 is to define which subarrays will be designated to perform receive combining for each user. The set $\mathcal{F}_n$ contains the indices of the users that will be served by the subarray n, and $\mathcal{D}_k$ contains the indices of the subarrays that serve the user k. The number of users served by the subarray n is $K_n = |\mathcal{F}_n|$, and the number of subarrays serving the user k is $N_k = |\mathcal{D}_k|$. If $k \in \mathcal{F}_n$, then $n \in \mathcal{D}_k$, and vice versa.

3.2.1. UL data transmission

During the UL, the received signal $\mathbf{r}_n \in \mathbb{C}^{M/N}$ at the subarray n is:

$$\mathbf{r}_n = \sum_{k=1}^{K} \mathbf{h}_{kn} x_k + \mathbf{n}_n \tag{22}$$

where $\mathbf{h}_{kn} = \mathbf{H}_{(\mathcal{M}_n, k)}$ and $\widehat{\mathbf{h}}_{kn} = \widehat{\mathbf{H}}_{(\mathcal{M}_n, k)}$ are respectively the channel vector and the estimated channel vector between the n-th subarray and the k-th user and $\mathbf{n}_n \tilde{} \mathcal{CN}(\mathbf{0}_{M/N}, \sigma_n^2 \mathbf{I}_{M/N})$. The estimated channel matrix of the n-th subarray is $\widehat{\mathbf{H}}_n = \widehat{\mathbf{H}}_{(\mathcal{M}_n, :)} \in \mathbb{C}^{(M/N) \times K}$, which contains only the rows corresponding to its antennas. If $k \in \mathcal{F}_n$, the subarray n will detect the signal transmitted by the user k:

$$y_{kn} = \mathbf{v}_{kn}^{\text{H}} \mathbf{r}_n \tag{23}$$

where the combining vector $\mathbf{v}_{kn} \in \mathbb{C}^{M/N}$ is given by

$$\mathbf{v}_{kn} = \begin{cases} \widehat{\mathbf{h}}_{kn} & \text{if } k \in \mathcal{F}_n, \\ \mathbf{0}_{M/N} & \text{otherwise.} \end{cases} \tag{24}$$

or

$$\mathbf{v}_{kn} = \begin{cases} \left[\widehat{\mathbf{H}}_n \left(\widehat{\mathbf{H}}_n^{\text{H}} \widehat{\mathbf{H}}_n \right)^{-1} \right]_{(:,k)} & \text{if } k \in \mathcal{F}_n, \\ \mathbf{0}_{M/N} & \text{otherwise.} \end{cases} \tag{25}$$

depending on whether MR or ZF is chosen, respectively. The matrix $\mathbf{V}_n = [\mathbf{v}_{1n} \ldots \mathbf{v}_{Kn}]$ is the collection of the combining vectors used by the subarray n. The CPU will then combine the detected signals $y_{kn}, n \in \mathcal{D}_k$ in each of the N_k subarrays, featuring a precision detector:

$$y_k = \frac{1}{\delta_k} \sum_{n \in \mathcal{D}_k} \theta_{nk} y_{kn} \tag{26}$$

where θ_{nk} and δ_k will be soon defined. Analogously to (18), the resulting SINR is given by:

$$\gamma_k = \frac{p_k t_{kk}}{\sum\limits_{\substack{k'=1 \\ k' \neq k}}^{K} p_{k'} t_{kk'} + \sigma_n^2 \sum\limits_{n=1}^{N} \theta_{nk}^2 \|\mathbf{v}_{kn}\|^2} \tag{27}$$

where

$$t_{kk'} = \left| \sum_{n=1}^{N} \theta_{nk} \mathbf{v}_{kn}^{\text{H}} \mathbf{h}_{k'n} \right|^2 \tag{28}$$

As defined in (24) and (25), if $k \notin \mathcal{F}_n$, then $\mathbf{v}_{kn}$ is an all-zero vector.

Notice that each subarray computes its receive combining matrix independently, based on the matrix $\widehat{\mathbf{H}}_n$, which contains only the rows of the matrix $\widehat{\mathbf{H}}$ that corresponds to the antennas that are part of the subarray n. Notice that the k-th column of the matrix $\mathbf{V}_n$ is all-zero if subarray n is not designated by Algorithm 2 to serve user k, *i.e.*, if $k \notin \mathcal{F}_n$.

3.2.2. FSS algorithm

In the context of fixed subarray selection methodology, Algorithm 2 assigns N_k subarrays with the highest θ_{nk} values to communicate with the user k. The algorithm computes the n-th entry of the vector $\boldsymbol{\theta}_k \in \mathbb{C}^N$ according to:

$$\theta_{nk} = \frac{Z_{kn}}{\sum_{\substack{i=1 \\ i \neq k}}^{K} Z_{in}} \tag{29}$$

where $\theta_{nk} = [\boldsymbol{\theta}_k]_n$. Notice that θ_{nk} in (29) is a metric that indicates the quality of the channel between the k-th user and the n-th subarray, while in (19) it indicates the quality of the channel between the user and each antenna individually. In order to normalize the combining evaluated in (26), we define δ_k as:

$$\delta_k = \sum_{n \in \mathcal{D}_k} \theta_{nk} \tag{30}$$

Being $\theta_{n_{ik}k}$ the i-th highest number in the set $\{\theta_{1k}, \ldots, \theta_{N_k k}\}$, N_k is the minimum number of subarrays that satisfies

$$\sum_{i=1}^{N_k} |Z_{kn_{ik}}|^2 \geqslant z_0 Z_k \tag{31}$$

where Z_{kn} is the *cumulative power associated to the k-th user in the n-th subarray*, given by:

$$Z_{kn} = \sum_{m \in \mathcal{M}_n} |\widehat{h}_{mk}|^2 \tag{32}$$

while Z_k in (21) can also be computed as:

$$Z_k = \sum_{n=1}^{N} Z_{kn} \tag{33}$$

Algorithm 2. FSS for receive combining in XL-MIMO systems

Input: $M, N, K, \widehat{\mathbf{H}}, z_0$
1: Initialize the set of the users that will be served by each subarray: $\mathcal{F}_n = \emptyset, n = 1, \ldots, N$.
2: Initialize the sets $\mathcal{M}_n = \left\{\frac{M}{N}\left(n-1\right) + 1, \ \ldots, \ \frac{M}{N}n\right\}$, which will be used to compute z_{kn} in line 6.
3: **for** $k = 1$ to K **do**
4: Reinitialize the set containing the indices of the N subarrays: $\mathcal{N} = \{1, \ldots, N\}$.
5: Initialize the set containing the indices of the subarrays that will communicate with the k-th user: $\mathcal{D}_k = \emptyset$.
6: Compute $Z_{kn}, n = 1, \ldots, N$, according to (32).
7: Compute Z_k, according to (33).
8: Compute $\boldsymbol{\theta}_k$, according to (29).
9: Initialize $z_k = 0$.
10: **while** $z_k < z_0 Z_k$ **do**
11: $n^* = \text{argmax}_{n \in \mathcal{N}} \ \theta_{nk}$
12: $z_k = z_k + Z_{kn^*}$
13: $\mathcal{D}_k = \mathcal{D}_k \cup \{n^*\}$
14: $\mathcal{F}_{n^*} = \mathcal{F}_{n^*} \cup \{k\}$
15: $\mathcal{N} = \mathcal{N} \backslash n^*$
16: **end while**
17: **end for**
Output: $\mathcal{F}_n, n = 1, \ldots, N$, and $\mathcal{D}_k, k = 1, \ldots, K$

If N_{act} denotes the number of non-empty $\mathcal{F}_n$ sets, and consequently the number of subarrays that serve at least one user, then $M_{\text{act}} = M \cdot N_{\text{act}} / N$ is the number of active antennas.

4. Computational complexity and power consumption model

4.1. FAS complexity

We first address the complexity of computing the ZF combining vectors, following (17). Multiplying $\widehat{\mathbf{H}}^{\text{H}}_{(\mathcal{D}_k,:)}$ by $\widehat{\mathbf{H}}_{(\mathcal{D}_k,:)}$ requires $\frac{K^2+K}{2}M_k$ complex multiplications,[2] using the Hermitian symmetry. According to [6], when the inverse of a matrix is multiplied by another matrix, the $\mathbf{LDL}^{\text{H}}$ decomposition can be used to achieve an efficient hardware implementation. The decomposition of $\widehat{\mathbf{H}}^{\text{H}}_{(\mathcal{D}_k,:)}\widehat{\mathbf{H}}_{(\mathcal{D}_k,:)}$ requires $\frac{K^3-K}{3}$ complex multiplications [6]. Finally, we need to multiply the matrix $\widehat{\mathbf{H}}_{(\mathcal{D}_k,:)}$ by the k-th column of the matrix $\left[\widehat{\mathbf{H}}^{\text{H}}_{(\mathcal{D}_k,:)}\widehat{\mathbf{H}}_{(\mathcal{D}_k,:)}\right]^{-1}$, which requires KM_k complex multiplications plus K complex divisions to compute $\mathbf{D}^{-1}$ [6,20]. Besides, considering complex division consumes 7 flops,[3] the complexity associated to the computation of the combining vector $\mathbf{v}_k$ is $3\left(\frac{K^2+K}{2}M_k + \frac{K^3-K}{3} + KM_k\right) + 7K$ flops per coherence block. Thus, computing the whole combining matrix $\mathbf{V}$ has a complexity of:

$$C^{\text{FAS}}_{\text{C-UL-ZF}} = K^4 + 6K^2 + \frac{3}{2}\left(K+3\right)K\sum_{k=1}^{K} M_k \ \left[\text{fpcb}\right] \tag{34}$$

MR combining does not require multiplications or divisions, as it is given directly from the channel estimates, as its k-th column is simply a copy of some entries of the k-th column of $\widehat{\mathbf{H}}$, according to (16). However, in practical implementations, we typically normalize the received signal y_k in (15) such that $\mathbf{v}_k^{\text{H}}\mathbf{h}_k$ in front of the desired signal x_k is close to one (or another constant). The complexity of this normalization is accounted by 1 complex division per user [6], what gives:

$$C^{\text{FAS}}_{\text{C-UL-MR}} = 7K \ \left[\text{fpcb}\right] \tag{35}$$

Recall that the k-th user combining vector was defined in (16) and (17) to have only M_k non-zero values. It reduces the complexity in obtaining y_k, as in (15), since BS will use M_k antenna-elements of the vectors $\mathbf{v}_k$ and $\mathbf{r}$, instead of M elements, resulting in $3M_k$ flops. As the information processing is done τ_{u} times per coherence block, the associated complexity results:

$$C^{\text{FAS}}_{\text{R/T}} = 3\tau_{\text{u}}\sum_{k=1}^{K} M_k \ \left[\text{fpcb}\right] \tag{36}$$

Obtaining Z_k in (21) requires M complex multiplications to compute $\left|\widehat{h}_{mk}\right|^2, m = \{1, \ldots, M\}$. Considering that there are K users, the total complexity is $3MK$ [fpcb]. Then, obtaining $\boldsymbol{\theta}_k, k = 1, \ldots, K$, requires only MK real divisions, as all the modulus were already computed. Finally, the associated complexity is given by:

$$C_{\text{FAS}} = 4MK \ \left[\text{fpcb}\right] \tag{37}$$

If there was no antenna selection, the complexities given by the Eqs. (34) and (36) would be higher, as all the M antennas would always be

[2] Multiplying two matrices $\mathbf{A} \in \mathbb{C}^{a \times b}$ and $\mathbf{B} \in \mathbb{C}^{b \times c}$ requires ac inner products between b-length vectors, corresponding to abc complex multiplications. However, if $\mathbf{B} = \mathbf{A}^{\text{H}}$, only a diagonal elements of $\mathbf{A}\cdot\mathbf{B}$ and half of the $a^2 - a$ off-diagonal elements need to be computed, due to the Hermitian symmetry, resulting in $\frac{a^2+a}{2}b$ complex multiplications [6].

[3] Let's $x = a + jb$ and $y = c + jd$, then $\frac{x}{y} = \frac{xy^*}{yy^*} = \frac{xy^*}{|y|^2}$. Computing xy^* and $|y|^2 = c^2 + d^2$ requires 3 and 2 real multiplications, respectively, while 2 real divisions are needed to compute the ratio $\frac{xy^*}{|y|^2}$, counting a total of 7 real operations.

active for all the K users, *i.e.*, $M_k = M, k = 1, \ldots, K$.

Finally, the total computational complexity associated to the FAS scheme, in flops per second,[4] can be established as:

$$C_{\text{tot-MR}}^{\text{FAS}} = \frac{B}{\tau_c}\left(C_{\text{CE}} + C_{\text{C-UL-MR}}^{\text{FAS}} + C_{\text{R/T}}^{\text{FAS}} + C_{\text{FAS}}\right) \quad \left[\text{fps}\right] \tag{38}$$

or

$$C_{\text{tot-ZF}}^{\text{FAS}} = \frac{B}{\tau_c}\left(C_{\text{CE}} + C_{\text{C-UL-ZF}}^{\text{FAS}} + C_{\text{R/T}}^{\text{FAS}} + C_{\text{FAS}}\right) \left[\text{fps}\right] \tag{39}$$

depending on whether MR or ZF is chosen, respectively.

4.2. FSS complexity

The multiplication of $\widehat{\mathbf{H}}_n^{\text{H}}$ by $\widehat{\mathbf{H}}_n$, according to (25), has a complexity of $\frac{K^2+K}{2}\frac{M}{N}$ flops per coherence block, using the Hermitian symmetry. The $\mathbf{LDL}^{\text{H}}$ decomposition of the matrix $\widehat{\mathbf{H}}_n^{\text{H}}\widehat{\mathbf{H}}_n$ requires $\frac{K^3-K}{3}$ complex multiplications. Multiplying $\widehat{\mathbf{H}}_n$ by the k-th column of $\left(\widehat{\mathbf{H}}_n^{\text{H}}\widehat{\mathbf{H}}_n\right)^{-1}$, in order to obtain $\mathbf{v}_{kn}, k \in \mathcal{F}_n$, requires $K\frac{M}{N}$ complex multiplications plus K complex divisions to compute $\mathbf{D}^{-1}$. Recalling that $|\mathcal{F}_n| = K_n$, the n-th subarray needs to compute the combining vectors of K_n users, and the complexity of obtaining the matrix $\mathbf{V}_n$ is $3\left(\frac{K^2+K}{2}\frac{M}{N} + \frac{K^3-K}{3} + K_nK\frac{M}{N}\right) + 7K$ flops per coherence block. Finally, the complexity to compute the combining matrix of the N subarrays, when employing ZF combining, is given by:

$$C_{\text{C-UL-ZF}}^{\text{FSS}} = NK^3 + \frac{3}{2}MK^2 + \frac{3}{2}\left(M + 4N\right)K + MK\sum_{n=1}^{N}K_n \left[\text{fpcb}\right] \tag{40}$$

Similarly to (35), the complexity associated with the computation of the MR combining matrix is given by:

$$C_{\text{C-UL-MR}}^{\text{FSS}} = 7\sum_{n=1}^{N}K_n \left[\text{fpcb}\right] \tag{41}$$

As $\mathbf{v}_{kn}$ and $\mathbf{r}_n$ are (M/N)-length vectors, obtaining y_{kn}, as in (23) requires M/N complex multiplications. This process is done τ_u times per coherence block. As the subarray n serves K_n users, the resulting complexity is $3\tau_u MK_n/N$ [fpcb]. Recalling that there are N subarrays, the total computational complexity is:

$$C_{\text{R/T}}^{\text{FSS}} = 3\tau_u\frac{M}{N}\sum_{n=1}^{N}K_n \left[\text{fpcb}\right] \tag{42}$$

To obtain Z_{kn}, given by (32), the BS does M/N complex multiplications to obtain $\left|\widehat{h}_{mk}\right|^2, m \in \mathcal{M}_n$. As there are N subarrays and K users, it results in a complexity of $3MK$ [fpcb]. Given the values of Z_{kn}, obtaining Z_k according to (33) does not involve any further multiplication or division. Finally, obtaining $\boldsymbol{\theta}_k, k = \{1, \ldots, K\}$, requires only NK real divisions, and the associated complexity is given by:

$$C_{\text{FSS}} = (3M + N)K \ [\text{fpcb}] \tag{43}$$

There is also an additional complexity due to the precision detector. To obtain δ_k, as in (30), N_k real multiplications are required. As there are K users, the resulting complexity, in [fpcb], is $\sum_{k=1}^{K}N_k$, which is equal to $\sum_{n=1}^{N}K_n$.

Multiplying θ_{nk} by y_{kn}, as in (26), costs 1 complex multiplication. It is done for the N_k subarrays that serve user k. Then, the sum obtained in (26) is divided by δ_k, which costs 1 complex division. It is done for the K users, τ_u times per coherence block, resulting in $\tau_u\sum_{k=1}^{K}(3N_k + 7) = 7\tau_u K + 3\tau_u\sum_{k=1}^{K}N_k$ [fpcb].

Thus, the total precision detector/precoder additional complexity is:

$$C_{\text{P}}^{\text{FSS}} = 7\tau_u K + \left(1 + 3\tau_u\right)\sum_{n=1}^{N}K_n \left[\text{fpcb}\right] \tag{44}$$

Finally, the total computational complexity associated to the FSS scheme, in flops per second, is:

$$C_{\text{tot-MR}}^{\text{FSS}} = \frac{B}{\tau_c}\left(C_{\text{CE}} + C_{\text{C-UL-MR}}^{\text{FSS}} + C_{\text{R/T}}^{\text{FSS}} + C_{\text{FSS}} + C_{\text{P}}^{\text{FSS}}\right) \left[\text{fps}\right] \tag{45}$$

or

$$C_{\text{tot-ZF}}^{\text{FSS}} = \frac{B}{\tau_c}\left(C_{\text{CE}} + C_{\text{C-UL-ZF}}^{\text{FSS}} + C_{\text{R/T}}^{\text{FSS}} + C_{\text{FSS}} + C_{\text{P}}^{\text{FSS}}\right) \left[\text{fps}\right] \tag{46}$$

depending on whether MR or ZF is chosen, respectively.

The while loop in Algorithm 1 and Algorithm 2 can be implemented with a sorting algorithm. The array to be sorted, θ_k, is M-length when adopting FAS1 or FAS2 schemes and N-length when adopting FSS1 or FSS2. As we can consider the sorting algorithms to have order of $M\log M$ with FAS1 or FAS2 and of $N\log N$ with FSS1 or FSS2 [21], the resulting complexity terms were neglected without compromising the accuracy of the total complexity equations developed in this section.

4.3. No Antenna Selection (noS) complexity

When there is no antenna selection (noS) scheme, the total computational complexity increases:

$$C_{\text{tot-MR}}^{\text{noS}} = \frac{B}{\tau_c}\left(C_{\text{CE}} + C_{\text{C-UL-MR}}^{\text{noS}} + C_{\text{R/T}}^{\text{noS}}\right) \left[\text{fps}\right] \tag{47}$$

or

$$C_{\text{tot-ZF}}^{\text{noS}} = \frac{B}{\tau_c}\left(C_{\text{CE}} + C_{\text{C-UL-ZF}}^{\text{noS}} + C_{\text{R/T}}^{\text{noS}}\right) \left[\text{fps}\right] \tag{48}$$

depending on whether MR or ZF is chosen, respectively. The terms $C_{\text{C-UL-MR}}^{\text{noS}}, C_{\text{C-UL-ZF}}^{\text{noS}}$ and $C_{\text{R/T}}^{\text{noS}}$ can be obtained from 41, 40 and 42, by simply taking $N = 1$ and replacing K_n with K, resulting in:

$$C_{\text{C-UL-MR}}^{\text{noS}} = 7K \ \left[\text{fpcb}\right] \tag{49}$$

$$C_{\text{C-UL-ZF}}^{\text{noS}} = K^3 + \frac{9}{2}MK^2 + \frac{3}{2}(M + 4)K \left[\text{fpbc}\right] \tag{50}$$

and

$$C_{\text{R/T}}^{\text{noS}} = 3\tau_u MK \left[\text{fpcb}\right] \tag{51}$$

4.4. SE and EE and power consumption model

The ergodic spectral efficiency is defined by [6]:

$$\text{SE} = \frac{\tau_u}{\tau_c}\sum_{k=1}^{K}\mathbb{E}\left\{\log_2\left(1 + \gamma_k\right)\right\} \tag{52}$$

where γ_k is the SINR of the k-th user, given in the XL-MIMO AS context

[4] As each coherence block contains τ_c symbols, B/τ_c is the number of coherence blocks per second. Therefore, if C is the complexity in [fpcb], the complexity in [fps] is given by BC/τ_c.

Table 1
System and Channel Parameter Values.

Parameter	Value
Pathloss attenuation exponent: γ	2.5
Median channel gain at a distance of 1 m: β_0	$2.95{\cdot}10^{-4}$
$[x_{min}, x_{max}]$	$[20\lambda, 200\lambda]$
$[y_{min}, y_{max}]$	$[-600\lambda, 600\lambda]$
Wavelength: λ	5 cm
Antenna separation: d	$\lambda/2$
Number of BS antennas (ULA): M	1000
Number of scatterers: S	50
Radium of the scatterers: r_s	5 m
Number of mobile users: K	{4; 8; 16; 32; 64; 100}
Loading factor $\mathcal{L}_{\%} = \frac{K}{M}100 \quad [\%]$	{0.4; 0.8; 1.6; 3.2; 6.4; 10}%
Transmission bandwidth: B	20 MHz
Channel coherence bandwidth: B_C	100 kHz
Channel coherence time: T_C	2 ms
Total UL noise power: σ_n^2	−100 dBm
UL pilot transmit power per user (EPA): p_p	0.1 W
UL data transmit power per user (EPA): p_{UL}	0.1 W
Power amplifier efficiency at the BSs: η^{UL}	0.5
Computational efficiency at the BS: L_{BS}	$75 \left[\frac{Gflop/s}{W}\right]$
Fixed power consumption: P_{FIX}	10 W
Power consumed by local oscillators at BS: P_{LO}	1.0 W
Power consumed by circuit components at BS: P_{BS}	0.5 W
Power consumed by circuit components at UE: P_{UE}	0.2 W
Power density for coding of data signals: $\mathcal{P}_{COD}$	$0.1 \left[\frac{W}{Gbit/s}\right]$
Power density for decoding of data signals: $\mathcal{P}_{DEC}$	$0.8 \left[\frac{W}{Gbit/s}\right]$
Power density for backhaul traffic: $\mathcal{P}_{BT}$	$0.25 \left[\frac{W}{Gbit/s}\right]$
Number of Monte-Carlo realizations: $\mathcal{T}$	1000

by (18) or (27), depending on the selection strategy.

The energy efficiency of a cellular network is defined in [6] as the number of bits that can be reliably transmitted per unit of energy. Thus, its unit is $\left[\frac{bit}{J}\right]$, which is the same as the throughput per unit of power $\left[\frac{bit/s}{W}\right]$. Alternatively, it can be defined as the throughput per unit of power:

$$EE = \frac{B{\cdot}SE}{P_{tot}} = \frac{B{\cdot}SE}{P_{TX}^{UL} + P_{TX}^{tr} + P_{CP}} \tag{53}$$

where the denominator contains the total power consumption (P_{tot}), including all power consumption terms required to make the wireless communication system operational. Being p_k the k-th user UL transmit power and η^{UL} the power amplifier efficiency at the BS, the term

$$P_{TX}^{UL} = \frac{\tau_u}{\tau_c}\frac{1}{\eta^{UL}}\sum_{k=1}^{K} p_k \tag{54}$$

refers to the UL power consumed for data transmission, while

$$P_{TX}^{tr} = \frac{\tau_p}{\tau_c}\frac{1}{\eta^{UL}} K p_p \tag{55}$$

accounts for the total power consumed by the power amplifiers during the UL pilot transmission. Based on [17,6], we utilized a detailed model for the circuit power consumption:

$$P_{CP} = P_{FIX} + P_{TC} + P_{CE/SP} + P_{C/D} + P_{BH} \tag{56}$$

Table 2
Average VR size. Adopted XL-MIMO channel parameters with $M = 1000$.

# antennas inside the BS-VR of an scatterer:	259.9
# antennas seen by each user via LoS propagation:	193.9
# antennas seen by each user via NLoS propagation:	406.2
# antennas seen by each user via LoS or NLoS propagation:	520.1
% users that don't see any antenna via LoS propagation:	49.5%
% users that don't see any antenna via NLoS propagation:	25.9%
% users don't see any antenna via neither LoS nor NLoS:	13.6%

The fixed power consumption (P_{FIX}) is a constant quantity that accounts for the power consumption required for site-cooling, control signaling and load-independent power of backhaul infrastructure and baseband processors [6,22]. The transceiver chains power consumption (P_{TC}) involves the power consumed by the BS local oscillator (P_{LO}), the circuit components (converters, mixers and filters) of each BS antenna (P_{BS}) and the circuit components (mixers, filters, amplifiers and oscillator) of each single-antenna user (P_{UE}), as described by:

$$P_{TC} = P_{LO} + M_{act}P_{BS} + KP_{UE} \tag{57}$$

The channel estimation and signal processing power consumption ($P_{CE,SP}$) can be obtained by simply dividing the total complexity in flops per second [fps], given in (38), (39), (45), (46), (47) or (48), by the computational efficiency at the BS (L_{BS}), which represents the number of flops per energy.

Finally, being $\mathcal{P}_{COD}, \mathcal{P}_{DEC}$ and $\mathcal{P}_{BT}$ the coding, decoding and backhaul traffic power densities, respectively, given in $\left[\frac{watt}{bit/s}\right]$, the channel coding and decoding power consumption can be expressed as:

$$P_{C/D} = B{\cdot}SE{\cdot}\left(\mathcal{P}_{COD} + \mathcal{P}_{DEC}\right) \tag{58}$$

The load-dependent backhaul power consumption, necessary for the data transmission between the BS and the core network, is modeled as

$$P_{BH} = B{\cdot}SE{\cdot}\mathcal{P}_{BT} \tag{59}$$

5. Numerical results

In the sequel we present numerical results based on Monte-Carlo simulations (MCS) in order to demonstrate that the proposed algorithms provide an EE increase while reducing considerably the computational complexity and the power consumption in the context of XL-MIMO systems. From these results, we can see the advantages of appropriately selecting the antennas subset (FAS or FSS schemes) against utilizing the whole antenna array to serve all users at the same time (noS scheme), and make comparisons between the two algorithms. We adopted equal power control policy, what means all UEs utilizes the same fixed transmit power, *i.e.*, $p_k = p_{UL}, k \in \{1,\ldots,K\}$. Table 1 contains a list of the main deployed parameter values, similar to those adopted in [6,17,22,23].

In the MCS, the antenna array contains $M = 1000$ antenna elements and the distance between the antennas is $d = \lambda/2$, where λ is the wavelength. The borders of the cell are defined by $x_{min} = 20\lambda, x_{max} = 200\lambda, y_{min} = -600\lambda$ and $y_{max} = 600\lambda$. Although the position of the users (and consequently the pathloss), the short-scale fading and the VRs are random variables, the numerical results represent an average over 1,000 independent realizations, therefore statistically relevant.

In all simulations, $S = 50$ scatterers and $r_s = 5$ m (radium for all scatterers) have been adopted. The NLoS-BS-VR of the s-th scatterer stands from $(0, y_s^{sc} - x_s^{sc}/2)$ to $(0, y_s^{sc} + x_s^{sc}/2)$. If the antenna m is in this interval, then $m \in \mathbf{\Phi}_s$. The LoS-BS-VR of the k-th user stands from $(0, y_k^{UE} - x_k^{UE}/2)$ to $(0, y_k^{UE} + x_k^{UE}/2)$, with probability of occurrence of

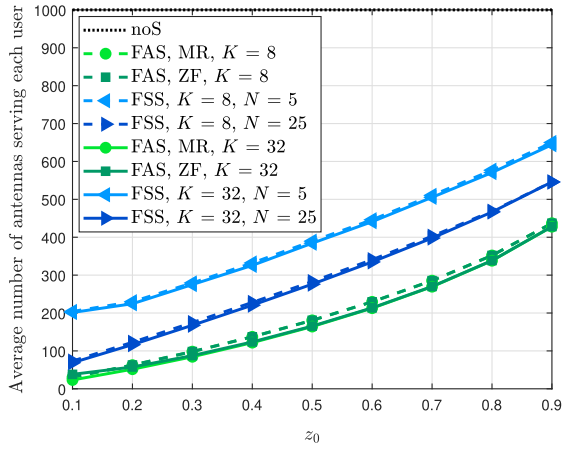

(a) Antennas per user

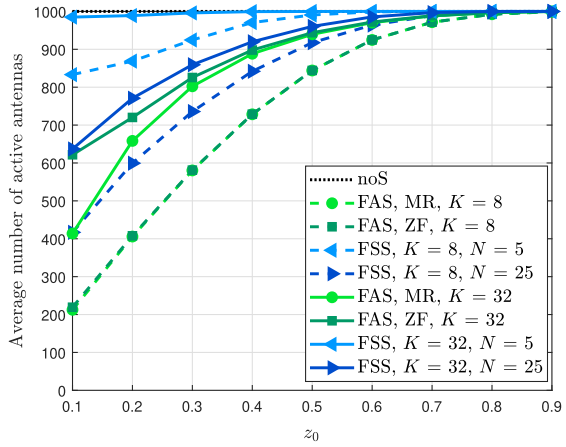

(b) Active antennas

Fig. 3. Impact of the z_0 on the average number of a) selected antennas to perform receive combining (each user); b) active antennas, for two different number of users, $K = 8$ and $K = 32$.

75%. If the antenna m is in this interval, and this VR exists, then $m \in \Xi_k$. Recall that (x_s^{sc}, y_s^{sc}) and (x_k^{UE}, y_k^{UE}) represent the points where the s-th scatterer and the k-th user are located, respectively. Under these conditions, one can obtain information about the length of the visibility regions associated to the users and the scatterers, via numerical simulation. For example, the BS-VR of a scatterer contains, on average, 259.9 antennas; each antenna is inside the BS-VR of 12.9 antennas, on average; and each user is inside the UE-VR of 2.0 scatterers, on average. Further information is presented in Table 2.

5.1. Impact of parameter z_0 and N on the energy efficiency

Numerical results demonstrate the impact of parameter z_0 and N value choice on the system energy efficiency and make comparisons among the noS, FAS and FSS selection schemes. Notice that algorithms FAS and FSS define the set $\mathcal{D}_k$ containing the antennas indexes deployed to select and detect the k-th user' signal in the UL data transmission phase, via receive combining, by utilizing MR or ZF processing. The number of selected antennas, $M_k = |\mathcal{D}_k|$, corresponds to the minimum number of antennas that satisfies the conditions (20) and (31), when employing FAS and FSS, respectively. Intuitively, increasing the z_0 value causes both algorithms to select more antennas to participate in the signal detection of each user. Consequently, the total number of active antennas and the power consumption also increase, as depicted in Figs. 3a, b, 4c and d.

When employing FSS, the number of subarrays (N) influences the average number of selected antennas per user, as well as the average number of active antennas. Dividing the antenna array into $N = 25$ subarrays, there are more degrees of freedom at selecting the antennas than if adopting $N = 5$ subarrays; hence, the condition in (31) can be attended with fewer antennas.[5] It comes at the cost of a more complex hardware implementation. Moreover, the maximum number of degrees of freedom is achieved taking $N = M$, where FSS would work like FAS. This is the reason why FAS activates less antennas than FSS. As P_{TC} is the most significant term in the total power consumption, the following pattern also holds:

$$P_{tot}^{fas} < P_{tot}^{fss} < P_{tot}^{noS},$$

as depicted in Figs. 4 c and d. Notice that there is a considerable power saving when employing FAS or FSS, comparing to the noS strategy, specially when adopting low z_0 values and when there are few active users; in such conditions, the antenna array is less likely to be entirely activated. Besides, the power consumption with ZF combiner is slightly higher than with MR, due to its higher computational complexity, as highlighted by Figs. 4a and b.

Elaborating further on the fraction of cumulative power values, z_0 in (20) and (31) influences the computational complexity of both AS methods (Figs. 4a and b). Higher z_0 implies that more antennas will be utilized to perform receive combining, which increases the complexity associated to multiplying the receive signal at the BS antennas with the combining vector, according to (36) and (42). Also, it is straightforward to conclude that a higher number of active users causes an increase in the XL-MIMO receiver complexity, since the ZF or MR combiner must be performed for more users. Finally, the FAS complexity exceeds the noS complexity when $z_0 > 0.7$ for $K = 32$ (or higher), mainly due to the impact of subarray size M_k over the C_{C-ZF}^{FAS}, eq. (34) , as FAS computes the combining vector of the k-th user based on the pseudo-inverse of a matrix of size $M_k \times K$, and it is done for the K users.

Fig. 5c shows that, by choosing a proper value for z_0, the FAS and FSS schemes can improve the throughput when employing MR, compared to the noS scheme. It means that the AS methods can reduce significantly the interference power at the reception while maintaining the desired signal power, resulting in a SINR increasing, and consequently higher data rates. Fig. 5d demonstrates that, as expected, ZF combiner provides much higher throughput than MR. Despite reducing the number of antennas at the receiver combining usually compromises the ZF ability to mitigate interference, FAS and FSS algorithms were capable to maintain the throughput level near to the noS strategy, as they reduce the received interference power by properly selecting the antennas. For instance, if we divide the antenna array into 5 subarrays, and employ FSS to select which subarray(s) will be used to detect the signal of each user, we can obtain about 90% of the throughput that we would obtain by utilizing the whole array in the detection, while reducing the power consumption. If we divide the antenna array into 25 subarrays, the XL-MIMO power consumption can be reduced further, but the throughput would fall to about 65% of the noS throughput.

Energy Efficiency. From Figs. 5a and b, one can intuitively conclude that it is possible to balance throughput and power consumption because, specially for the cases of $K = 8$ and $K = 32$ under ZF combining (Fig. 5b), the EE can be improved by both the FAS and FSS strategies. One only needs to select z_0 and N accordingly. We also observe that when there are few active users ($K = 8$), it is possible to increase the system EE near the levels of $K = 32$, because under the analyzed antenna selection algorithms it is more likely to reduce considerably the number of active antennas, leading to a power saving while not compromising

[5] But with a number of antennas sufficiently large to guarantee channel hardening features.

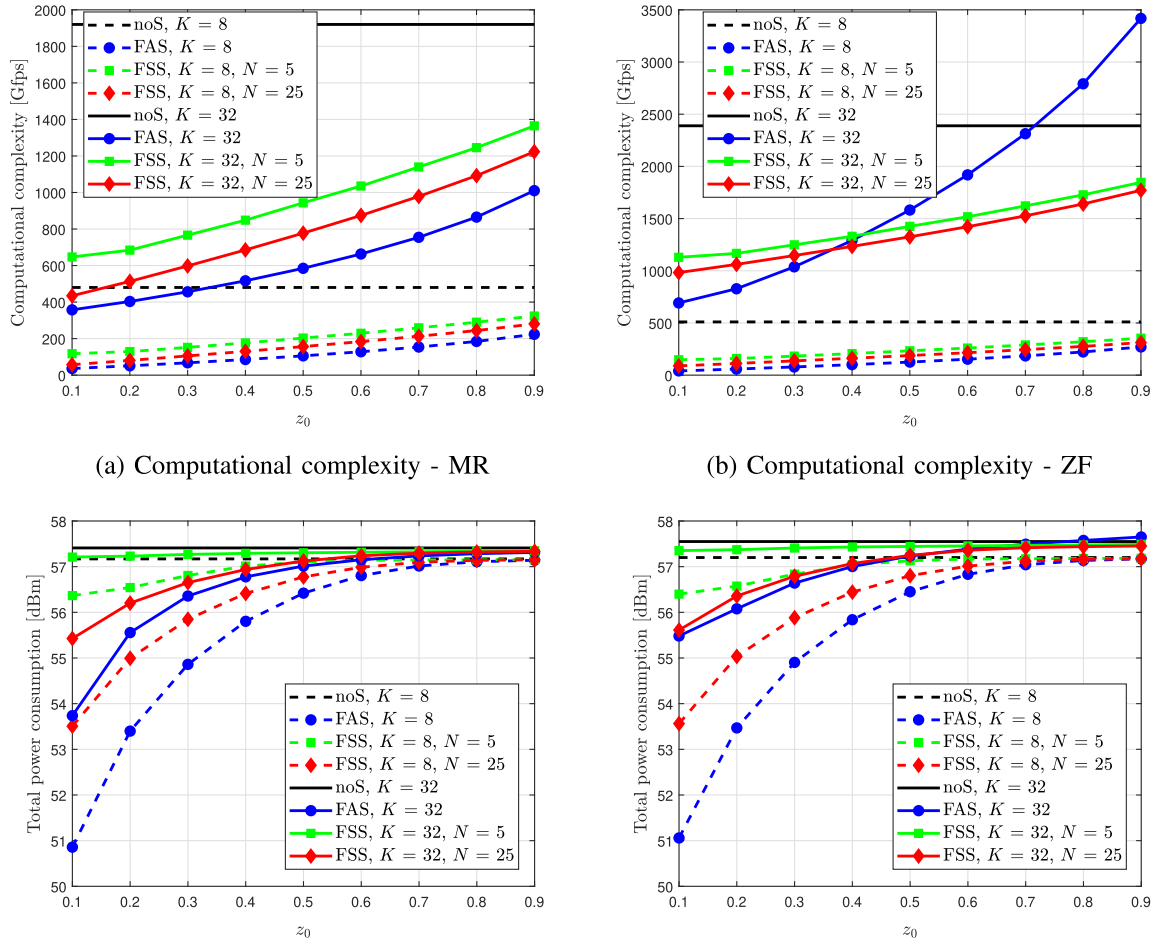

(a) Computational complexity - MR

(b) Computational complexity - ZF

(c) Power consumption - MR

(d) Power consumption - ZF

Fig. 4. Computational complexity and power consumption with FSS and FAS antenna selection schemes and MR or ZF combiners.

the throughput. As a result, the system EE attained with both AS methods can be increased when the fraction of the selected antenna within the cumulative received power decreases below $z_0 < 0.6$. When employing MR, as the FAS and FSS can improve the throughput (what seems not to be possible with ZF), the EE can be easily increased. However, the ZF combiner provides much higher EE than MR due to its capability in mitigating multiuser interference.

5.2. How much can FAS and FSS boost the EE, by properly choosing z_0 and N?

Can z_0 and N in the FAS and FSS algorithms be optimized in order to maximize the system EE? Fig. 6 compares the three selection schemes (noS, FAS and FSS) in terms of computational complexity, power consumption, throughput (B·SE) and per user rate (B·SE/K), for different number of users and for the two most common massive MIMO linear combining schemes (MR and ZF). Table 3 contains the optimal value of z_0 and N, denoted by z_0^* and N^*, for several numbers of active users. If $K \leq 32$, it is advantageous, in order to maximize the EE, to activate only few antennas. Otherwise, the considerable power consumption increase would not justify the small throughput gain. Consequently, z_0^* is very low for both algorithms. Thus, the AS strategies were effective at reducing the average number of selected antennas per user (see Fig. 6a), particularly under very low loading factor scenario ($\mathcal{L}_{\%} \leqslant 3\%$). In this scenario, the number of active antennas is therefore considerably reduced when compared to the noS strategy, and consequently so does the power consumption and the computational complexity (see Figs. 6c and d).

If $K \geqslant 64$, the optimal z_0^* increases a lot, what means the algorithms need to select much more antennas in order to handle with the increasing interference levels, resulting in higher power consumption as the whole antenna array is active, Fig. 6b. Hence, considering XL-MIMO with ULA configurations, one can determine the loading factor range under which simple AS methods bring remarkable gains in terms of system EE-SE tradeoff and complexity reduction: $\mathcal{L}_{\%} \in \{3;\ 6.5\}$ %.

Elaborating further, simple FAS and FSS methods work well in two different ways depending on the goal (EE or SE maximization) in XL-MIMO systems. If $K \leqslant 32$ ($\mathcal{L}_{\%} \leqslant 3.2\%$), the EE is maximized with very low z_0 values, which means few antennas selected per user. In this scenario, the computational complexity is considerably reduced when compared to the traditional strategy (noS). Another consequence is that the number of active antennas may be much lower than M, causing a great power saving. As the channel is non-stationary, which means that the majority of the energy sent by one user achieves only a small portion

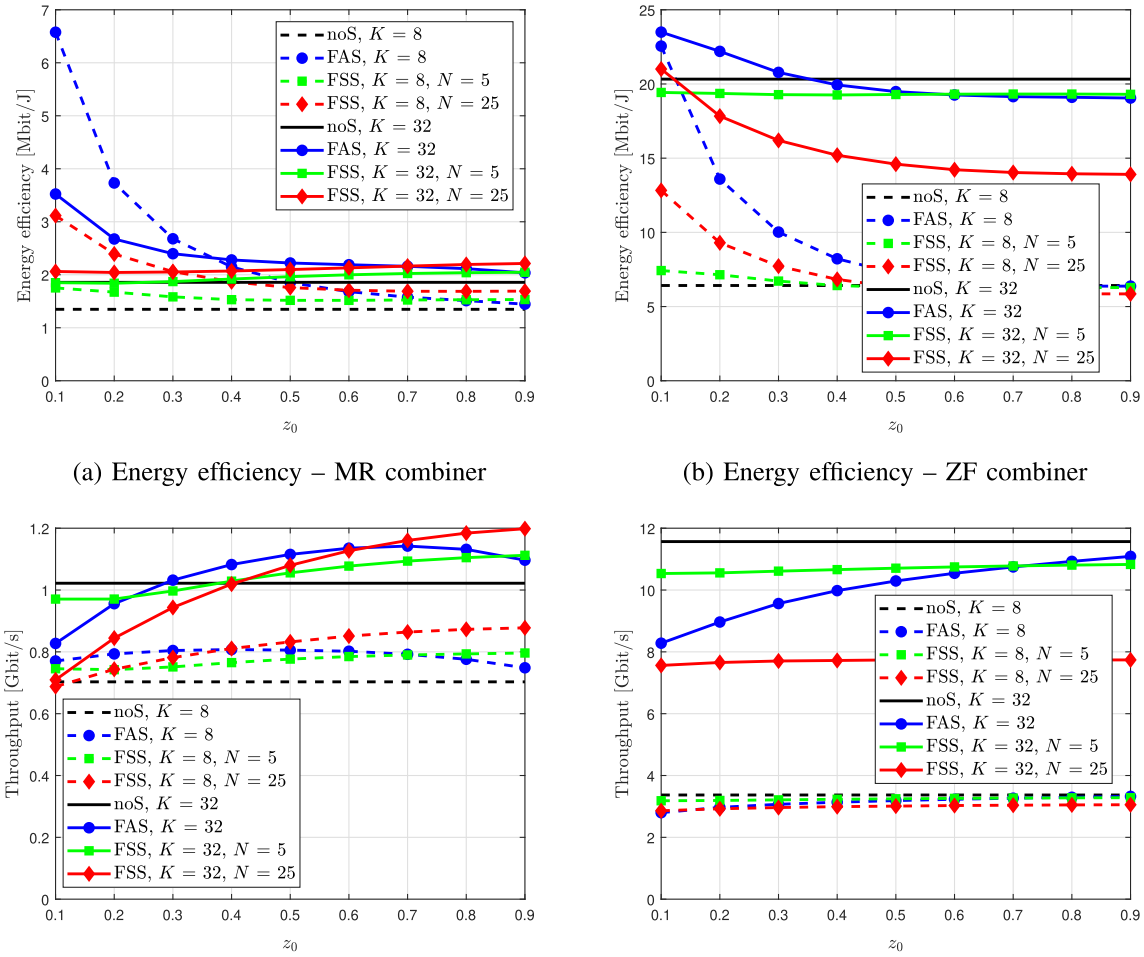

(a) Energy efficiency – MR combiner

(b) Energy efficiency – ZF combiner

(c) Throughput – MR combiner

(d) Throughput – ZF combiner

Fig. 5. Energy efficiency and throughput, with FSS and FAS antenna selection schemes and MR or ZF combiners.

of the array, performing receive combining with only some of the M antennas will not compromise the throughput considerably, as long as this selection is done appropriately, via antenna selection method. As a result, one can obtain a huge EE improvement regarding the no-selection strategy (noS), according to Fig. 7.

On the other hand, if $K \geqslant 64$ ($\mathcal{L}_{\%} \geqslant 6.4\%$), the interference power from overleaped VRs in XL-ULA grows such that both FAS and FSS need to select much more antennas for the signal detection. In this scenario, the (almost) whole ULA array must be activated and the power consumption cannot be reduced; as a consequence, in such scenario, the EE cannot be improved; besides, the multiuser inter-antenna interference must be mitigated (ZF combiner), yet reducing the system throughput, Fig. 6f.

As expected, the ZF performance, considering both the throughput and the energy efficiency, Fig. 6e and 7, respectively, is much better than the MR when deploying the same AS methods, while its power consumption is not much higher and its computational complexity is not prohibitive. Hence, the ZF combiner at XL-MIMO receiver combined with the FSS or FAS antenna selection method results in the best EE-SE tradeoff. Finally, the performance of the FAS and FSS schemes are very similar. The only relevant difference is under higher loading factor ($\mathcal{L}_{\%} \geqslant 3.2\%$), when FSS performs better than FAS, considering ZF combiner in each massive MIMO subarray.

6. Conclusion

Increasing the number of antennas at the BS of a massive MIMO network is useful to provide higher rates and energy efficiency. However, increasing the antenna separation is opportune to make real advantage from an array dimension of the order of hundreds or thousands of antennas. Consequently, the array length increases a lot and channel spatial non-stationary properties appear, which means that the majority of the energy sent by a given user achieves only a small portion of the antenna array. Thus, selecting the antennas that will participate in the receive combining of the signal sent by each user, instead of using all the available antennas, may be very useful strategy to reduce considerably the power consumption without degrading the throughput. The numerical results corroborated it for both antenna selection schemes proposed in this work (FAS and FSS). Up to loading factor $\mathcal{L}_{\%} \leqslant 3.2\%$, at least, FAS and FSS provided huge EE improvement, by properly choosing the values of the parameters z_0 and N. It is important to say that, considering the cell dimensions, $K = 32$ is a realistic scenario. On the other hand, in a scenario with 64 users or more, FAS and FSS could not prevent the whole antenna array to be activated simultaneously, and the system EE could not be improved accordingly. Finally, considering that the FAS and FSS schemes resulted in a very similar performance,

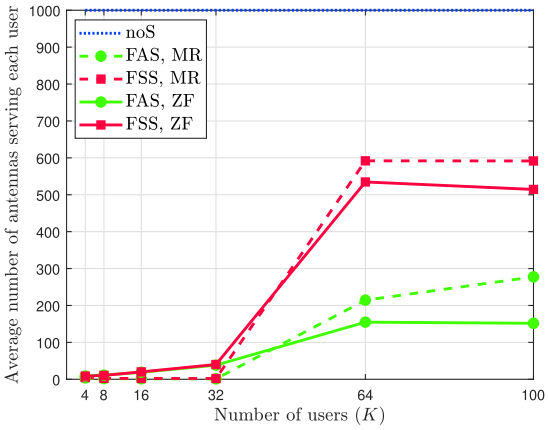

(a) # antennas selected to detect each user information

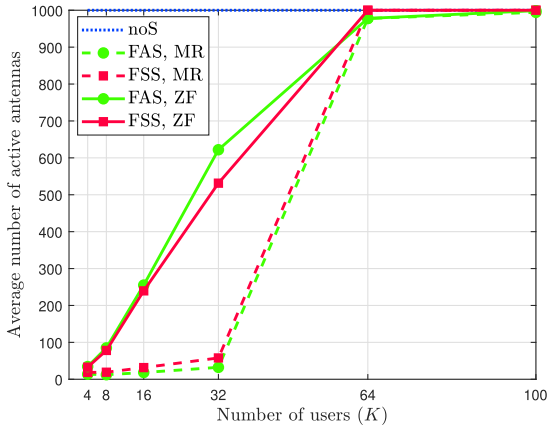

(b) Average number of active antennas

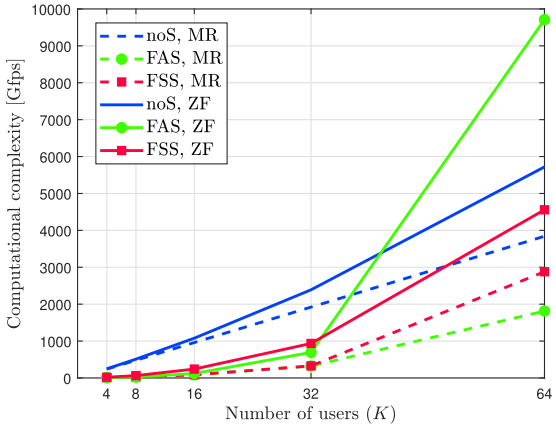

(c) Computational complexity

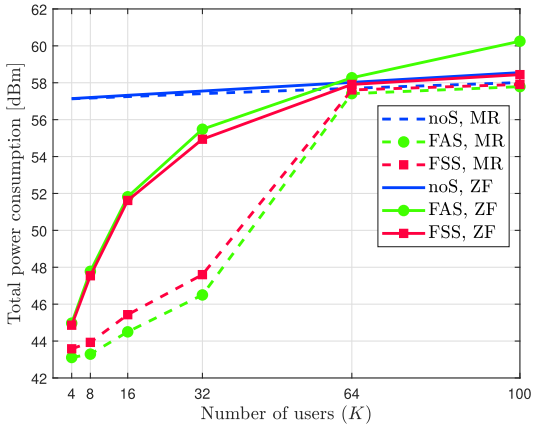

(d) Total power consumption

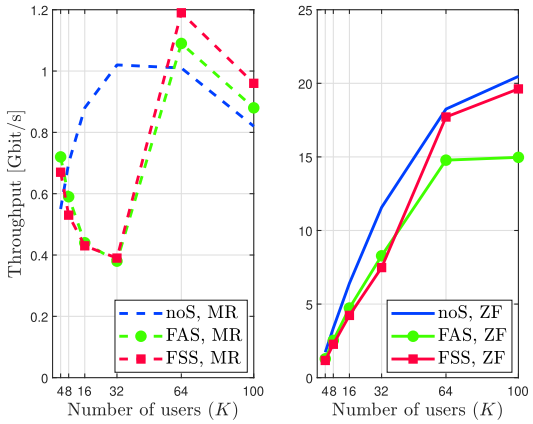

(e) Throughput (sum rate)

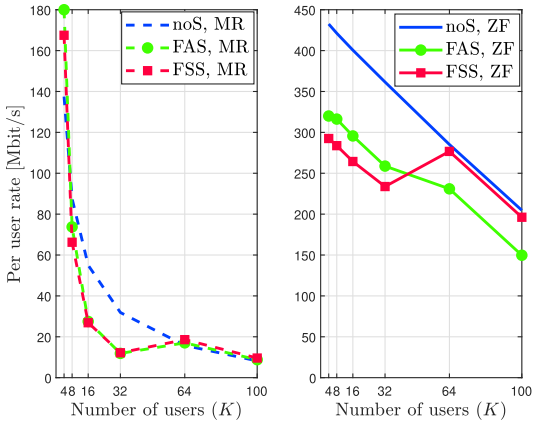

(f) Per user rate

Fig. 6. Comparison among the three antenna selection strategies (noS, FAS and FSS), when the optimal values of z_0 and N are adopted to maximize the EE, $M = 1000$ BS antennas.

Table 3
Optimal values of z_0 and N for maximizing EE when employing FAS or FSS, depending on the number of users and on the linear combining technique (MR or ZF), the average number of selected subarrays ($\mathbb{E}\{N_k\}$) and selected antennas ($\mathbb{E}\{M_k\}$) per user, with $M = 1000$.

	FAS				FSS							
	MR		ZF		MR				ZF			
K	z_0^*	$\mathbb{E}\{M_k\}$	z_0^*	$\mathbb{E}\{M_k\}$	z_0^*	N^*	$\mathbb{E}\{N_k\}$	$\mathbb{E}\{M_k\}$	z_0^*	N^*	$\mathbb{E}\{N_k\}$	$\mathbb{E}\{M_k\}$
4	0.004	3.6	0.004	8.8	0.003	500	2.42	4.8	0.003	200	1.69	8.5
8	0.004	1.6	0.004	11.1	0.003	500	1.23	2.8	0.003	100	1.05	10.5
16	0.004	1.2	0.004	19.0	0.003	500	1.05	2.1	0.003	50	1.00	20.0
32	0.004	1.1	0.100	38.2	0.003	500	1.03	2.1	0.003	25	1.00	40.0
64	0.609	214.4	0.471	154.8	0.960	50	29.60	591.9	0.459	2	1.07	534.7
100	0.718	277.4	0.434	151.7	0.960	50	29.58	591.6	0.390	2	1.03	514.4

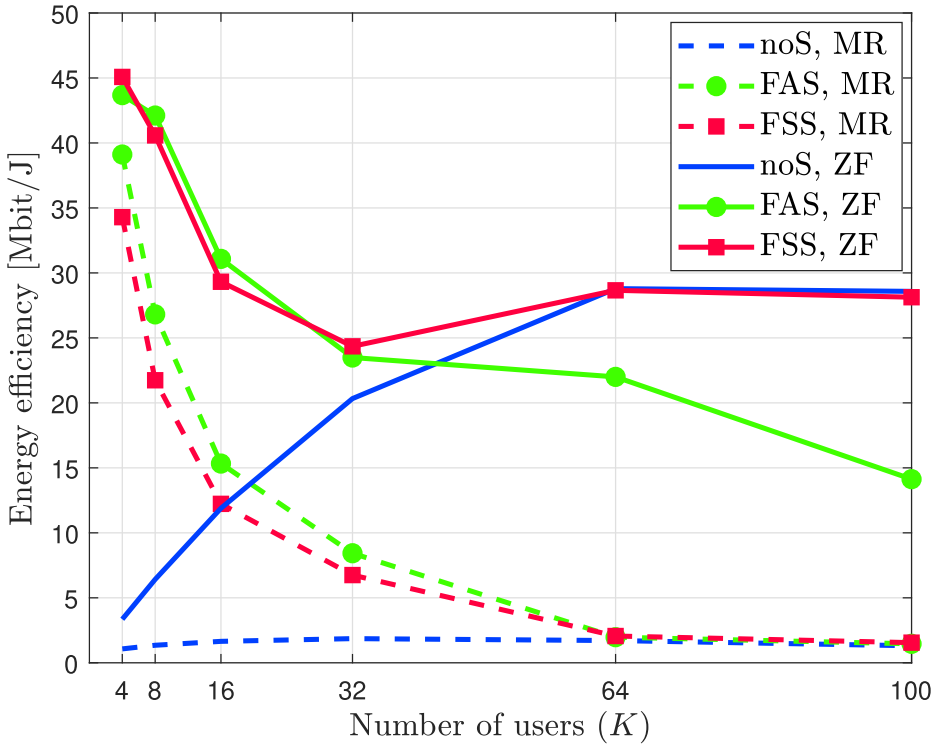

Fig. 7. Energy efficiency×K active users for the three antenna selection strategies (noS, FAS and FSS) and ZF, MR combiners, when the optimal values of z_0 and N are adopted to maximize the EE.

FSS may be advantageous, as its hardware implementation is simpler.

Declaration of Competing Interest

The authors declare that they have no known competing financial interests or personal relationships that could have appeared to influence the work reported in this paper.

Acknowledgements

This study was financed in part by the Coordenação de Aperfeiçoamento de Pessoal de Nível Superior - Brazil (CAPES) - Finance Code 001; in part it was supported by the National Council for Scientific and Technological Development (CNPq) of Brazil under Grants 304066/2015-0 and 404079/2016-4; in part by Londrina State University, Paraná State Government (UEL).

Appendix A. Supplementary material

Supplementary data associated with this article can be found, in the online version, at https://doi.org/10.1016/j.aeue.2020.153568.

References

[1] Marzetta TL. Noncooperative cellular wireless with unlimited numbers of base station antennas. IEEE Trans Wirel Commun 2010;9(11):3590–600. https://doi.org/10.1109/TWC.2010.092810.091092.
[2] Chockalingam A, Rajan BS. Large MIMO Systems. Cambridge University Press; 2014. https://doi.org/10.1017/CBO9781139208437.
[3] Boccardi F, Heath RW, Lozano A, Marzetta TL, Popovski P. Five disruptive technology directions for 5g. IEEE Commun Mag 2014;52(2):74–80.
[4] Carvalho ED, Ali A, Amiri A, Angjelichinoski M, Heath RW. Non-stationarities in extra-large-scale massive mimo. IEEE Wirel Commun 2020;27(4):74–80.
[5] Wang H, Kosasih A, Wen C, Jin S, Hardjawana W. Expectation propagation detector for extra-large scale massive mimo. IEEE Trans Wirel Commun 2020;19(3):2036–51.
[6] Björnson E, Hoydis J, Sanguinetti L. Massive MIMO networks: Spectral, energy, and hardware efficiency. Found Trends® Signal Process 2017;11(3–4):154–655. https://doi.org/10.1561/2000000093.
[7] Han Y, Jin S, Wen C, Ma X. Channel estimation for extremely large-scale massive mimo systems. IEEE Wirel Commun Lett 2020. 1–1.
[8] Flordelis J, Li X, Edfors O, Tufvesson F. Massive mimo extensions to the cost 2100 channel model: Modeling and validation. IEEE Trans Wirel Commun 2020;19(1):380–94.
[9] Yin X, Wang S, Zhang N, Ai B. Scatterer localization using large-scale antenna arrays based on a spherical wave-front parametric model. IEEE Trans Wirel Commun 2017;16(10):6543–56.

[10] Ali A, Carvalho ED, Heath RW. Linear receivers in non-stationary massive mimo channels with visibility regions. IEEE Wirel Commun Lett 2019;8(3):885–8. https://doi.org/10.1109/LWC.2019.2898572.
[11] Amiri A, Angjelichinoski M, de Carvalho E, Heath RW. Extremely large aperture massive mimo: Low complexity receiver architectures. In: 2018 IEEE Globecom Workshops (GC Wkshps); 2018. p. 1–6.
[12] Hou S, Wang Y, Zeng T, Wu S. Sparse channel estimation for spatial non-stationary massive mimo channels. IEEE Commun Lett 2020;24(3):681–4.
[13] Li J, Ai B, He R, Yang M, Zhong Z, Hao Y, Shi G. The 3d spatial non-stationarity and spherical wavefront in massive mimo channel measurement. In: 2018 10th International Conference on Wireless Communications and Signal Processing (WCSP); 2018. p. 1–6.
[14] Chen J, Yin X, Cai X, Wang S. Measurement-based massive mimo channel modeling for outdoor los and nlos environments. IEEE Access 2017;5:2126–40. https://doi.org/10.1109/ACCESS.2017.2652983.
[15] Huang Y, He S, Wang J, Zhu J. Spectral and energy efficiency tradeoff for massive mimo systems. IEEE Trans Veh Technol 2018. https://doi.org/10.1109/TVT.2018.2824311. 1–1.
[16] Amiri A, Manch'on CN, de Carvalho E. Deep learning based spatial user mapping on extra large mimo arrays; 2020. arXiv: 2002.00474.
[17] Ubiali GA, Abrão T. Xl-mimo energy-efficient antenna selection under non-stationary channels. Phys Commun 2020;43:101189. https://doi.org/10.1016/j.phycom.2020.101189. http://www.sciencedirect.com/science/article/pii/S1874490720302664.
[18] Flordelis J, Rusek F, Tufvesson F, Larsson EG, Edfors O. Massive mimo performance-tdd versus fdd: What do measurements say? IEEE Trans Wirel Commun 2018;17(4):2247–61. https://doi.org/10.1109/TWC.2018.2790912.
[19] Marzetta T, Larsson E, Yang H, Ngo H. Fundamentals of Massive MIMO, Fundamentals of Massive MIMO. Cambridge University Press; 2016. URL https://books.google.com.br/books?id=IM0iDQAAQBAJ.
[20] Boyd S, Vandenberghe L. Convex Optimization. Cambridge University Press; 2004. https://doi.org/10.1017/CBO9780511804441.
[21] Cormen TH, Leiserson CE, Rivest RL, Stein C. Introduction to Algorithms, vol. 5. Cambridge: MIT Press; 2001.
[22] Filho JCM, Panazio C, Abrão T, Tomasin S. Total energy efficiency of tr-mrc and fd-mrc receivers for massive mimo uplink. IEEE Syst J 2019;13(3):2285–96.
[23] Björnson E, Sanguinetti L, Hoydis J, Debbah M. Optimal design of energy-efficient multi-user mimo systems: Is massive mimo the answer? IEEE Trans Wirel Commun 2015;14(6):3059–75. https://doi.org/10.1109/TWC.2015.2400437.